

Syracuse University

**SURFACE**

---

Physics - Dissertations

College of Arts and Sciences

---

12-2011

## Interacting Stochastic Processes: from Viciousness to Caging to Force Chains

Shiliyang Xu  
*Syracuse University*

Follow this and additional works at: [https://surface.syr.edu/phy\\_etd](https://surface.syr.edu/phy_etd)



Part of the [Physics Commons](#)

---

### Recommended Citation

Xu, Shiliyang, "Interacting Stochastic Processes: from Viciousness to Caging to Force Chains" (2011).  
*Physics - Dissertations*. 119.  
[https://surface.syr.edu/phy\\_etd/119](https://surface.syr.edu/phy_etd/119)

This Dissertation is brought to you for free and open access by the College of Arts and Sciences at SURFACE. It has been accepted for inclusion in Physics - Dissertations by an authorized administrator of SURFACE. For more information, please contact [surface@syr.edu](mailto:surface@syr.edu).

## Abstract

This thesis documents a quest to develop and study several novel interacting stochastic processes. As for the first example, we generalize a system of vicious random walkers in which the only interaction between any two random walkers is that when they intersect, both walkers are annihilated. We define a system of  $N$  vicious accelerating walkers with each walker undergoing random acceleration and compute the survival probability distribution for this system. We also define and study a system of  $N$  vicious Lévy flights in which any two Lévy flights crossing one another annihilate each other. The average mean-squared displacement of a Lévy flight is not proportional to time, but scales with what is known as the Lévy index divided by two. In both cases, vicious accelerating walkers and vicious Lévy flights, we are motivated by ultimately generalizing our understanding of Gaussian random matrices via non-Markovian and non-Gaussian extensions respectively. Moreover, inspired by recent experiments on periodically sheared colloids at low densities, we define and investigate several new contact processes, or interacting stochastic processes, with conserved particle number and three-or-more-body interactions. We do so to characterize the periodically sheared colloidal system at higher densities. We find two new dynamical phase transitions between an active phase, where some fraction of the colloids are always being displaced from their position at the beginning and end of each shear cycle, and an inactive phase in which all colloids return to their initial positions at the end of each shear cycle. One of the transitions is discontinuous, while the second, which is due to a caging, or crowding, effect at

high densities, appears to be continuous and in a new universality from what is known as conserved directed percolation. The latter transition may have implications for the onset of glassiness in dense, particulate systems. In addition, this thesis also includes analysis of the heterogeneous force network present in amorphous solids near the onset of rigidity, or jamming. The onset of rigidity can, in some sense, be viewed an interacting stochastic process with added constraints to enforce force-balance on each particle, for example. Our analysis yields string-like correlations in the locally-large forces in the system. Such correlations are reminiscent of force chains. While force chains have been readily observed in experiments, it is the first time these correlations have been observed in conjugate gradient simulations of repulsive soft spheres. We also study the contact geometry of the force network and explore a link with spin systems, namely spin glasses, to search for signatures of chaos due to marginal stability, for instance. Connections between jamming systems and spin glass systems will hopefully open up new avenues of theoretical investigation for both systems. Finally, we explore the quantum version of an individual stochastic process, namely the fractional Schrödinger equation. We prove that previously claimed exact solutions for certain potentials are incorrect and determine a new exact solution for a Lévy index of unity and the harmonic oscillator potential. While our results contribute to the realm of mathematical physics, a physical realization of the fractional Schrödinger equation will indeed launch a new subfield of quantum mechanics.

# Interacting Stochastic Processes: From Viciousness to Caging to Force Chains

By

Shiliyang Xu

B. Sc., USTC 2006

DISSERTATION

Submitted in partial fulfillment of the requirements for the  
degree of Doctor of Philosophy in Physics  
in the Graduate School of Syracuse University

December 2011

Copyright 2011 Shiliyang Xu

All rights reserved

## **Acknowledgements**

My deepest gratitude is to my advisor, Prof. Schwarz, for her guidance, understanding, patience and most importantly, her friendship during my graduate years. Without her help, none of the thesis would have been even possible.

My time at Syracuse was made enjoyable by my friends. There are too many names to mention individually, and I just want to say that no matter how far apart we might be in the future, I always wish you the best.

I also owe a huge debt of gratitude to my parents, for never complaining about how infrequently I call, and always being there when I need them. They are simply wonderful, and deserve far better than I can possibly give.

My final thank you must go to Zoey, who entirely brightens my life. For all that, and for being everything I am not, she has my everlasting love.

# Contents

<b>Chapter Summaries</b>	<b>xiii</b>
<b>1 Vicious accelerating walkers and vicious Lévy flights</b>	<b>1</b>
1.1 Background . . . . .	1
1.1.1 Vicious random walkers . . . . .	1
1.1.2 Lévy flights . . . . .	7
1.2 Inquiry . . . . .	9
1.3 $N \leq 3$ vicious accelerating walkers . . . . .	12
1.4 $N > 3$ vicious accelerating walkers . . . . .	19
1.5 Vicious Lévy flights . . . . .	20
1.6 Discussion . . . . .	24
<b>2 Particle-conserving interacting stochastic processes in crowded environments</b>	<b>26</b>
2.1 Background . . . . .	26
2.1.1 Directed percolation . . . . .	26
2.1.2 Conserved directed percolation . . . . .	32
2.1.3 Caging and kinetically constrained models of the glass transition . . . . .	32
2.2 Inquiry . . . . .	34
2.3 The model . . . . .	36
2.4 Mean field analysis . . . . .	38

---

2.5	Two-dimensional simulations . . . . .	46
2.5.1	Simulation protocol . . . . .	46
2.5.2	Results . . . . .	47
2.6	Discussion . . . . .	54
<b>3</b>	<b>Force network analysis of amorphous solids near the onset of rigidity</b>	<b>57</b>
3.1	Background . . . . .	57
3.2	Inquiry . . . . .	60
3.3	Force bonds and spatial correlations . . . . .	62
3.4	Contact number and spins . . . . .	71
3.5	Jammed solids, spin glasses, and some speculation . . . . .	76
3.6	Discussion . . . . .	80
<b>4</b>	<b>On the non-locality of the fractional Schrödinger equation</b>	<b>83</b>
4.1	Background . . . . .	83
4.1.1	Free particle . . . . .	85
4.1.2	Dirac $\delta$ potential . . . . .	86
4.2	Inquiry . . . . .	86
4.3	Infinite one-dimensional square well . . . . .	88
4.4	Other systems . . . . .	91
4.5	The fractional harmonic oscillator . . . . .	92
4.5.1	WKB approximation . . . . .	92
4.5.2	An exact solution for $\alpha = 1$ . . . . .	93
4.6	Discussion . . . . .	94
<b>A</b>	<b>Long-range, one-dimensional Potts glass</b>	<b>96</b>
	<b>Bibliography</b>	<b>101</b>



# List of Figures

1.1	Schematic plot of a directed polymer brush of five polymers as the trajectories of five vicious random walkers [11]. . . . .	3
1.2	Trajectories of discrete vicious random walkers. The fluctuation of position of the leftmost walker $P1$ converges to the famed Tracy-Widom distribution as proved by Baik [10]. . . . .	4
1.3	Realization of a one-dimensional Lévy flight (short-dashed blue) and the comparison with an ordinary random walk (black) and an accelerating random walk (long-dashed red). The inset is a blow-up of the ordinary random walk. . . . .	9
1.4	Log-log plot of survival probability distribution versus time for $N = 2$ and $N = 3$ vicious accelerating walkers in line and for a single accelerating walker in a $\frac{\pi}{3}$ wedge geometry. The line denotes a survival probability exponent of $1/4$ , while the dashed line denotes a survival probability exponent of $3/4$ . . . . .	15
1.5	Survival probability exponent for a two dimensional accelerating walker in a wedge geometry as a function of the opening angle. The line denotes $\alpha = \frac{\pi}{4\theta}$ . Inset: Log-log plot to emphasize the difference between the data and $\alpha = \frac{\pi}{4\theta}$ . The error bars are smaller than the symbols. . . . .	17

1.6	Log-log plot of the survival probability distribution for the $N = 3$ mixed cases of vicious accelerating walkers (A) and vicious random walkers (R). The line denotes a first passage time probability exponent of $\beta = \frac{3}{2}$ . . . . .	18
1.7	Survival probability exponent $\alpha$ for vicious accelerating walkers (solid squares) and vicious Gaussian walkers (solid circles) systems up to $N = 10$ . The simulation results for vicious Gaussian walkers agree very well with theory prediction $\alpha = N(N - 1)/4$ (black curve). However, the results for vicious accelerating walkers deviate from a method of images prediction of $\alpha = N(N - 1)/8$ (blue dashed curve). . . . .	20
1.8	Log-log plot of the the survival probability distribution for $N = 3$ vicious Lévy flights for different values of the Lévy index, $\mu$ . The curve denotes a survival probability exponent of $\alpha = \frac{3}{2}$ . Inset: The survival probability exponent for $N = 2$ and $N = 3$ vicious Lévy flights as a function of the Lévy index. For $\mu > 2$ , we obtain the vicious random walker results. . . . .	21
2.1	Directed percolation as an interacting stochastic process. The filled (hollow) circles denote active (inactive) sites. . . . .	27
2.2	Pictorial representation of diffusion and reaction processes in directed percolation. . . . .	28
2.3	Directed percolation realizations below, at, and above the transition. . . . .	28
2.4	Map of a typical trajectory of a particle in solution at packing fraction, $\phi = 0.56$ . The trajectory is imaged over 100 minutes and it took the particle approximately 500 seconds to go from one cage to the other. Adapted from Ref. [48]. . . . .	33

2.5	A two-dimensional schematic of the three-dimensional experiment presented in Ref. [6]. The red circles denote active particles and the blue denote inactive ones. . . . .	35
2.6	Plot of the fraction of active particles as a function of time for two different strain amplitudes. Adapted from Ref. [6]. . . . .	35
2.7	Mean-field phase diagram for the two-body activation process. . . . .	39
2.8	Mean field phase diagram with caging effect with $z = 2$ . . . . .	43
2.9	Mean field phase diagram for the three-body activation process with via two active particles. . . . .	45
2.10	The dynamical behavior for the active particles for the $A + 2B$ contact process at different total occupation probabilities. . . . .	48
2.11	Log-log plot of the off-critical scaling collapse, $\rho_A t^\theta$ vs. $t \rho - \rho_c ^{\nu_\parallel}$ with $\rho_c = 0.450(2)$ . . . . .	49
2.12	Dynamical behavior of density of active particles $\rho_A$ at critical density $\rho_c$ for different system sizes. . . . .	50
2.13	Log-log plot for finite size scaling at the critical point $\rho = \rho_c$ , $\rho_A t^\theta$ vs. $t/L^z$ . . . . .	50
2.14	The dynamical behavior for the active particles for the $2A + B$ contact process at different total occupation probabilities. . . . .	51
2.15	Log-log plot of the off-critical scaling collapse for the caging transition. The scaling parameters used are $\theta = 0.29(2)$ and $\nu_\parallel = 1.37(3)$ . . . . .	52
2.16	Log-log plot of finite size scaling collapse for different system sizes at the caging transition. Inset: unscaled data. . . . .	53
2.17	The measured caging transition point vs. linear system size, $L$ . The fitted line is an exponential with $\rho_c \sim 0.884$ as $L \rightarrow \infty$ . . . . .	54

2.18	Surviving sample averages for $\rho_A(\rho)$ for different $L$ s. Inset: The magnitude of the jump in $\rho_c$ vs. linear system size. The fitted line is a power-law with a slope of approximately 0.96. . . . .	55
3.1	Jamming phase diagram. Adapted from Ref. [56] . . . . .	58
3.2	Contact force distribution in an experiment. Adapted from Ref. [83] . . . . .	58
3.3	Contact force distribution from simulations. Adapted from Ref. [87] . . . . .	59
3.4	Top: $P(\theta)$ and $P(\theta_{lg})$ for $\phi = 0.841$ , $N = 512$ , and $\lambda = 3/2$ . Bottom: $P_{z=4}(\theta)$ and $P_{z=4}(\theta_{lg})$ for the same parameters. The bin size is $2^\circ$ . . . . .	66
3.5	$P(\theta)$ and $P(\theta_{lg})$ for $\phi = 0.91$ , $N = 512$ , and $\lambda = 3/2$ for a monodisperse system. . . . .	67
3.6	Top: $P(\theta)$ and $P(\theta_{lg})$ for $\phi = 0.843$ , $N = 512$ , and $\lambda = 3/2$ . Bottom: $P_{z=4}(\theta)$ and $P_{z=4}(\theta_{lg})$ for the same parameters. . . . .	68
3.7	Left: $P_{z=3}(\theta_{lg})$ for $\phi = 0.843$ , $N = 512$ , and $\lambda = 3/2$ . Right: $P_{z=4}(\theta_{lg})$ for the same parameters. Bottom: $P_{z=5}(\theta_{lg})$ for the same parameters. . . . .	69
3.8	Jammed configuration for $\phi = 0.841$ , $N = 1024$ . The particles participating along the largest force chain (dark blue) as distinguished from the other particles (light blue). . . . .	71
3.9	The probability of spanning in either direction, $P_s$ , for the largest force chain. . . . .	72

- 
- 3.10 Log-log plot of the average number of particles in the largest force chain that span,  $N_{FC}$ , the average number of particles in the largest force spanning cluster,  $N_{LF}$ , and the average number of particles in the smallest force spanning cluster,  $N_{SF}$ , as a function of  $N$ . The error bars are smaller than the symbols. The straight lines are fits to the data. Here,  $\phi = 0.843$  and  $\lambda = 3/2$ . . . . . 72
- 3.11 Jammed configuration (same as above) colored via coordination number. Light blue denotes  $z = 0$ , magenta denotes  $z = 3$ , red denotes  $z = 4$ , blue depicts  $z = 5$ , orange depicts  $z = 6$ , and purple denotes  $z = 7$  (possible for 1.4 diameter ratio bidisperse system). . . . . 76
- 3.12 Plot of  $r$  as a function of  $N$  for several  $\delta$ s. Inset: Plot of  $r$  for  $N = 128$  as a function of  $\delta$ . The error bars are smaller than the symbols. . . . . 77

# Chapter Summaries

*Note to the reader:* The following section contains a birdseye view of the thesis along with summaries of each chapter. In other words, it is an abstract of unconstrained length. As for the chapters, each chapter begins with a background section followed by an inquiry section. The background section provides the reader with enough material and/or references to more firmly grasp the context of the results of each chapter, while the inquiry section relays the overall question driving the research performed in each chapter. A compilation of all the background sections could provide for an overall introduction to the thesis, however, we have decided to make each chapter self-contained and, hence, chosen this particular construction. We should also note that the variables invoked within each chapter are self-contained.

The study of interacting stochastic processes impacts upon a wide range of systems ranging from magnetism to epidemic spreading to the competition between species. While numerous examples exist, two celebrated ones are the contact process [1] and the exclusion process [2]. The contact process considers active, or infected, sites and inactive, or healthy, sites on a hypercubic lattice. Inactive sites become activated by nearest neighbor active sites at a rate proportional to the number of nearest neighbor active sites. In addition, active sites become inactive (recover their health) at a rate of unity. There exists a critical value of the propor-

tionality constant below which the infection (the presence of active sites) dies out. As for the exclusion process, particles diffuse freely on a lattice with the constraint that they cannot overlay and must avoid each other in order to cross (in dimensions higher than unity). The system may exchange particles with some infinite reservoir at the boundaries, or may be closed. One of the initial motivations for studying this process, at least in one dimension, was to model mRNA translation where the particles correspond to ribosomes moving along mRNA strands [3].

One of the main quests documented in Chapters 1 and 2 is to construct and study new models of interacting stochastic processes. The new models are motivated by two different, though related topics, the first being generalizations of random matrix ensembles and the second being glassiness in disordered systems. These two topics are related by the idea that the Instantaneous Normal Modes of fluids near the glass transition can be characterized by a random matrix whose elements depend on the Euclidean distance between points randomly distributed in space [4]. Another main quest documented in Chapter 3 is the study of the implications of a previously developed interacting stochastic process—the onset of rigidity in amorphous solids, otherwise known as jamming. Jamming involves an intricate interplay between forces and contact geometry in order to balance the forces on each particle. We go beyond the usual distribution of forces to look for spatial correlations in the forces generated as well as investigate perturbations in the contact geometry and find an effect linked to chaos in spin glass systems near the onset of jamming. Finally, Chapter 4 addresses a mathematical physics problem we discovered while developing a new interacting stochastic process now dubbed vicious Lévy flights. The problem involves building correct, exact solutions for the fractional Schrodinger equation in which the ordinary Laplacian operator is replaced with the fractional Laplacian operator. The fractional Laplacian operator describes Lévy flights (in the continuum limit).

## Chapter 1

Consider the following interacting stochastic process. There are  $N$  random walkers on a line. When any two walkers intersect, both are annihilated. This system is known as vicious random walkers with the viciousness referring to the annihilation [5]. There exists a link between vicious random walkers and the Gaussian random matrices. In an effort to ultimately go beyond Gaussian random matrices, we study a system of  $N$  vicious accelerating walkers with the acceleration undergoing Gaussian fluctuations, as opposed to the velocity. We numerically compute the survival probability exponent,  $\alpha$ , for this system, which characterizes the probability for any two walkers not to intersect. For example, for  $N = 3$ ,  $\alpha = 0.71 \pm 0.01$ . Based on our numerical data, we conjecture that  $\frac{1}{8}N(N-1)$  is an upper bound on  $\alpha$ . We also numerically study  $N$  vicious Lévy flights and find, for instance, for  $N = 3$  and a Lévy index  $\mu = 1$  that  $\alpha = 1.31 \pm 0.03$ . While vicious accelerating random walkers may prove relevant for a non-Markovian extension of Gaussian random matrices, vicious Lévy flights may be relevant for random Lévy matrices. Moreover, vicious accelerating walkers relate to no-crossing configurations of semiflexible polymer brushes just as vicious random walkers relate to no-crossing configurations of flexible polymer brushes. This work was published in *Europhysics Letters* in 2011.

## Chapter 2

Periodically sheared colloids at low densities demonstrate a dynamical phase transition from an inactive to active phase as the strain amplitude is increased [6]. To begin to answer the question of what happens to this system at higher densities approaching that of the colloidal glass transition, we build and investigate a conserved-particle-number interacting stochastic process with a three-body inter-



action as opposed to the usual two-body interaction. In particular, one active (diffusing) particle collides with two inactive (non-diffusing) particles such that they can become active. In mean-field, this system exhibits a continuous absorbing phase transition belonging to standard conserved directed percolation universality class. Simulations on two-dimensional lattices support our result. In contrast, the three-body interaction with two active particles colliding and activating one inactive particle exhibits a first-order transition. Inspired by kinetically-constrained models of the glass transition, we investigate the "caging effect" at even higher particle densities to look for a second dynamical phase transition back to an inactive phase. Again, mean-field calculations demonstrate a continuous transition. Two-dimensional lattice simulations suggest a continuous dynamical phase transition, however, the universality class appears to be a different from the standard conserved directed percolation universality class. This difference is presumably due to the localized geometric constraint of caging. This work is in preparation.

## Chapter 3

Jamming is an interacting stochastic process involving force balance, isostaticity and local mechanical stability. Using a system of repulsive, soft particles as a model for an amorphous solid, we analyze its force network as characterized by the magnitude of the contact force between two particles, the local contact angle subtended between three particles, and the local coordination number. In particular, we measure the local contact angle distribution as a function of the magnitude of the local contact force. We find the suppression of small contact angles for locally larger contact forces, suggesting the existence of chain-like correlations in the locally larger contact forces. We also investigate perturbations in the contact geometry. Using a coordination number-spin state mapping, we measure chaos

due to marginality in the jammed system similar to what is found in spin glass systems at the spin glass transitions. By coupling the force-chain results with the coordination number-spin state mapping we suggest the possibility of a jammed (amorphous) solid being described by a sea of weakly interacting spins providing for long-range interactions along a chain-like backbone of more strongly interacting spins. This suggestion may easily explain the mean-field nature observed in numerical simulations of the jamming transition. This work is under review at *Physical Review E*.

## Chapter 4

A number of papers over the past eight years have claimed to solve the fractional Schrödinger equation for systems ranging from the one-dimensional infinite square well to the Coulomb potential to one-dimensional scattering with a rectangular barrier. However, some of the claimed solutions ignore the fact that the fractional diffusion operator is inherently nonlocal, preventing the fractional Schrödinger equation from being solved in the usual piecewise fashion. We focus on the one-dimensional infinite square well and show that the purported groundstate, which is based on a piecewise approach, is definitely not a solution of the fractional Schrödinger equation for general fractional parameters  $\alpha$ . On a more positive note, we present a solution to the fractional Schrödinger equation for the one-dimensional harmonic oscillator with  $\alpha = 1$ . This work was published in the *Journal of Mathematical Physics* in 2010.

# Chapter 1

## Vicious accelerating walkers and vicious Lévy flights

### 1.1 Background

#### 1.1.1 Vicious random walkers

**A** random walk is the simplest stochastic process for an individual particle. It also provides the basis for numerous interacting stochastic processes. For instance, consider  $N$  random walkers in one-dimension. These random walkers act independently unless two random walkers intersect or cross. Then, the pair of walkers annihilate each other, hence the term "vicious". The  $N$  vicious walkers system dies leaving behind an  $N - 2$  vicious walkers system. This interaction was introduced by M. E. Fisher in 1984 during his Boltzmann Medal lecture [5].

Why choose such an interaction? It was originally proposed to study interfacial wetting in 1+1 dimensions, which is driven by the interaction of different interfaces

(the various random walkers) [5, 7]. Close to the wetting transition, the interface is pinned to the wall with alternate segments either attached to the wall or staying apart from the wall to form bubbles. The fluctuations of the interface normal to the wall can be modeled with random walks, while the direction parallel to the wall is treated as time. Therefore, the wetting transition is equivalent to having the random walks (different segments of the interface) annihilate upon contact such that the entire interface is attached to the wall, or wetted. A similar situation occurs in the one-dimensional Ising spin system with Glauber spin-flip mechanism, where the domain walls act as random walks and disappear when they intersect [5, 7].

Later on it was noted that the fermionic nature of vicious walkers (where no two walkers can occupy the same lattice site in a discretized version of vicious walkers) provides for a Coulomb gas description [8]. Interestingly, the partition function of a log-potential Coulomb gas in one dimension is equivalent to the partition function of an ensemble of Gaussian random Hermitian matrix (at three particular temperatures with each temperature relating to the three types of Gaussian random matrices—orthogonal, unitary, and symplectic) [9]. Furthermore, Baik [10] proved that a particular limiting conditional distribution of the displacement of the leftmost walker is equivalent to the Tracy-Widom distribution for Gaussian random Hermitian matrices. The Tracy-Widom distribution characterizes the fluctuations in the largest eigenvalue in a Gaussian random Hermitian matrix. In addition, vicious walker configurations correspond to directed polymer brushes with the vicious mechanism capturing the non-intersecting property of the polymers [11]. See Fig. 1.1 for a schematic of a polymer brush. Polymer brushes consist of polymers adhered to a surface at high densities such that there is crowding among the polymers forcing them to elongate away from the surface to avoid overlapping with other polymers or themselves (no self-avoidance). So

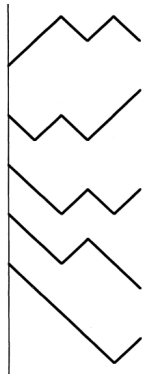


Figure 1.1: Schematic plot of a directed polymer brush of five polymers as the trajectories of five vicious random walkers [11].

while the study of vicious walkers has attracted attention from the mathematical physics community, a number of different physical applications also drive its study.

Let us start with the fundamentals characterizing vicious random walkers. A single random walker in one-dimension with position  $x(t)$  as a function of time  $t$  is described by the equation of motion,

$$\dot{x} = \eta(t), \quad (1.1)$$

where  $\eta(t)$  is Gaussian noise  $\langle \eta(t) \rangle = 0$  and  $\langle \eta(t)\eta(t') \rangle = 2D\delta(t - t')$ . The corresponding Fokker-Planck equation is simply

$$D \frac{\partial^2}{\partial x^2} p(x, t) = \frac{\partial}{\partial t} p(x, t), \quad (1.2)$$

where  $p(x, t)$  is the probability density distribution for the one-dimensional random walk. For an  $N$  vicious random walkers system, since the  $N$  random walkers behave independently, the joint probability density distribution  $p(x_1, \dots, x_N, t)$  obeys

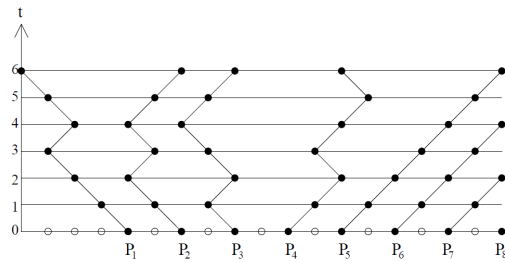


Figure 1.2: Trajectories of discrete vicious random walkers. The fluctuation of position of the leftmost walker  $P_1$  converges to the famed Tracy-Widom distribution as proved by Baik [10].

the Fokker-Planck equation

$$D \sum_{i=1}^N \frac{\partial^2}{\partial x_i^2} p(x_1, \dots, x_N, t) = \frac{\partial}{\partial t} p(x_1, \dots, x_N, t). \quad (1.3)$$

In order to implement the vicious interaction between random walkers, we assign the boundary condition  $p(x_1, \dots, x_N, t) = 0$  if  $\exists(i, j)$  such that  $x_i = x_j$ . If all the walkers are ordered initially  $x_i < x_j \forall i < j$ , the vicious interaction preserves the order since the dynamics of a random walk is local and no crossing is allowed. For a schematic of the vicious walker trajectories, see Fig. 1.2.

We are interested in a particular time scale in the system. In particular, for how long can the  $N$  vicious random walkers avoid each other so that the system survives? To investigate this problem, one can introduce a survival probability for the system  $s(t)$ , defined as the probability that the system is still alive up to time  $t$ . For  $N = 1$ ,  $s(t) = 1$ .

For  $N = 2$ , we have two vicious random walkers on a line and the system dies only if they meet. That is, as long as the distance between them is not zero, the system survives. One can then define a new variable  $x(t) = x_1(t) - x_2(t)$

and perform the change of variable on the Fokker-Planck equation for the  $N = 2$  system to obtain

$$2D \frac{\partial^2}{\partial x^2} p(x, t) = \frac{\partial}{\partial t} p(x, t). \quad (1.4)$$

This is the Fokker-Planck equation for a single 1D random walker (with diffusion constant  $2D$ ) and  $x(0) = x_1(0) - x_2(0) < 0$ . The boundary condition is now  $p(x = 0, t) = 0$ . We now have in fact converted the  $N = 2$  vicious random walkers problem into the first-passage problem of one random walk. If one defines a first-passage probability function  $f(t)$ , it is related to the survival probability function  $s(t)$  via

$$\begin{aligned} s(t) &= 1 - \int_0^t f(t') dt' \\ \frac{ds(t)}{dt} &= -f(t). \end{aligned} \quad (1.5)$$

The solution to the first-passage problem of a 1D random walk is well-known. At long times,  $f(t) \sim t^{-3/2}$ . Thus, for  $N = 2$  vicious walkers, the survival probability distribution scales as  $s(t) \sim t^{-1/2}$ .

For  $N = 3$  vicious random walkers on a line, we can first use a relative coordinate change of variables. Specifically, set  $x = x_1 - x_2$ ,  $y = x_2 - x_3$ . The Fokker-Planck equation is now

$$2D \left( \frac{\partial^2}{\partial x^2} + \frac{\partial^2}{\partial y^2} - \frac{\partial^2}{\partial x \partial y} \right) p(x, y, t) = \frac{\partial}{\partial t} p(x, y, t). \quad (1.6)$$

To get rid of the coupled term, apply a second set of coordinate transformations,  $u = x + y$  and  $v = -(x - y)/\sqrt{3}$ , to arrive at

$$2D \left( \frac{\partial^2}{\partial u^2} + \frac{\partial^2}{\partial v^2} \right) p(u, v, t) = \frac{\partial}{\partial t} p(u, v, t). \quad (1.7)$$

The absorbing boundaries now lie at  $v = \pm u/\sqrt{3}$ . By the two-step change of variables, we have mapped the  $N = 3$  vicious walkers problem to a single two-dimensional random walk in an absorbing wedge geometry with a  $60^\circ$  wedge angle.

The first-passage properties of a two-dimensional random walk in an absorbing wedge has been solved. One way to solve it is conformal mapping[32]. Given the rotational invariance of the diffusion operator, one can use the transformation  $z' = z^{\pi/\theta}$  to map a wedge with angle  $\theta$  to the upper-half plane, and the absorbing boundary now lies on the x-axis. Since the random walk in x-direction is actually freed, the problem is reduced to a 1D random walk with absorbing wall in y-direction, and the survival probability is presented above as  $s(t) \sim t^{-1/2}$ . Use the inverse mapping, one can obtain that the survival probability of a 2D random walk in an absorbing wedge with angle  $\theta$  is then  $s(t) \sim t^{-\pi/2\theta}$ . For the  $60^\circ$  we have obtained for the  $N = 3$  vicious walkers problem, the survival probability is  $s(t) \sim t^{-3/2}$ .

The same technique can be applied to arbitrary values of  $N$  to map the vicious random walkers problem to an  $N - 1$  dimensional random walk in an absorbing wedge geometry. In addition, for any infinite domain with absorbing boundaries, the survival probability of a random walk generally decays as a power-law relation at long times, i.e.  $s(t) \sim t^{-\alpha}$ , while for a bounded domain, the survival probability decays exponentially. The first-passage probability distribution for an infinite domain is then also power-law as  $f(t) \sim t^{-\beta}$  at long times with  $\beta = \alpha + 1$ .

In a related derivation, Fisher [5] has shown that the long-time asymptotic distribution for the  $N$  vicious random walkers is

$$p(x_1, \dots, x_N, t) = \frac{e^{-\sum_{i=1}^N x_i^2/2t}}{(2\pi t)^{N/2}} e^{-N(N-1)(2N-1)/12t} \prod_{i>j}^N (e^{x_i/t} - e^{x_j/t}). \quad (1.8)$$

The first factor is the product of  $N$  independent random walks without any in-



teraction. The second exponential term approaches unity in the long time limit  $t \rightarrow \infty$ . The most important factor is the third one, or  $\prod_{i>j}^N (e^{x_i/t} - e^{x_j/t})$ , which is denoted as the "death factor" in Fisher's derivation. The product in the death factor has  $N(N-1)/2$  terms in itself, and one of each corresponds to a pair of vicious random walkers  $(x_i, x_j)$ . The survival probability can be obtained from the asymptotic distribution above by integrating it over all possible set of  $x_i$ 's subject to the boundary condition  $x_1 < x_2 \dots < x_{N-1} < x_N$ , where the integral will eventually become again a product of individual death factors  $D_{ij}$  for the pair  $(x_i, x_j)$ . As we already know each pair  $(x_i, x_j)$  generates a survival probability  $s(t) \sim t^{-1/2}$ , the probability for all the  $N(N-1)/2$  pairs to survive is  $s(t) \sim t^{-N(N-1)/4}$ , or the survival probability exponent  $\alpha = N(N-1)/4$ . This is one of the central analytical results for vicious random walkers.

### 1.1.2 Lévy flights

As a foundation for vicious Lévy flights, we would like to introduce the properties of an individual Lévy flight. Lévy flights are generalizations random walks in that they retain the Markovian nature of a random walk. However, the step-size distribution (or Lévy distribution) of a Lévy flight as an infinite mean and/or variance. In particular, the Lévy distribution can be asymptotically expressed as  $f(x) \sim x^{-1-\mu}$ , where  $\mu$  is the Lévy index. When  $\mu > 2$ , the variance of a Lévy distribution is finite, however, when  $1 < \mu \leq 2$ , the variance is infinite (but mean finite) and when  $0 < \mu < 1$ , both the mean and variance are infinite. For  $0 < \mu \leq 2$ , because of the broad tail in the Lévy distribution, Lévy flights can make long jumps in contrast to step-size distributions with finite mean and/or variances. See Fig. 1.3. Lévy flights have been observed in many systems, including animal foraging patterns, DNA-binding protein searching for binding sites, kinetic Ising model with long-range interactions, and light waves transporting in

certain materials [12, 13, 14, 15].

When  $\mu > 2$ , the variance of a Lévy distribution is finite and the Central Limit Theorem holds such that a Lévy flight is equivalent to a Gaussian random walk at long times. When  $\mu < 2$ , however, the variance and/or mean of the step-size distribution diverges and one expects to see qualitatively different behavior from a Gaussian random walk since one of the assumptions invoked in the Central Limit Theorem no longer applies. Then, the mean square displacement of a Lévy flight with Lévy index  $\mu$  follows  $\langle r^2 \rangle \sim t^{2/\mu}$ , where for  $\mu = 2$  the linear, normal random walk behavior is recovered. One might remember that for anomalous diffusion, the mean square displacement also grows non-linearly in  $t$  such that Lévy flights may describe anomalous diffusion.

The long jumps of a Lévy flight make the process non-local such that it can overshoot a given target without hitting. People have investigated the distribution of leapovers  $p(l)$ , where the leapover  $l$  is defined as the length of overshooting to a given target, for Lévy flights in one-dimension. The leapover distribution scales as  $p(l) \sim l^{-\mu/2}$ , meaning that for  $1 < \mu < 2$  even if the average step length is finite, the average overshooting length could be diverging [16]. Nevertheless, the first passage time probability distribution of a Lévy flight in 1D scales as  $f(t) \sim t^{-3/2}$  independent of the value of  $\mu$ , which is a result of the Sparre-Andersen theorem. The Sparre-Andersen theorem states that for any symmetric step size distribution, the first passage probability distribution in 1D always has the same exponent as a Gaussian random walk. It is quite a powerful statement and we will invoke it later on in this chapter.

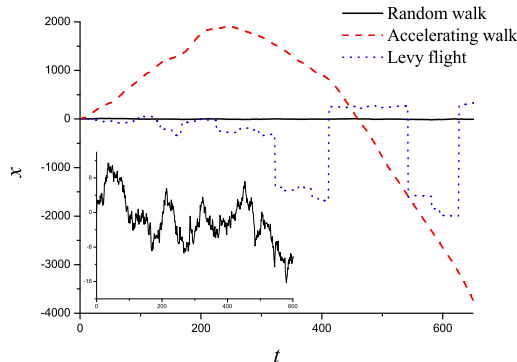


Figure 1.3: Realization of a one-dimensional Lévy flight (short-dashed blue) and the comparison with an ordinary random walk (black) and an accelerating random walk (long-dashed red). The inset is a blow-up of the ordinary random walk.

## 1.2 Inquiry

There have been generalizations of vicious walkers to dissimilar walkers [17], walkers with drift [18], and walkers with external potentials [19]. Here, we introduce a system of  $N$  accelerating vicious walkers and ask the question: What is the survival probability,  $s(t)$ , the probability for having none of the  $N$  accelerating walkers annihilated up to time  $t$  in the long-time limit?

In one-dimension, a randomly accelerating walker,  $x(t)$ , is defined by

$$\frac{d^2x(t)}{dt^2} = \eta(t), \quad (1.9)$$

where  $\eta(t)$  is Gaussian noise with  $\langle \eta(t) \rangle = 0$  and  $\langle \eta(t)\eta(t') \rangle = 2D\delta(t - t')$ . If we introduce the velocity variable  $v = dx/dt$ , the above equation of motion can be rewritten as

$$\begin{aligned} dv &= \sqrt{dt}M_t(0, 1) \\ dx &= vdt, \end{aligned} \quad (1.10)$$

where the right-hand-side of the equation for  $dv$  is the Markov propagator of a Wiener process as called in the mathematical literature with  $M_t(0, 1)$  denoting normal distributed number with mean zero and variance unity. A detailed explanation of this representation can be found in Ref.[20]. The basic idea is that even if  $\sqrt{dt}$  is larger than  $dt$  as  $dt \rightarrow 0$ , the fluctuation of a normal distributed number,  $M_t(0, 1)$  (also proportional to  $\sqrt{dt}$  as seen in ordinary diffusion), will regulate the right-hand-side of the equation of  $dv$  back to the order of  $dt$ .

To eventually arrive at the corresponding Fokker-Planck equation, for an arbitrary smooth function  $f(x, v)$ , one can compute the total derivative up to the order of  $dt$  as

$$\begin{aligned} df &= \frac{\partial f}{\partial x} dx + \frac{\partial f}{\partial v} dv + \frac{\partial^2 f}{\partial v^2} \frac{(dv)^2}{2} \\ df &= \frac{\partial f}{\partial x} v dt + \frac{\partial f}{\partial v} M_t(0, 1) \sqrt{dt} + \frac{\partial^2 f}{\partial v^2} \frac{dt}{2}. \end{aligned} \quad (1.11)$$

Also, given the probability density distribution,  $p(x, v, t)$ , one has the following identity

$$\int \int dx dv \frac{\partial p}{\partial t} f(x, v) = \left\langle \frac{df(x, v)}{dt} \right\rangle. \quad (1.12)$$

Now insert the total derivative for  $f(x, v)$  as derived in Eq.(1.11) (along with  $\langle M_t(0, 1) \rangle = 0$ ) to arrive at

$$\begin{aligned} \int \int dx dv \frac{\partial p}{\partial t} f(x, v) &= \left\langle v \frac{\partial f}{\partial x} + \frac{1}{2} \frac{\partial^2 f}{\partial v^2} \right\rangle \\ \int \int dx dv \frac{\partial p}{\partial t} f(x, v) &= \int \int dx dv \left( v \frac{\partial f}{\partial x} + \frac{1}{2} \frac{\partial^2 f}{\partial v^2} \right) p(x, v, t). \end{aligned} \quad (1.13)$$

Integrating the right-hand-side by parts and dropping surface terms will lead to

$$\int \int dx dv \frac{\partial p}{\partial t} f(x, v) = \int \int dx dv f(x, v) \left( -v \frac{\partial p}{\partial x} + \frac{1}{2} \frac{\partial^2 p}{\partial v^2} \right). \quad (1.14)$$

Since  $f(x, v)$  is arbitrary, the above equation yields the Fokker-Planck type equation we need

$$\frac{\partial}{\partial t} p(x, v, t) = \frac{1}{2} \frac{\partial^2}{\partial v^2} p(x, v, t) - v \frac{\partial}{\partial x} p(x, v, t), \quad (1.15)$$

where the prefactor  $1/2$  can be dropped via a rescaling of  $x$  and  $v$  such that the final version of the Fokker-Planck equation for a random acceleration process in one-dimension is

$$\left[ D \frac{\partial^2}{\partial v^2} - v \frac{\partial}{\partial x} \right] p(x, v, t) = \frac{\partial}{\partial t} p(x, v, t). \quad (1.16)$$

Note that the final result is a special case of the Kramers equation[21]. In Ref.[21] the general Fokker-Planck equation for Brownian motion in a potential is written as

$$\frac{\partial}{\partial t} p(x, v, t) = - \left( \frac{K(x)}{m} \frac{\partial}{\partial v} + v \frac{\partial}{\partial x} \right) p(x, v, t) + \frac{\zeta}{m} \frac{\partial}{\partial v} \left( \frac{k_B T}{m} \frac{\partial}{\partial v} + v \right) p(x, v, t), \quad (1.17)$$

where  $m$  is the mass of the Brownian particle,  $\zeta$  is the friction constant,  $k_B$  is the Boltzmann constant,  $T$  is the temperature, and  $K(x) = -\partial V(x)/\partial x$  is the external field of force associate with a given potential  $V(x)$ .

As one can see from the above equation (Eq. 1.16), a randomly accelerating walker is presumably the simplest non-Markovian stochastic process. Given the fermionic interaction between vicious accelerating walkers, one can explore the possibility of a non-Markovian analogue to the log-potential Coulomb gas and, hence, a potentially new class of non-Markovian random matrices [8, 9]. Recently, Fukushima and collaborators [22] have revisited Dyson's original Brownian motion model for random matrices [9] and found a non-Markovian stochastic process after generalizing the coefficients of the matrices. We anticipate further generalizations in the future.

In addition, a randomly accelerating walker appears in the Boltzmann weight of

an extensible, semiflexible polymer of length  $L$  with non-zero bending energy [23]. For a given displacement vector  $\vec{r}(z)$  from some reference point along a contour length,  $z$ , the Hamiltonian,  $H$ , is given by

$$H(\vec{r}(z), \vec{u}(z); z) = \frac{\kappa}{2} \int_0^L dz \left( \frac{d^2 \vec{r}(z)}{dz^2} \right)^2, \quad (1.18)$$

where  $\vec{u}(z)$  denotes the tangent vector and  $\kappa$  characterizes the bending rigidity. Mapping the contour length  $z$  to time  $t$  and the displacement vector  $\vec{r}$  to  $\vec{x}(t)$ , the equation of motion for this system corresponds to a randomly accelerating walker in the corresponding dimension. Implementing the vicious interaction between  $N$  random accelerating walkers, therefore, corresponds to the statistics of non-intersecting semiflexible polymer brushes [24].

### 1.3 $N \leq 3$ vicious accelerating walkers

We begin by considering  $N = 2$  vicious accelerating walkers in one-dimension with equal diffusion constants  $D_1 = D_2 = D$ . The two accelerating walkers are governed by the equation,

$$\begin{aligned} & D \left( \frac{\partial^2}{\partial v_1^2} + \frac{\partial^2}{\partial v_2^2} \right) p(x_1, x_2, v_1, v_2, t) \\ & - \left( v_1 \frac{\partial}{\partial x_1} + v_2 \frac{\partial}{\partial x_2} \right) p(x_1, x_2, v_1, v_2, t) = \\ & \frac{\partial}{\partial t} p(x_1, x_2, v_1, v_2, t) \end{aligned} \quad (1.19)$$

with the initial condition,  $p(x_1, x_2, v_1, v_2, t = 0) = \delta(x_1 - x_{1,i})\delta(x_2 - x_{2,i})\delta(v_1)\delta(v_2)$ , with  $x_{1,i} < x_{2,i}$ . In addition, to compute the survival probability,  $s(t)$ , we implement the boundary condition,

$$p(x_1 = x_2, v_1 > v_2, t) = 0 \quad (1.20)$$

such that the system “dies” when the two walkers meet in space and have ingoing velocities. Note that the boundary condition in  $v$  is redundant since, due to the initial positions, the two walkers cannot meet with a relative outgoing velocity.

We then choose the relative coordinate system to reduce the  $N = 2$  vicious accelerating walkers to one random accelerating walker in the presence of an absorbing wall. This change of variables takes the form,  $x = x_1 - x_2$  and  $v = v_1 - v_2$ . The Fokker-Planck equation thereby reduces to

$$\left[ 2D \frac{\partial^2}{\partial v^2} - v \frac{\partial}{\partial x} \right] p(x, v, t) = \frac{\partial}{\partial t} p(x, v, t), \quad (1.21)$$

with the boundary condition,  $p(x = 0, v > 0, t) = 0$ .

The survival probability for this process is nontrivial in that one cannot invoke the method of images as is done for the ordinary random walker. Using properties of the integral of a Brownian curve, Sinai [26] proved that the asymptotic survival probability distribution is given by

$$s(t) \sim t^{-1/4} \quad (1.22)$$

at long times. Note that the first-passage time distribution,  $f(t)$ , where the first passage time is defined by the time at which any of the two walkers meet is given by  $f(t) = -\frac{ds(t)}{dt}$  such that  $f(t) \sim t^{-5/4}$ . In general, if the survival probability distribution is given by  $s(t) \sim t^{-\alpha}$  at large times, then  $f(t) \sim t^{-\beta}$  with  $\beta = \alpha + 1$ .

A heuristic argument, based on Sinai’s approach, for  $\alpha = 1/4$  was given in Ref. [27]. First, a new time counter,  $M$ , is defined by each “original” time the velocity crosses zero. In other words, the original time is now defined by the distribution of first-passage time of a random walk undergoing a Lévy flight with Lévy index  $\mu = 1/2$ . Moreover, with this new counting, the position variable is also a Lévy flight with Lévy index  $\mu = 1/3$ . By invoking the powerful superuniversality

of the Sparre-Andersen theorem in one-dimension [28, 29, 30], the first passage time distribution for the position in terms of  $M$  is the same as for a random walk, i.e.  $M^{-3/2}$ . To convert back to the original time, one simply needs to compute the integral

$$f(t) \sim \int \frac{1}{M^{\frac{3}{2}}} \frac{M}{t^{\frac{3}{2}}} \exp(-t^2/M) dM, \quad (1.23)$$

where  $\frac{M}{t^{\frac{3}{2}}} \exp(-t^2/M)$  is the limiting distribution for the sum of  $M$   $\mu = 1/2$  Lévy variables. We should also mention that Burkhardt [23] made the use of Marshall-Watson functions [25] to solve for the Laplace transform version of Eq. 1.21 with the absorbing boundary condition.

To numerically check for  $\alpha = 1/4$  result (and other results), we implement the go-with-the winners algorithm [31]. We do this because as  $N$  increases, the first passage time exponent  $\beta$  increases, making it more difficult to sample the tail of the distribution. The go-with-the winners algorithm iterates replica systems in parallel. Once the number of surviving replicas fall below a preset fraction, those surviving replicas are copied over to the "dead" replicas so that the total number of running replicas remains a roughly same value. We choose that fraction to be one-half such that each copy generated carries a relative weight of  $1/2^c$ , where  $c$  is the number of copies, which is then incorporated into the survival probability. The number of replicas range between 1,000 and 10,000. The number of runs averaged over range between 10 and 40. Fluctuations between the runs are then used for error analysis.

Having calibrated our results for the  $N = 2$  case, we now consider  $N = 3$  vicious accelerating walkers with equal diffusion constants. The Fokker-Planck equation is given by

$$\sum_{j=1}^3 \left[ D \left( \frac{\partial^2}{\partial v_j^2} \right) - \left( v_j \frac{\partial}{\partial x_j} \right) \right] p(X, V, t) = \frac{\partial}{\partial t} p(X, V, t), \quad (1.24)$$



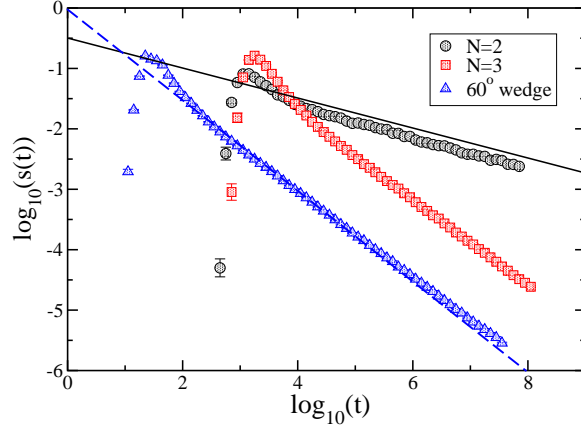


Figure 1.4: Log-log plot of survival probability distribution versus time for  $N = 2$  and  $N = 3$  vicious accelerating walkers in line and for a single accelerating walker in a  $\frac{\pi}{3}$  wedge geometry. The line denotes a survival probability exponent of  $1/4$ , while the dashed line denotes a survival probability exponent of  $3/4$ .

where  $X = \{x_1, x_2, x_3\}$ , and  $V = \{v_1, v_2, v_3\}$ .

We apply change of variables  $v = v_1 - v_2$ ,  $u = v_2 - v_3$ ,  $x = x_1 - x_2$ ,  $y = x_2 - x_3$  such that the LHS operator for two relative coordinates becomes

$$2D \left( \frac{\partial^2}{\partial v^2} + \frac{\partial^2}{\partial u^2} - \frac{\partial^2}{\partial v \partial u} \right) - \left( v \frac{\partial}{\partial x} + u \frac{\partial}{\partial y} \right) \quad (1.25)$$

with the absorbing boundary at  $x = 0$ ,  $y = 0$ ,  $u > 0$  and  $v > 0$ . Again, here, boundary conditions on the velocities are redundant. To remove the coupled term in  $u$  and  $v$ , we perform another set of linear transforms,  $u = \frac{l-q/\sqrt{3}}{2}$ ,  $v = \frac{-l-q/\sqrt{3}}{2}$ ,  $x = \frac{-z-w/\sqrt{3}}{2}$ , and  $y = \frac{z-w/\sqrt{3}}{2}$  to obtain

$$6D \left( \frac{\partial^2}{\partial q^2} + \frac{\partial^2}{\partial l^2} \right) - \left( q \frac{\partial}{\partial w} + l \frac{\partial}{\partial z} \right) \quad (1.26)$$

with absorbing boundaries,  $z = \pm w/\sqrt{3}$ , i.e. a  $\frac{\pi}{3}$  wedge in the  $z - w$  plane.

We have reduced three vicious accelerating walkers in one-dimension to one accelerating walker in two-dimensions in a wedge geometry. While there is currently no analytical solution for the survival probability distribution for an accelerating

walker in a  $\frac{\pi}{3}$  wedge geometry, for a  $\frac{\pi}{2}$  wedge, the Sparre-Andersen theorem can be invoked for the two independent directions to arrive at an asymptotic power-law survival probability distribution with  $\alpha = \frac{1}{2}$ . In addition, for a  $\pi$  wedge,  $\alpha = \frac{1}{4}$ . While the Sparre-Andersen theorem is quite powerful and can easily be extended to as many independent dimensions as needed, the  $\frac{\pi}{3}$  wedge geometry couples the two directions (for  $N = 3$ , at least) and, therefore, the Sparre-Andersen theorem, as it stands, cannot be invoked.

However, to smoothly interpolate between the  $\frac{\pi}{2}$  and  $\pi$  cases, we conjecture that for other wedge angles, the survival probability distribution also asymptotes to a power-law with survival probability exponent,  $\alpha$ , with  $\alpha$  decreasing continuously as the wedge angle increases. To test this conjecture, we resort to numerical simulation of both the wedge geometry for one accelerating walker and the line geometry for three accelerating walkers. The result is presented in Fig. 1.4. We measure a survival probability exponent of  $\alpha = 0.71 \pm 0.01$  for  $N = 3$  vicious accelerating walkers in a line, which agrees with the  $\frac{\pi}{3}$  wedge geometry result (with essentially the same error bar). Also, referring back to the accelerating walker-Lévy flight mapping implemented to demonstrate the  $\alpha = \frac{1}{4}$  exponent for an absorbing accelerating walker in one-dimension, simulating a  $\mu = 1/3$  Lévy flight in a  $\frac{\pi}{3}$  wedge geometry with the opening angle,  $\theta$ , between 0 and  $\frac{\pi}{3}$ , yields  $\alpha = 0.71 \pm 0.03$ .

Figure 1.5 tests our conjecture that  $\alpha$  continuously decreases with increasing wedge angle. Both the numerical values of  $\alpha$  for the  $\frac{\pi}{2}$  and  $\pi$  wedges agree well with their analytical counterparts. For comparison purposes, we have also plotted the curve  $\alpha = \pi/4\theta$ , which agrees with the two analytical solutions and can be viewed as a trivial extension of the random walker solution. While the agreement looks reasonable at larger angles, the deviation becomes more apparent at smaller angles. It also appears that the divergence in  $\alpha$  as  $\theta$  decreases to zero is slower

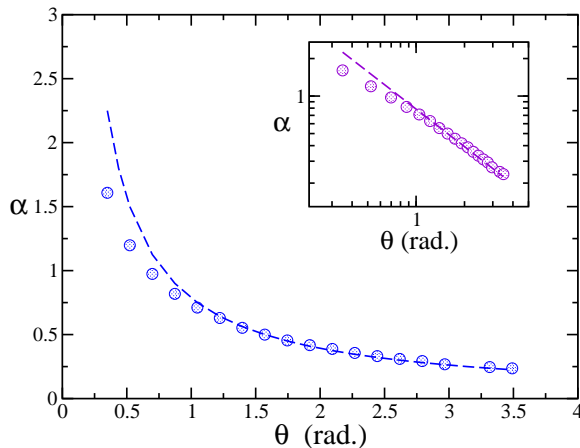


Figure 1.5: Survival probability exponent for a two dimensional accelerating walker in a wedge geometry as a function of the opening angle. The line denotes  $\alpha = \frac{\pi}{4\theta}$ . Inset: Log-log plot to emphasize the difference between the data and  $\alpha = \frac{\pi}{4\theta}$ . The error bars are smaller than the symbols.

than  $1/\theta$ .

In the interest of studying a mixture of flexible and semiflexible polymer brushes, one can study a mixture of vicious accelerating and random walkers. Consider a mixture of vicious accelerating and random walkers—an example of a vicious walkers system with dissimilar members. For one random walker and one random accelerator, the random walker can be approximated as an absorbing boundary at rest since the displacement of a random walker scales as  $x(t) \sim t^{1/2}$ , while for a random accelerating walker, the velocity scales as  $v(t) \sim t^{1/2}$  such that the displacement scales as  $x(t) \sim t^{3/2}$ . Thus, in long time limit, the displacement of a normal random walker is negligible compared with that of a random accelerator. In other words, one can simply take the normal random walker as a fixed absorbing wall to fulfill the vicious mechanism. Simulations of one random walker and one accelerating walker that annihilate upon crossing verify this.

Now to address the  $N = 3$  mixed case. We use the "A" to denote an accelerating walker and "R" to denote a normal one in the present discussion. The two pure states "RRR" and "AAA" are trivial with the former following Fisher's

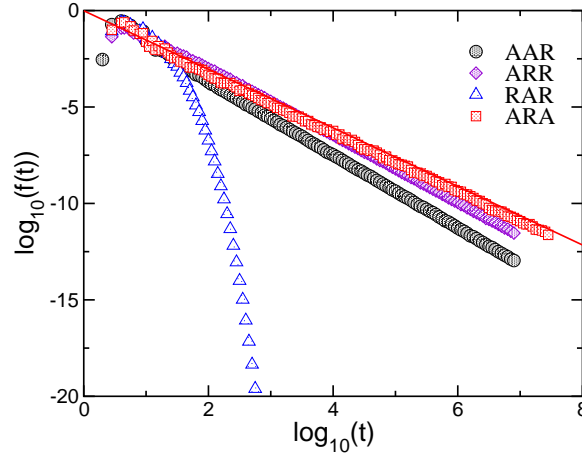


Figure 1.6: Log-log plot of the survival probability distribution for the  $N = 3$  mixed cases of vicious accelerating walkers (A) and vicious random walkers (R). The line denotes a first passage time probability exponent of  $\beta = \frac{3}{2}$ .

general solution and latter demonstrated by our numerical simulation described earlier in the paper. The combination with two normal walkers and one accelerator can have two forms, namely "RRA" and "RAR". The former can be treated as one absorbing random walker and one absorbing accelerating acting independently such that  $\alpha = 3/4$ . The latter is an accelerating walker sandwiched between two random walkers, i.e. a bounded domain, and hence the survival probability decays instead exponentially in time. A detailed analysis can be found in Ref.[33]. Simulations support both results. See Figure 1.6. For "ARA", there is an absorbing wall in between two accelerating walkers, i.e. a pair of decoupled accelerator-wall systems, hence  $\alpha = 1/2$ . The last possible configuration, "AAR", is nontrivial in that it can be reduced to one accelerating walker in a  $\frac{\pi}{4}$  wedge geometry, just as two vicious random walkers in the presence of an absorbing wall can be mapped to one random walker in a  $\frac{\pi}{4}$  wedge geometry. We measure a nontrivial survival probability exponent of  $\alpha = 0.89 \pm 0.01$  for this case, which is consistent with our wedge measurements.

## 1.4 $N > 3$ vicious accelerating walkers

Now, we numerically address  $N > 3$  vicious accelerating walkers. To compare with ordinary vicious walkers, based on the method of images, Fisher [5, 7] considered one compound walker in  $N$  dimensions that cannot cross any of the  $x_1 = x_2, x_2 = x_3, \dots$ , or  $x_{N-1} = x_N$  linear manifolds. Using the method of images, as long as the initial positive and negative weights (corresponding to unrestricted positive and negative walkers) are chosen such that probability distribution is antisymmetric under reflection within each linear manifold, then the distribution will satisfy the absorbing boundary conditions for all future times. These weights can be represented as a Vandermonde determinant, which can be factorized to yield a product of  $\frac{1}{2}N(N-1)$  pairings such that  $\alpha(N) = N(N-1)/4$ , where  $\alpha(2) = 1/2$ . Previous and the current simulations verify this prediction. See Figure 1.7. By the same argument, if the survival exponent for two (one pair of) vicious accelerating walkers is  $1/4$ , the survival exponent for  $N$  vicious accelerating walkers system should be  $N(N-1)/8$ . However, for vicious accelerating walkers, the method of images fails.

Based on the  $N = 2$  and  $N = 3$  results, combined with the fact that  $N$  vicious accelerating walkers can be mapped to one accelerating walker in  $N - 1$  dimensions in an unbounded domain, we expect the power-law survival probability distribution extends to  $N > 3$ . In Figure 1.7 we present the simulation results of survival probability exponents for vicious accelerating walkers system up to  $N = 10$ , as well as the too trivial prediction,  $\alpha = N(N-1)/8$ . The deviation is apparent at large  $N$ . We find that  $N(N-1)/8$  is clearly an upper bound for the measured  $N$ . The non-Markovian nature of the accelerating walker enables the system to survive longer and in a way that cannot be accounted for by individual pairings.

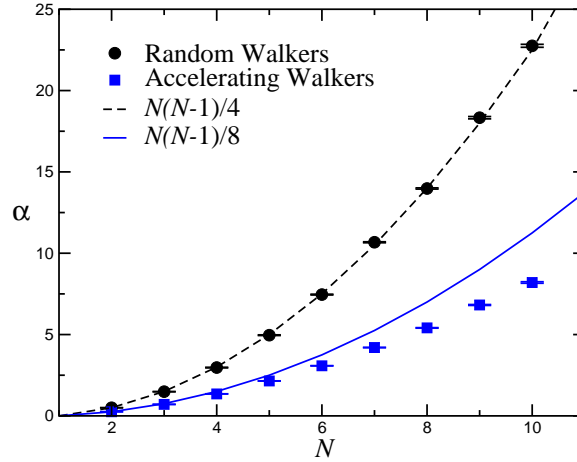


Figure 1.7: Survival probability exponent  $\alpha$  for vicious accelerating walkers (solid squares) and vicious Gaussian walkers (solid circles) systems up to  $N = 10$ . The simulation results for vicious Gaussian walkers agree very well with theory prediction  $\alpha = N(N - 1)/4$  (black curve). However, the results for vicious accelerating walkers deviate from a method of images prediction of  $\alpha = N(N - 1)/8$  (blue dashed curve).

## 1.5 Vicious Lévy flights

As mentioned previously, vicious Gaussian walkers problem is closely related to the Gaussian random matrix theory. A matrix with random entries falls into this category as long as the entries are independent and identically distributed (iid) variables with a finite second moment of the corresponding distribution. A generalization of the random Gaussian matrix is the random Lévy matrix [34], where the entries are drawn from a broader distribution, namely a Lévy distribution. The most important characteristic of Lévy distribution is a heavy power-law tail step-size  $S$  distribution,  $P(S) \sim S^{-1-\mu}$  for large  $S$ . When  $\mu \geq 2$ , the variance of the distribution is finite and, hence, the central limit theorem holds for the distribution of the sum of independently drawn Lévy variables. Similarly, the random Lévy matrices reduce to random Gaussian matrices. However in the regime  $\mu < 2$ , the variance of the distribution diverges and hence random Lévy matrices behave qualitatively different from random Gaussian matrices. For example, the famous

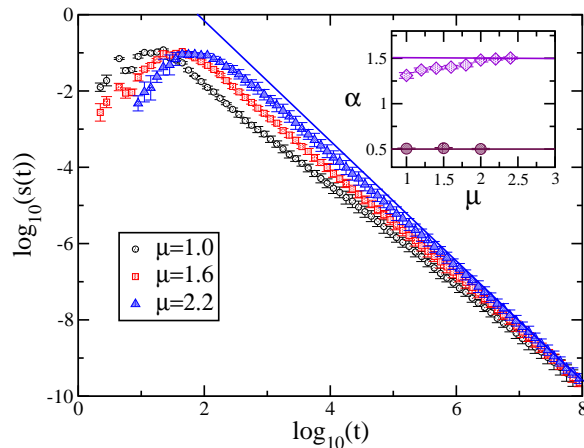


Figure 1.8: Log-log plot of the survival probability distribution for  $N = 3$  vicious Lévy flights for different values of the Lévy index,  $\mu$ . The curve denotes a survival probability exponent of  $\alpha = \frac{3}{2}$ . Inset: The survival probability exponent for  $N = 2$  and  $N = 3$  vicious Lévy flights as a function of the Lévy index. For  $\mu > 2$ , we obtain the vicious random walker results.

Wigner-Dyson semicircular law is replaced with a density of states that extends over the entire eigenvalue axis [34].

Inspired by the connection between vicious Gaussian walkers and random Gaussian matrices as well as the connection between Lévy flights and random accelerating walkers, we study the problem of vicious Lévy flights. Given  $N$  Lévy flights in one-dimension, we define the vicious interaction between pairs. Because Lévy flights are nonlocal, two Lévy flights jump over each other without meeting at some exact point. Hence, there could be two ways to define the vicious interaction, to prohibit the jump-overs or to allow for jump-overs and the annihilation occurs upon intersection within some range, irrespective of the ordering. The latter has been recently studied [35]. However, we are more interested in the former case, in which the set of Lévy flights annihilate whenever a crossing occurs. In other words, a surviving system strictly maintains the initial ordering of all flights, which is the same as for the vicious Gaussian walkers.

The Fokker-Planck equation for a system of  $N$  one-dimensional vicious Lévy

flights is described as

$$\sum_{j=1}^N \frac{\partial^\mu}{\partial |x_j|^\mu} p(X, t) = \frac{\partial}{\partial t} p(X, t), \quad (1.27)$$

where the normal Laplacian is replaced by the Riesz-Feller derivative of fractional order  $2 > \mu > 0$  [36, 37]. This derivative has an integral representation, which more easily reveals its nonlocal nature, or

$$\frac{d^\alpha}{d|x|^\alpha} f(x) = -\frac{1}{2 \cos((m-a)\pi/2)} (D_+^\alpha - D_-^\alpha), \quad (1.28)$$

where

$$\begin{aligned} D_+^\alpha &= \frac{1}{\Gamma(\alpha)} \int_a^x dy (x-y)^{m-\alpha-1} f^{(m)}(y) \\ D_-^\alpha &= \frac{1}{\Gamma(\alpha)} \int_x^b dy (y-x)^{m-\alpha-1} f^{(m)}(y), \end{aligned} \quad (1.29)$$

with  $\alpha \in (m-1, m)$ ,  $m$  integer, and  $x \in \Omega = [a, b]$  [36]. The initial condition is still  $p(X, t=0) = \prod_{j=1}^N \delta(x - x_{j,i})$ , with  $x_{j,i} < x_{k,i}$  for all  $j < k$ . The boundary condition for the non-crossing vicious interaction as we described above is then  $p(x_j, t) = 0$ , if  $x_j \geq x_k$  for any  $j < k$ .

The  $N = 2$  case is, again, equivalent to the first-passage problem of a single Lévy flight via a transformation to relative coordinates (and integrating out the center of mass coordinate). The only difference with a random walker is that the absorbing boundary condition at the origin has to be modified to an absorbing region occupying the positive x-axis to preserve the non-crossing property. The first-passage property of a Lévy flight is governed by the Sparre-Andersen theorem [28, 29, 30], which implies that the first-passage time distribution for any symmetric step size distribution in one-dimension asymptotes to the same as that of a Gaussian walker. Thus, the survival probability exponent for  $N = 2$  is  $\alpha = 1/2$



independent of  $\mu$ . We verify this result in our simulation. See Figure 1.8. Note that this result is very different from the result obtained in Ref. [35] where  $\alpha$  depends on  $\mu$  for  $N = 2$  and higher.

We also simulate  $N = 3$  vicious Lévy flights. Because of the linearity of fractional derivatives, the mapping of two vicious Lévy flights to a single Lévy flights in an absorbing plane holds. However, due to the lack of rotational invariance of the Riesz-Feller derivative, the wedge mapping that holds for vicious walkers and now for vicious accelerating walkers, does not apply to vicious Lévy flights. In order to make progress, since for  $N = 2$  there exists a power-law distribution, we conjecture that the survival probability distribution scales as a power-law at long times for  $N > 2$  and measure  $\alpha$ . Figure 1.8 plots the survival probability exponents for  $N = 3$  vicious Lévy flights for several different Lévy indices. For  $N = 2$  all values of  $\mu$  yield the same survival probability exponent of  $1/2$ , in agreement with the Sparre-Andersen theorem. However, the  $N = 3$  exponents appear to vary with  $\mu$ . For instance, for  $\mu = 1$ ,  $\alpha = 1.31 \pm 0.03$ . While the 0.19 difference between  $\mu = 1.0$  and  $\mu = 2$  is small, the difference grows with  $N$ . For example, for  $N = 4$  and  $\mu = 1$ ,  $\alpha = 2.3 \pm 0.1$  and for  $\mu = 2$ ,  $\alpha = 2.91 \pm 0.09$ . Based on this data, we speculate that for  $N > 2$ ,  $\alpha$  depends on  $\mu$ .

A few comments on the technical aspects of the simulations are in order. We implement an upper cut-off on the Lévy steps so that at long enough times, the survival probability distribution approaches the random walker result [38]. The convergence also depends on the Lévy index. For example, for  $\mu = 1$  and stepsize cut-off  $S_c = 10 - 100$ , the convergence to the random walker result is fast such that the asymptote to a power-law beyond  $t \approx 10^2$  is in agreement with the random walker result to within one standard deviation. In contrast for  $\mu = 1.6$ ,  $S_c = 10^9$ , and time scales beyond  $t \approx 10^8$ , convergence to the random walker result is observed. Secondly, for  $\mu = 1$  we also generated Cauchy distributed numbers

directly and found good agreement with the power-law generated  $\mu = 1$  result.

## 1.6 Discussion

To summarize, we have generalized the vicious walker problem in two different ways: (1) vicious accelerating walkers and (2) vicious Lévy flights as defined by non-crossing. For both generalizations, the typical analytical technique of the method of images fails. Analytical results for  $N = 2$  are readily obtainable since both problems can be mapped to the first passage problem of a single accelerating walker or Lévy flight with the appropriate absorbing boundary or region. We demonstrate that the  $N$  vicious walker mapping to one walker in  $N - 1$  dimensions in a wedge geometry generalizes to vicious accelerating walkers. We also conjecture, based on our numerical data, that there exists an upper bound on the survival probability exponent of  $\alpha = \frac{1}{8}N(N - 1)$  for  $N$  vicious accelerating walkers. An analytical calculation for the  $N = 3$  case corresponding to one accelerating walker in a two-dimensional wedge geometry would be the next logical step. The heuristic argument for the absorbing accelerating walker in one-dimension using a new time counter and Lévy flights may eventually become useful for analyzing the two-dimensional wedge problem. However, the non-locality of the Riesz-Feller derivative makes the inclusion of boundary conditions rather difficult. There also exists a recent numerical result for the survival probability distribution for the two-dimensional Fractional Brownian motion process, originally introduced by Kolmogorov [39], in a wedge [40]. We anticipate more study of non-Markovian processes in dimensions higher than unity in the near future. Indeed, a non-Markovian extension of Dyson's Brownian motion model to, for example, include inertia, may be related to  $N$  vicious accelerating walkers to arrive at a new class of random matrices. It may also be interesting to investigate other ordering prob-

lems of randomly accelerating walkers on a line such as the Gaussian equivalent of the "leader" and the "laggard" problem [41].

Finally, given our numerical results, we speculate that the survival probability exponent for  $N$  vicious Lévy flights (as defined by no-crossing) depends on  $\mu$  for fixed  $N > 2$ . We also refer to a new result where vicious Lévy flights are defined as annihilating when any two Lévy flights come within some range of each other and  $\alpha$  depends on  $\mu$  even for  $N = 2$  [35]. While the survival probability exponent in one-dimension is independent of the Lévy index, as a consequence of the powerful Sparre-Andersen theorem, we anticipate that this superuniversality may be broken in dimensions higher than unity and the universality of each Lévy index becomes exposed. In light of our results, a higher dimensional generalization (or modification) of the Sparre-Andersen theorem should be on the forefront of at least several statistical physicists and mathematicians minds.

# Chapter 2

## Particle-conserving interacting stochastic processes in crowded environments

### 2.1 Background

#### 2.1.1 Directed percolation

Consider making coffee. To make coffee, water passes through coffee grinds absorbing the grind's chemical compounds that give coffee its taste, color, and smell. If the coffee grinds are compacted so tightly, then water cannot pass through them anymore. To understand this clogging transition, one can model the coffee grinds as a lattice with randomly-diluted bonds. The probability of a bond to be open is denoted as  $p$  and so clogged is  $1 - p$ . Two limiting cases are,  $p = 0$  where no water can flow across the lattice, and  $p = 1$  where the lattice is fully connected and water easily flows. In other words, there are two phases: the non-percolating (clogged)

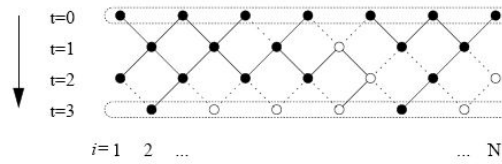


Figure 2.1: Directed percolation as an interacting stochastic process. The filled (hollow) circles denote active (inactive) sites.

phase and the percolating (flowing) phase. There exists a critical threshold value of  $p_c$  below which the system becomes clogged [42]. This transition is purely a geometric process and the value of  $p_c$  depends on the structure of the underlying lattice.

Coffee percolating is a particularly interesting example since it demonstrates a special case of percolation that is directed. Due to gravity, the liquid (water) only flows downward through the coffee grinds, but not upward. The directed percolation transition is quantitatively different from isotropic case. Directed percolation is important because it potentially explains a wide range of non-equilibrium phase transitions as explained below.

Let us return to the main theme of interacting stochastic processes. Even though percolation and directed percolation are both determined by geometry, they can be interpreted as stochastic processes [43]. Sites on the lattice with water are denoted as active ( $A$ ) and sites without water are labeled inactive ( $\emptyset$ ). The percolation process then contains the following possible dynamics. An active site may continue to transfer water via open channels (occupied bonds on the lattice). For a directed percolation on an oriented square lattice, the number of possible out-channels (lower bonds) is 2 for every site and the number of possible in-channels (upper bonds) is also 2. If no out-channel bonds are occupied, the active site ends its trip and turns inactive ( $A \rightarrow \emptyset$ ). If both lower bonds are occupied, the water will continue to flow through both channels and generate 2

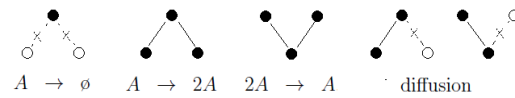


Figure 2.2: Pictorial representation of diffusion and reaction processes in directed percolation.

new active sites ( $A \rightarrow 2A$ ). If only one out-channel is available (one lower bond is occupied), water will continue to flow and possibly diffuse from side to side. Plus, if a site gets water from both of 2 in-channels, those 2 in-channels can generate only 1 new active site ( $2A \rightarrow A$ ). In summary, the directed percolation process can be interpreted as a combination of diffusion and three possible reaction processes



See Figs. 2.1 and 2.2 for a pictorial representation of the above discussion.

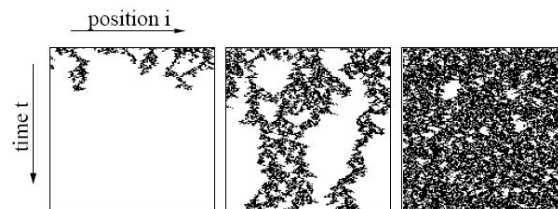


Figure 2.3: Directed percolation realizations below, at, and above the transition.

As mentioned previously, directed percolation has two possible steady state

phases, an active phase (a finite fraction of active sites survive and so the system flows) and an inactive phase (all sites are inactive and the system is clogged). See Fig. 2.3. Therefore, the order parameter is chosen to be the fraction of active sites  $\rho_A$ . The inactive phase is an absorbing state because the system cannot spontaneously generate active sites and, thus, possibly leave the inactive state. The absorbing state phase transition does not thus obey detailed balance and it is a non-equilibrium phase transition. Similar to continuous equilibrium phase transitions, absorbing state phase transitions can be characterized by scaling exponents and then grouped into universality classes. Close to, but above, the transition into the active phase, the order parameter should scale as a power-law with the distance from transition, i.e.,

$$\rho_A \sim (p - p_c)^\beta, \quad (2.2)$$

where  $\beta$  is the order parameter exponent. In addition, the correlation time  $\xi_{\parallel}$  and length  $\xi_{\perp}$  both diverge approaching transition but with different exponents, or

$$\xi_{\parallel} \sim (p - p_c)^{-\nu_{\parallel}} \quad (2.3)$$

$$\xi_{\perp} \sim (p - p_c)^{-\nu_{\perp}}. \quad (2.4)$$

The time evolution is also important in these stochastic processes. In particular, the order parameter  $\rho_A$  at the transition scales as a power-law in time, or

$$\rho_A \sim t^{-\theta}, \quad (2.5)$$

and the correlation length grows as

$$\xi_{\perp} \sim t^{1/z}, \quad (2.6)$$

where the exponents have scaling relations,  $\theta = \beta/\nu_{\parallel}$  and  $z = \nu_{\parallel}/\nu_{\perp}$ . In a finite system of linear length  $L$ , since the correlation length cannot exceed  $L$ , the time,  $t$ , it takes to reach the absorbing state at the transition is proportional to  $L^z$ . These exponents are all accessible via numerical simulation. For directed percolation on a square lattice,  $\beta = 0.58$ ,  $\nu_{\parallel} = 1.30$ , and  $\nu_{\perp} = 0.73$  [43].

If we introduce a set of interaction rates for the reaction processes used to describe directed percolation, namely the removal process  $A \rightarrow \emptyset$  with rate  $k_1$ , the offspring process  $A \rightarrow 2A$  with rate  $k_2$ , and the coalescence process  $2A \rightarrow A$  with rate  $k_3$ , it is possible to set up a mean-field dynamical equation for the order parameter,  $\rho_A$  [43]. The equation is

$$\frac{\partial \rho_A}{\partial t} = -k_1 \rho_A + k_2 \rho_A - k_3 \rho_A^2. \quad (2.7)$$

We can look for a steady-state solution to the dynamical equation above. Set the left hand of the equation to zero and we have

$$0 = ((k_2 - k_1) - k_3 \rho_A) \rho_A. \quad (2.8)$$

The solution  $\rho_A = 0$  corresponds to the absorbing state when no active sites survive. But, as we can see, there is another possible non-zero solution,  $\rho_A = (k_2 - k_1)/k_3$  (if  $k_2 \neq k_1$ ). This non-zero steady-state value of  $\rho_A$  corresponds to the active state. Since all  $k_i$ 's must be positive and so is  $\rho_A$ , the transition occurs at  $k_2 = k_1$ . For  $k_2 < k_1$ , the active state solution is negative and hence non-physical. The only physical solution is the absorbing one. For  $k_2 > k_1$ , the active solution is physical, and from  $\rho_A \sim (k_2 - k_1)$  we observe that the mean-field order parameter exponent  $\beta = 1$ . At the critical point  $k_2 = k_1$ , the solution to the dynamical equation is  $\rho_A(t) \sim 1/k_3 t$ , and we get the mean-field scaling exponent  $\theta = 1$ .



A Langevin-type field-theoretic approach for directed percolation can be set up using the above dynamic equation [43]. We have to include the diffusion term for active sites as well as an appropriate noise term. The Langevin equation is then

$$\frac{\partial}{\partial t}\rho_A(\vec{r}, t) = D\nabla^2\rho_A(\vec{r}, t) + (k_2 - k_1)\rho_A(\vec{r}, t) - k_3\rho_A^2(\vec{r}, t) + \eta(\vec{r}, t), \quad (2.9)$$

where  $\eta(\vec{r}, t)$  is the usual multiplicative Gaussian noise field satisfying the correlations,

$$\begin{aligned} \langle \eta(\vec{r}, t) \rangle &= 0 \\ \langle \eta(\vec{r}, t)\eta(\vec{r}', t') \rangle &= \kappa\rho_A(\vec{r}, t)\delta(t - t')\delta(\vec{r} - \vec{r}'), \end{aligned} \quad (2.10)$$

where  $\kappa$  is the amplitude of the noise. The right-hand side of the second equation is proportional to  $\rho_A(\vec{r}, t)$  so that there is no fluctuation in the absorbing  $\rho_A(\vec{r}, t) = 0$  phase to ensure that the system cannot escape to an active phase. The upper critical dimension of the field theory is  $d_c = 4$ , above which the mean-field results should hold, while below the critical dimension fluctuations become relevant.

It is worth mentioning that the universality class of directed percolation is very robust. In other words, a wide range of stochastic processes combining diffusion and reactions similar to the dynamical rules explained above fall into the same universality class (yielding the same set of scaling exponents). To be more specific, an interacting stochastic process belongs to the directed percolation universality class if it satisfies the famous Janssen-Grassberger conditions [44],

1. The model exhibits a continuous transition from a fluctuating active phase to a unique absorbing phase,
2. The model is characterized by a non-negative, one-component order parameter,

3. The model has only short-ranged dynamic rules,
4. There is no additional symmetry such as conservation laws or quenched disorder in the system.

### **2.1.2 Conserved directed percolation**

According to the above Janssen-Grassberger criteria [44], one can construct a model that does not fall into the directed percolation universality class by introducing additional symmetries. A conservation law in the total number of particles would do the trick, thereby yielding a new universality class of conserved directed percolation. Models that belong to this universality class include the Manna model [45], the conserved lattice gas model [46], and the particle-conserving interacting stochastic process that we will discuss in detail [47].

### **2.1.3 Caging and kinetically constrained models of the glass transition**

Let us now discuss a seemingly unrelated topic, namely the glass transition. The glass transition is presumably related to a wider set of phenomena collectively termed, dynamical arrest, or the process by which many particles in a liquid dramatically slow down in a concerted manner. One interpretation is as follows: for simple repulsive interactions, with increasing density, the progress loss of space around a typical particles leads it to become effectively trapped by its neighbors. This phenomenon is often dubbed caging. Occasionally, the particle can escape from the cage and make larger movements before becoming trapped in another cage. Caging has been observed in experiments near the colloidal glass transition where directly imaged poly-(methylmethacrylate) particles in solution at a packing fraction of 0.56 spent most of the time in their cages and only made significant

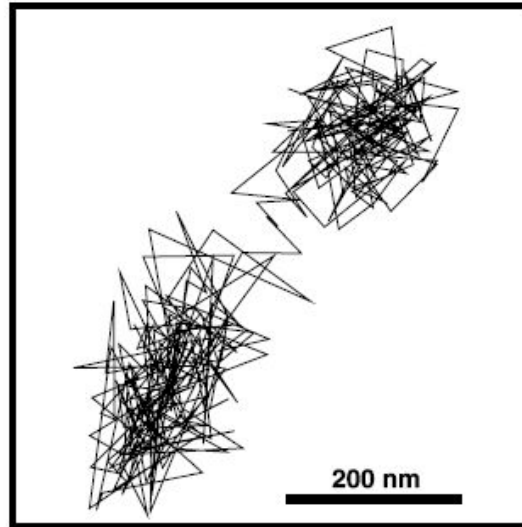


Figure 2.4: Map of a typical trajectory of a particle in solution at packing fraction,  $\phi = 0.56$ . The trajectory is imaged over 100 minutes and it took the particle approximately 500 seconds to go from one cage to the other. Adapted from Ref. [48].

displacements during quick cage rearrangements [48]. See Fig. 2.4.

Kinetically constrained models, such as the one introduced by Kob and Andersen, represent the intra-cage behavior of glassy systems on a lattice to presumably produce blocked, nonergodic states [49]. The Kob-Andersen model is defined simply by rendering a particle mobile if the number of occupied neighbors is equal to or less than some number  $m$  before and after the hop to a neighboring empty site. We say empty site because there is no multiple occupancy on any site. Numerical simulations for  $m = 3$  on the cubic lattice initially indicated that there was a dynamical phase transition from particles being able to diffuse on the lattice to a spanning cluster of caged (stuck) particles as the density increased. This transition presumably occurred at a density of around 0.88. However, it was later proven that in the infinite system limit, the transition occurs only in fully occupied lattices, i.e. no transition at a finite fraction of occupation [50]. Another kinetically constrained model, the Frederick-Andersen model also does not exhibit a dynamical

transition [51]. These results have been somewhat discouraging for such models. It would be interesting to find an example of a kinetically-constrained model that indeed yielded a dynamical phase transition from an ergodic to a nonergodic state space, if you will.

## 2.2 Inquiry

A recent experiment of colloidal suspensions under shear at low Reynolds number [6] can be viewed as a realization of an interacting stochastic process in a colloidal system. Plastic beads are suspended in a very viscous fluid and the system is periodically sheared in a Couette geometry. The viscosity of the fluid is about 3000 times that of water and makes the dynamics of the beads over-damped (inertialess). Upon one cycle of shearing, some particles become displaced and may collide with others. If no collision happens, the particle will arrive back at its original place after a full shear cycle. Any collision will displace the participating colloids and may trigger an avalanche of collisions. After a number of shearing cycles, the system either organizes itself into a state where every particle will not meet others upon shearing, or that collisions are unavoidable, depending on the strain amplitude. See Fig. 2.5 for a two-dimensional schematic of the three-dimensional experiment.

It has been argued that the dynamics of periodically sheared colloids in suspension can be modeled as an absorbing state phase transition. The particles displaced from their initial positions during shearing will either relax into the highly viscous fluid (become inactive) or turn other inactive particles into active particles via collisions. As the strain amplitude is increased, the system goes from an inactive phase to an active phase with some fraction of particles getting always displaced from their initial positions during a shear cycle. See Fig. 2.6. It

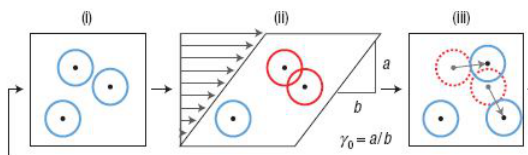


Figure 2.5: A two-dimensional schematic of the three-dimensional experiment presented in Ref. [6]. The red circles denote active particles and the blue denote inactive ones.

is thought that this dynamical phase transition resembles the conserved directed percolation universality class.

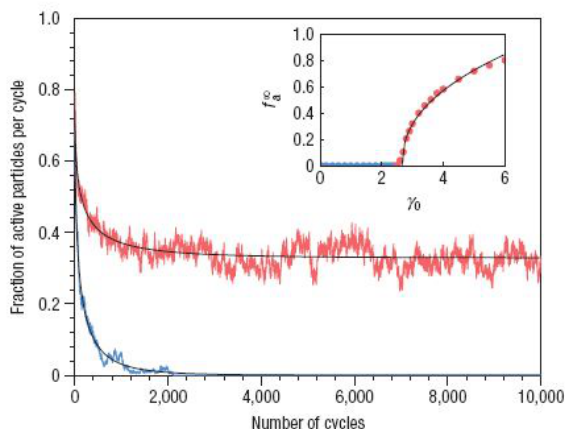


Figure 2.6: Plot of the fraction of active particles as a function of time for two different strain amplitudes. Adapted from Ref. [6].

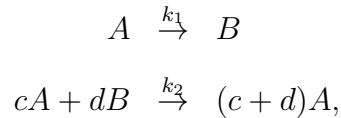
Now, this experiment was conducted at low packing fraction such that most collisions are presumably two-body collisions. We pose the following question: What happens to the dynamics of the colloids as the packing fraction is increased? What happens when the packing fraction is increased towards the colloidal glass transition? Increasing the packing fraction increases the possibility of three or more particle collisions, thereby justifying the study of higher-order contact processes. Of course, from a renormalization group perspective, higher-order interactions are less relevant and so one may not expect the scaling near the absorbing state phase

transition to differ from the lowest-order interaction case unless the rate of two-body collisions was tuned to zero. While this may be difficult in an experiment, it is not the case for simulations.

In addition to studying the role of higher-order interactions on the absorbing state phase transition, we study the effect higher density has on the diffusion of the active particles. If the active particles are prevented from diffusing due to surrounding particles via caging then the active particles are rendered inactive. In the highly dense limit, the system will ultimately become inactive due to this additional deactivation rate. We will study the properties of this presumably new absorbing state phase transition.

## 2.3 The model

Consider a lattice model with two types of particles—particle type A to denote the active members and particle type B for inactive ones. The inactive particles are “inactive” because they do not diffuse, while the active particles diffuse. Moreover, the particles obey an excluded volume rule implemented on the lattice by not allowing more than one particle per lattice site. We consider the following transformation rules:



where  $k_1$  denotes the inactivation rate and  $k_2$  denotes activation rate. Note that these rules conserve particle number no matter which order of interaction (values of  $c$  and  $d$ ) is present. We will also consider a nearest neighbor density-dependent inactivation rate, i.e. the caging effect, where the inactivation rate is unity (in time units of the simulation) if an active particle is fully surrounded by either

active or inactive particles (the local total density). In other words, the active particle has no empty neighboring site to diffuse to and so becomes inactive.

In the absence of the caging effect, if we consider the dynamics of the individual particles to be diffusive (as is usually done), the dynamical equations for the space-time density of active particles,  $\rho_A$ , and inactive particles,  $\rho_B$ , are

$$\begin{aligned}\frac{d\rho_A}{dt} &= D_A \nabla^2 \rho_A - k_1 \rho_A + k_2 d \rho_A^c \rho_B^d \\ \frac{d\rho_B}{dt} &= D_B \nabla^2 \rho_B + k_1 \rho_A - k_2 d \rho_A^c \rho_B^d,\end{aligned}\tag{2.11}$$

where we have included a diffusion term for the A particles with a diffusion constant  $D_A$  and a diffusion constant  $D_B$  for the inactive particles.

To date, there has been no field theory analysis of the above problem even in the absence of excluded volume and a constant diffusion constant. However, if one allows for the inactive particles to diffuse (and both diffusion constants are indeed constant), for the lowest-order interaction ( $c = d = 1$ ) there exists analytical (renormalization group) analysis [52]. It turns out that the ratio  $D_A/D_B$  affects the phase diagram. In particular, in the regime of  $D_A/D_B \geq 1$  (active particles diffuse faster or at least as fast) and the absorbing phase transition is second-order, while the regime of  $D_A/D_B < 1$  remains unsolved with the possibility of a first-order transition. In social networks, it is reasonable to consider two different diffusion constants. For example, infected people may have lower mobility than healthy people. However, in Brownian particle systems, the diffusion constant is inversely proportional to the radius of the particle, therefore, particles of the same size have the same diffusion constant. In the experiment above, the suspension prevents the particles from diffusing individually. Only colliding particles diffuse via the random nature of their collisions. Therefore, the inactive particles (non-colliding particles) do not diffuse,  $D_B = 0$ . As pointed out in Ref. [47], the limit

of  $D_B \rightarrow 0$  in the field theory is non-analytic, hence we expect a different critical behavior in this driven colloidal system.

## 2.4 Mean field analysis

We first analyze the mean field limit of the model (in the absence of caging). Mean field theory is simple and sheds light on the nature of the phase transition—is it continuous or discontinuous? Typically, a transition that is continuous in mean field is also continuous in finite-dimensions (though there are exceptions to the “rule” [53]). The lowest-order stochastic process studied previously follows the dynamical rules of



where  $s$  is the activation rate upon contact between an active particle and an inactive one, and  $r$  is the spontaneous deactivation rate of active particles regardless of its neighborhood. This model yields a dynamical equation of

$$\frac{d\rho_A}{dt} = D_A \nabla^2 \rho_A - r\rho_A + s\rho_A\rho_B, \tag{2.13}$$

where we have included a diffusion term for the active particles. For mean field analysis, we first average over space such that the diffusion term vanishes, and set the time derivative to be zero for steady state analysis to arrive at

$$\frac{d\rho_{As}}{dt} = -r\rho_{As} + s\rho_{As}\rho_{Bs} = 0. \tag{2.14}$$



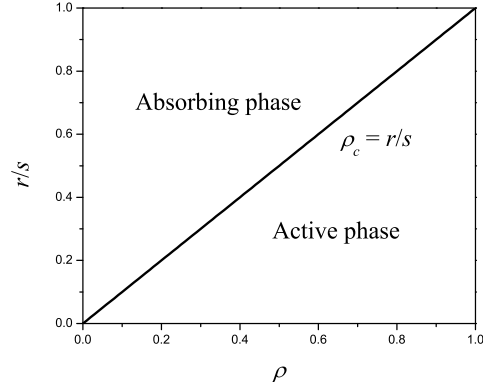


Figure 2.7: Mean-field phase diagram for the two-body activation process.

We set the conserved total particle density to be  $\rho = \rho_A + \rho_B$ , and the above equation can be rearranged as

$$\rho_{As} \left( \rho - \frac{r}{s} - \rho_{As} \right) = 0. \quad (2.15)$$

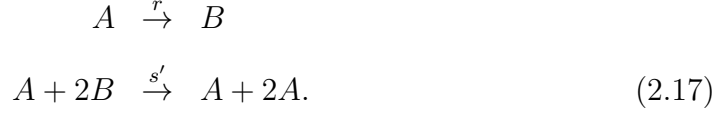
We observe two solutions for the steady state active particle density,  $\rho_{As}$ ,

$$\rho_{As} = \begin{cases} 0, & \rho < \rho_c = \frac{r}{s}, \\ \rho - \rho_c, & \rho \geq \rho_c, \end{cases} \quad (2.16)$$

predicting a continuous phase transition with linear scaling,  $\rho_A = (\rho - \rho_c)^\beta$  for  $\rho \geq \rho_c$  with order parameter exponent  $\beta = 1$ . See Fig. 2.7 for a mean-field phase diagram.

As the particle density is increased, it is reasonable to consider three-or-more body interactions such that an active particle can collide with more than one inactive particles in its path. The pure next-lowest-order contact process thus

obeys



Following the same steps as above to set up a mean field, steady state equation for the active particles, we have

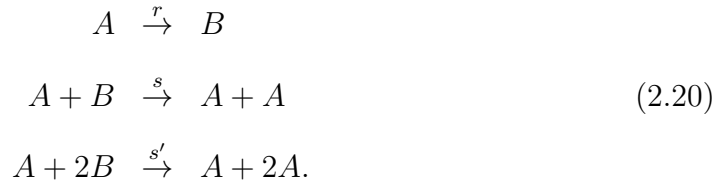
$$\begin{aligned} \frac{d\rho_{As}}{dt} &= -r\rho_{As} + 2s'\rho_{As}\rho_{Bs}^2 = 0 \\ \rho_{As}((\rho - \rho_{As})^2 - \frac{r}{2s'}) &= 0, \end{aligned} \quad (2.18)$$

with the solution

$$\rho_{As} = \begin{cases} 0, & \rho < \rho_c = \sqrt{\frac{r}{2s'}}, \\ \rho - \rho_c, & \rho \geq \rho_c. \end{cases} \quad (2.19)$$

We see the same type of continuous transition with a shift in the transition location.

If we have a mixture of the two lower order interactions (and this is presumably closer to what happens in reality), then the dynamical rules are



These rules correspond to a steady state equation of

$$\begin{aligned} \frac{d\rho_{As}}{dt} &= -r\rho_{As} + s\rho_{As}\rho_{Bs} + 2s'\rho_{As}\rho_{Bs}^2 = 0 \\ \rho_{As}(2s'(\rho - \rho_{As})^2 + s(\rho - \rho_{As}) - r) &= 0, \end{aligned} \quad (2.21)$$

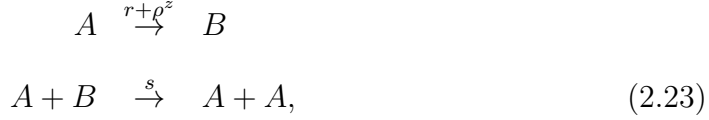
with the solution

$$\rho_{As} = \begin{cases} 0, & \rho < \rho_c = \frac{\sqrt{s^2 + 8rs'} - s}{4s'} \\ \rho - \rho_c, & \rho \geq \rho_c. \end{cases} \quad (2.22)$$

The solution does not appear that intuitive. Let us examine the condition under which the transition occurs, that is  $0 < \rho_c < 1$ . Since both the numerator and the denominator are positive for any positive values of the transition rates  $r, s, s'$ , the condition  $\rho_c > 0$  is always satisfied to guarantee an absorbing phase. On the other hand, the upper bound  $\rho_c < 1$  can be shown to be equivalent to  $r < s + 2s'$ . It simply says that, in a mean field system, close to the absorbing transition, all active particles are exposed to a continuum background of inactive particles, and the net production of active particles is proportion to  $s + 2s' - r$ . In summary, a combined lowest-order and next-lowest-order contact process exhibits, again, a continuous absorbing phase transition with order parameter exponent  $\beta = 1$ . This conclusion is also in agreement with field theory calculations, since close to transition, the higher-order interaction terms are generally less relevant and do not change the critical behavior. However in finite-dimensional simulations, we might expect different behavior since the  $D_B = 0$  limit of the field-theory is not well-behaved.

As the density of particles in the system is increased, there will eventually be no space for the active particles to displace to and, thus, they become inactive. In a lattice model, we model this effect with an active particle becoming an inactive one when all of its neighboring sites are occupied (by active or inactive particles). For a lattice with coordination number  $z$  and in mean field, this is equivalent to adding another deactivation process with probability,  $\rho^z$ . If we consider only the lowest-order contact process with this new "caging" effect, the dynamical rules

are now



with corresponding steady state equation,

$$\begin{aligned} \frac{d\rho_{As}}{dt} &= -(r + \rho^z)\rho_{As} + s\rho_{As}\rho_{Bs} = 0 \\ \rho_{As}(r + \rho^z - s\rho + s\rho_{As}) &= 0. \end{aligned} \quad (2.24)$$

The solutions are

$$\rho_{As} = \begin{cases} 0, \\ \rho - \frac{\rho^z}{s} - \frac{r}{s}. \end{cases} \quad (2.25)$$

In general, the absorbing transitions occur at the roots of equation:  $-\rho^z/s + \rho - r/s = 0$ . We denote the roots as  $\rho_c$ , and within a vicinity of  $\rho_c$ , say  $\rho = \rho_c + \delta\rho$  where  $\delta\rho \ll \rho_c$ , we have

$$\begin{aligned} \rho_{As} &= \rho - \frac{\rho^z}{s} - \frac{r}{s} \\ &= \rho_c + \delta\rho - \frac{(\rho_c + \delta\rho)^z}{s} - \frac{r}{s} \\ &= \rho_c + \delta\rho - \frac{1}{s}\rho_c^z \left(1 + \frac{\delta\rho}{\rho_c}\right)^z - \frac{r}{s} \\ &= \rho_c + \delta\rho - \frac{\rho_c^z}{s} \left(1 + z\frac{\delta\rho}{\rho_c}\right) - \frac{r}{s} \\ &= \delta\rho - \frac{z}{s}\rho_c^{z-1}\delta\rho \\ &= \left(1 - \frac{z}{s}\rho_c^{z-1}\right)\delta\rho \\ &\sim (\rho - \rho_c)^\beta, \end{aligned} \quad (2.26)$$

where  $\beta = 1$ . It shows that for any value of  $z$ , as long as the absorbing transitions

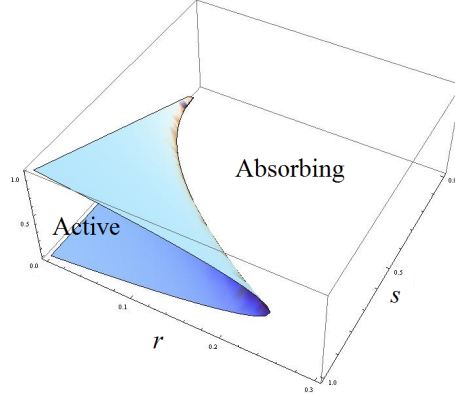


Figure 2.8: Mean field phase diagram with caging effect with  $z = 2$ .

occur (in a certain volume of  $\{z, r, s\}$  phase space), the transition is continuous with order parameter exponent  $\beta = 1$ . As an example, for a 1D lattice  $z = 2$ , the active phase solution is

$$\rho_{As} = -\frac{\rho^2}{s} + \rho - \frac{r}{s}, \quad (2.27)$$

and we see an active phase  $\rho_{As} > 0$  when  $\rho_{c-} < \rho < \rho_{c+}$  where  $\rho_{c\pm} = \frac{1}{2}(s \pm \sqrt{s^2 - 4r})$ . The condition for an active phase to exist is  $s^2 - 4r \geq 0$ . The transition at  $\rho_{c-}$  is the usual absorbing phase transition at low density, and the reentrant to absorbing phase at higher density represents the second transition due to caging. See Fig. 2.8.

For the "caging effect", one may think that if an active particle is caged by other active particles, the active particle might actually be unjammed from the boundary and then it is able to move. Based on this argument, one can also let an active particle turn inactive by caging only if its neighboring sites are all occupied by inactive particles. That is

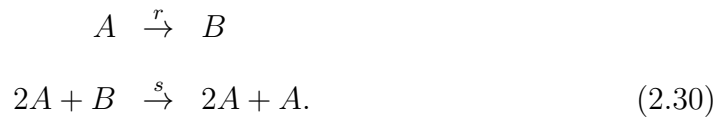


The corresponding mean-field steady-state rate equation is

$$\frac{d\rho_{As}}{dt} = 0 = -(r + \rho_{Bs}^z)\rho_{As} + s\rho_{As}\rho_{Bs}. \quad (2.29)$$

There is still an absorbing state solution  $\rho_{As} = 0$ . The active state solution corresponds to the solution of  $s(\rho - \rho_{As}) - r - (\rho - \rho_{As})^z = 0$ . If one assumes that the transition occurs at  $\rho_{As} = 0$ , then the critical value of  $\rho = \rho_c$  is the root of equation  $s\rho - r - \rho^z = 0$ , and it is clear that  $\rho_{As} = \rho - \rho_c$ , which indicates, again, a continuous transition with order parameter exponent  $\beta = 1$ .

There is another type of three-body contact process in the form of



In the experiment described above, this process corresponds to the activation of an inactive particle occurring when two active particles impact it at the same time. The mean field, steady state equation for this particular process is

$$\begin{aligned} \frac{d\rho_{As}}{dt} &= -r\rho_{As} + s\rho_{As}^2\rho_{Bs} = 0 \\ \rho_{As}(r - s\rho_{As}\rho_{Bs}) &= 0. \end{aligned} \quad (2.31)$$

The absorbing state solution  $\rho_{As} = 0$  is still valid. For an active state solution,

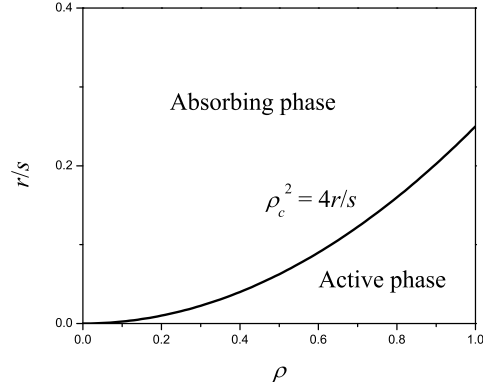


Figure 2.9: Mean field phase diagram for the three-body activation process with two active particles.

given that  $\rho_{Bs} = \rho - \rho_{As}$ , we arrive at

$$\begin{aligned}
 r - s\rho_{As}(\rho - \rho_{As}) &= 0 \\
 s\rho_{As}^2 - s\rho\rho_{As} + r &= 0 \\
 \rho_{As} &= \frac{s\rho \pm \sqrt{s^2\rho^2 - 4rs}}{2s} \\
 \rho_{As} &= \frac{\rho}{2} \pm \frac{1}{2}\sqrt{\rho^2 - \frac{4r}{s}}.
 \end{aligned} \tag{2.32}$$

This solution is physical only when  $\rho \geq \rho_c = \sqrt{4r/s}$ , and at the critical point  $\rho = \rho_c$ ,  $\rho_{As} = \rho/2 = \sqrt{rs} \neq 0$ . We have thus generated a first-order absorbing phase transition at the mean field level. This activation process is very different from the one driven by a single active particle, which is continuous. See Fig. 2.9 for a mean-field phase diagram for this process.

## 2.5 Two-dimensional simulations

### 2.5.1 Simulation protocol

We begin with a square lattice of linear size  $L$ . For initialization, the particles are distributed on sites according to a preset probability/density,  $p$ . The initial ratio of active to inactive particles is denoted by  $q$ . Data suggest that the steady state dynamical phase transition behavior does not depend on the value of  $q$ , however  $q$  affects the initial transients. Each site is occupied by at most one particle at any time (fermionic interaction). Periodic boundary conditions are also implemented. At every time step,

(1) Each active particle hops to one of its empty neighboring sites with equal probability, i.e. diffusion. Active particles must hop as long as they have at least one empty neighboring site. If no empty neighbor is available, the active particle does not hop and becomes inactive (caging effect).

(2) Each active particle can activate one nearest inactive neighbor at random choice with probability  $s$ . As for three-body interactions, one active particle can activate two neighboring inactive particles with probability  $u$ , two active particles can activate one commonly neighboring inactive particle with probability  $v$ .

(3) Each active particle has probability  $r$  to become inactive independent of its neighborhood.

The simulation is carried out until steady state is reached defined by the number of active particles on average not changing. From the steady state mean-field analysis, the ratio of now  $r$  to  $s$ , for example, alters the competition between



activation and deactivation and, therefore, determines the usual absorbing state transition point. In lattice simulations, however, due to finite size effects, the actual values of  $r$  and  $s$  are also important, in addition to the ratio.

## 2.5.2 Results

We are primarily interested in how the system responds to a change in the occupation probability of particles since it is this parameter,  $\rho$ , which is proportional to  $\rho$  that drives the transition. The lowest-order contact process with conserved total particle number and one non-diffusive particle type is already known to fall into the universality class of conserved lattice gas model [46] and the Manna model [45]. See Ref. [47]. Though the scaling relations mentioned above were initially thought to be violated numerically, recent work claims to have resolved the inconsistencies, with the key factor being distinguishing averaging over all samples and averaging over survival samples [54].

For the next-lowest order contact process  $c = 1, d = 2$ , presumably occurs at a higher occupation probability. Recall that the mean-field analysis shows a similar continuous absorbing phase transition to  $c = d = 1$ . If one keeps both  $A + B$  and  $A + 2B$  processes in the system, the former would dominate and it is more difficult to determine the effects of the latter. Therefore, we tune  $s = 0$  and  $u = 0.5$  to better identify the dynamical behavior of the pure next-lowest order contact process. The spontaneous deactivation probability is fixed at  $r = 0.25$ . The simulation results for  $\rho_A(t)$  at different total densities are plotted in Fig. 2.10.

If the transition is indeed continuous, one would expect a series of scaling relations similar to the ones presented in the discussion on directed percolation. In particular, the density of active particles at the critical point would decay as a power-law in time, or  $\rho_A \sim t^{-\theta}$ . Also, the correlation time would scale by the distance to transition, or  $\tau \sim |\rho - \rho_c|^{\nu_{\parallel}}$ . Thus, one expects a scaling function in

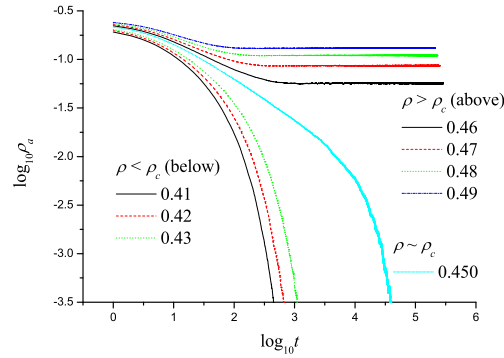


Figure 2.10: The dynamical behavior for the active particles for the  $A+2B$  contact process at different total occupation probabilities.

the form of

$$\rho_A(t) = t^{-\theta} F(t/\tau) = t^{-\theta} F(t/|\rho - \rho_c|^{\nu_{\parallel}}), \quad (2.33)$$

where  $F(x)$  is the universal off-critical scaling function. Moreover, the steady state density should follow  $\rho_{As} \sim (\rho - \rho_c)^{\beta}$  in the long time limit,  $t \gg \tau$ . Hence, the scaling relation  $\beta = \theta\nu_{\parallel}$  should hold similar to the one for directed percolation. For  $L = 256$ , the data collapses nicely according to the scaling function (see Fig.2.11). We measure the values of  $\theta$  and  $\nu_{\parallel}$  to be  $\theta = 0.43(1)$  and  $\nu_{\parallel} = 1.45(2)$ , which agrees well with the corresponding exponents of conserved directed percolation universality class [54]. Therefore, our results suggest a continuous transition with corrections to the mean field exponents.

In addition, due to the finite-size fluctuations involved in the lattice simulations, the system will eventually reach the absorbing state in some finite time at the critical density. This is explicitly shown in Fig.2.12. Power-law decays at early times are clear with a universal power. At late times the finite size effect drives the exponential fall-off of the order parameter. The correlation length near the critical point scales as the linear system size  $L$  as  $\xi \sim |\rho - \rho_c|^{\nu_{\perp}} \sim L$  and, thus,  $|\rho - \rho_c| \sim L^{-1/\nu_{\perp}}$  as pointed out for directed percolation transition. The scaling

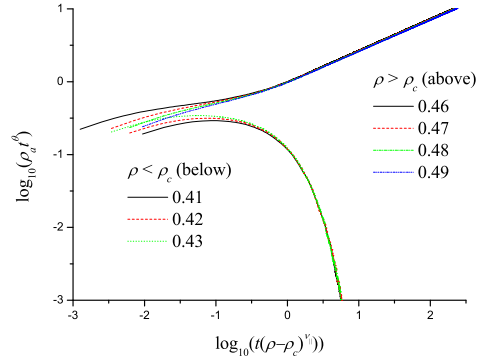


Figure 2.11: Log-log plot of the off-critical scaling collapse,  $\rho_A t^\theta$  vs.  $t|\rho - \rho_c|^{\nu_\parallel}$  with  $\rho_c = 0.450(2)$ .

functions described above can be rewritten as

$$\rho_A(t) = t^{-\theta} G(t/L^z), \quad (2.34)$$

where  $z = \nu_\parallel/\nu_\perp$  is the dynamic exponent and  $G(x)$  is the universal finite-size scaling function. Again, the data are very well collapsed according to the scaling function as shown in Fig. 2.13. We found that  $z = 1.35(4)$  in our simulation. All exponents measured are in agreement with the values of conserved directed percolation universality class, which is consistent with the mean-field result that the next-lowest-order interaction does not generate a different transition. It is also consistent with the fact that the inactive particles are “enslaved” to the active ones. In other words, they cannot move around without the help of the active ones so that fact that changing the number of inactive particles activated does not change the universality class (as it may with usual higher-order interactions), while changing the number of activated should change the universality class. A check on this claim is borne out not only in mean-field but in finite-dimensions where the  $\rho_A(t)$  curves for different  $\rho$ s look qualitatively different from the  $A + 2B$  case such that a standard scaling collapse is not possible. See Fig. 2.14.

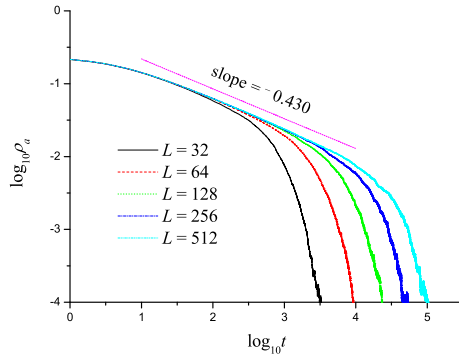


Figure 2.12: Dynamical behavior of density of active particles  $\rho_A$  at critical density  $\rho_c$  for different system sizes.

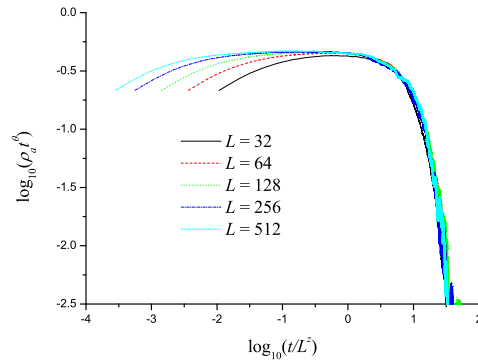


Figure 2.13: Log-log plot for finite size scaling at the critical point  $\rho = \rho_c$ ,  $\rho_A t^\theta$  vs.  $t/L^z$ .

The caging mechanism (an active particle becomes inactive if no empty neighboring site is present at any given time step) introduced in our simulation protocol does not change the absorbing phase transition behavior discussed above occurring at “low” densities (for the single active particle processes). Close to the first dynamical transition, the density of particles is low enough such that there is almost always at least one available empty site for an active particle to diffuse.

However, as we increase the occupation probability, or density, the caging effect becomes more significant. We should observe a second absorbing phase transition

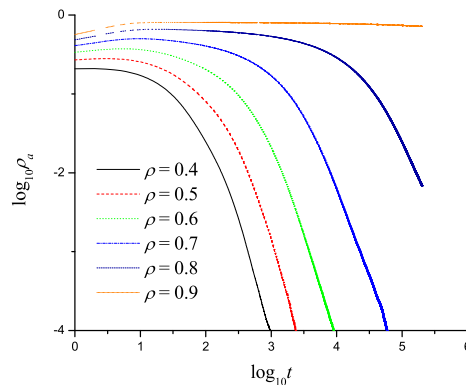


Figure 2.14: The dynamical behavior for the active particles for the  $2A+B$  contact process at different total occupation probabilities.

at high densities back to an inactive (or stuck) state where active particles turn inactive due to the local geometrical constraint. Recall that the cage mechanism brings in a local density dependent deactivation rate in addition to the spontaneous deactivation in conventional contact process description.

In our simulation, since this second transition occurs at high particle density for a given set of parameters. If one allows the caging effect to take place only with inactive particles occupying the neighboring sites of an active particle, for the chosen parameter set  $s = 0.5$  and  $r = 0.25$ , the second transition never occurs. Of course, one could increase the uniform inactivation rate, but then the first transition would not necessarily be observed. On the other hand, the caging effect brought by having both types of particles in the cages exhibits an absorbing phase transition for the chosen parameter set.

According to the mean-field analysis, this transition is a continuous transition with order parameter exponent  $\beta = 1$ , i.e. the same type as the first absorbing state phase transition at low density. Thus, the scaling functions  $F(x)$  and  $G(x)$  derived above should apply and data should show the same type of scaling behavior. However, the off-critical scaling collapse does not look as satisfactory for the

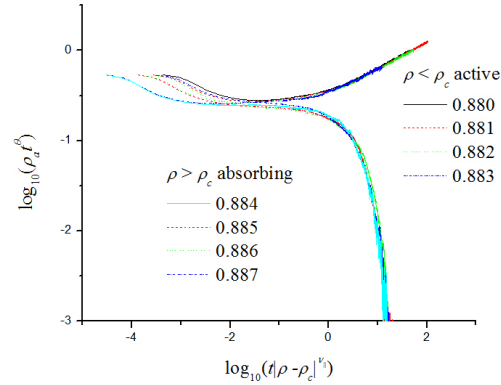


Figure 2.15: Log-log plot of the off-critical scaling collapse for the caging transition. The scaling parameters used are  $\theta = 0.29(2)$  and  $\nu_{\parallel} = 1.37(3)$ .

branch above the caging transition where system ends up in absorbing state (see Fig.2.15). We do not have an explanation for this currently, but are investigating several avenues. In any event, the measured values of  $\theta$  and  $\nu_{\parallel}$  are reasonably different from the conserved directed percolation universality class, suggesting a new universality class. For example,  $\theta = 0.41$  in the latter case and  $\theta = 0.28(2)$  in the former.

We also tried finite-size scaling at the caging transition. The trial scaling collapse is presented in Fig. 2.16 with a measured value of  $z = 2.35(2)$ . Here, the scaling collapse is reasonable. This  $z$  is rather different from the conserved directed percolation of  $z = 1.35(4)$ .

In order to clarify the nature of the transition, we must also determine if the transition actually exists. This question is prompted by the fact that some kinetically constrained models claimed to exhibit a transition, as suggested by lattice simulations, but eventually it was proven that the transition occurs at  $\rho_c = 1$  in the thermodynamic limit. We tried to fit the measured transition point  $\rho_c(L)$  against the system size  $L$  to see if the transition density approaches some finite value in the infinite system size limit. The fit is presented in Fig. 2.17. It

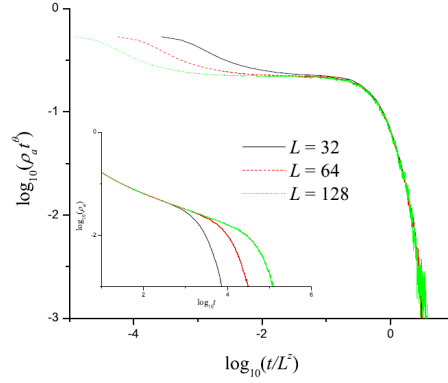


Figure 2.16: Log-log plot of finite size scaling collapse for different system sizes at the caging transition. Inset: unscaled data.

suggests that as  $L \rightarrow \infty$ , the value of  $\rho_c$  approaches a constant less than unity. However, we have no proof at this time. The fact that our model contains a uniform inactivation rate may “save” us from the absence of a transition in the thermodynamic limit as compared to previously explored caging models.

Assuming that the transition occurs at a total occupation probability less than unity, we have gone one step further to look for more evidence of a continuous transition as suggested by the mean-field analysis. We analyze the relation between system size and the magnitude of the jump in the order parameter (steady state density) at the transition due to finite-size fluctuations. See Fig. 2.18. The scaling relation involved is  $\rho_A(t) = t^{-\theta}G(t/L^z)$ , and we can rewrite it using  $z\theta = \beta/\nu_\perp$  to arrive at

$$\rho_A(t) = L^{-\beta/\nu_\perp}H(t/L^z). \quad (2.35)$$

The slope as seen in the inset of Fig. 2.18 should correspond to  $-\beta/\nu_\perp$ . However, the measured exponents do not follow the scaling relations. In particular, the scaling relations,  $\beta = \theta\nu_\parallel$  and  $\nu_\perp = \nu_\parallel/z$ , would suggest  $\beta = 0.4$  and  $\nu_\perp = 0.58$ . Then,  $\beta/\nu_\perp = 0.69$  is not consistent with this measurement suggesting  $\beta/\nu_\perp = 0.96$ . A similar broken scaling relation has been reported to exist in the conserved

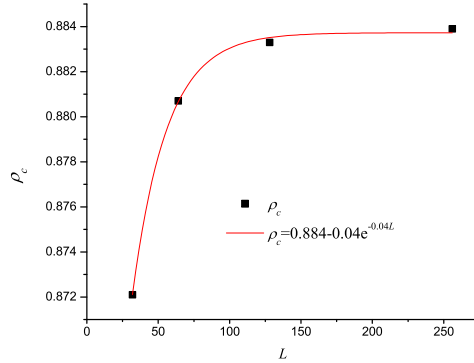


Figure 2.17: The measured caging transition point vs. linear system size,  $L$ . The fitted line is an exponential with  $\rho_c \sim 0.884$  as  $L \rightarrow \infty$ .

lattice model. However, it was resolved in the work by Lee and Lee [54]. We have followed this more recent analysis protocol used in Ref. [54] and still get the inconsistency. Our result might suggest that the absorbing phase transition due to caging has some special features, presumably from the highly local inactivation mechanism.

## 2.6 Discussion

We introduce novel higher-order interactions in contact processes with conserved total particle number to understand how a periodically sheared colloidal system may undergo a dynamical phase transition at even higher densities than previously explored in experiments. We find that a simple three-body collision of one active (diffusing) particle activating two inactive (nondiffusing) particles does not change the nature of the absorbing phase transition found at lower densities due to a two-body collision. This is due to the fact that the inactive particles are enslaved to the active particles such that the inactive particles simply form a continuous background that an active particle can always access. In other words, the differ-



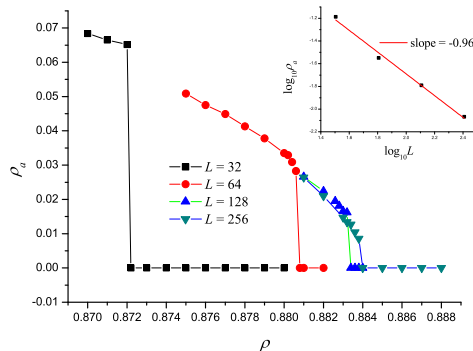


Figure 2.18: Surviving sample averages for  $\rho_A(\rho)$  for different  $L$ s. Inset: The magnitude of the jump in  $\rho_c$  vs. linear system size. The fitted line is a power-law with a slope of approximately 0.96.

ence between activating one inactive particle ( $A + B$ ) and activating two inactive particles ( $A + 2B$ ) is effectively a change in the activation rate and not the fundamental mechanism of activation. In square lattice simulations, the two processes yield same values for the set of scaling exponents, and the scaling relation derived for two-body contact process holds.

On the other hand, further investigation regarding the collective activation process  $2A + B \rightarrow 3A$  would be promising in terms of looking for a new transition of a very different nature as indicated by mean-field calculations and by numerical simulations on the square lattice. Close to the critical point, the fraction of active particles might be very small, and the  $2A + B$  process requires that the active particle community must be clustered to maintain the possibility to generate more active particles, so that to stay in the active phase. On the other hand, those isolated active particles would be eliminated very fast for they cannot reproduce. The possibility of having a first-order transition in the collective activation model may be comparable to a recent modification of the asymmetric exclusion process where a particle can hop to its right only if its left neighbor is occupied to arrive at very different features from the usual asymmetric exclusion process [55].

The caging mechanism may be responsible for dynamical arrest in glasses. We incorporate this mechanism in our model for the dynamics of periodically sheared colloidal suspensions to search for such a transition. We numerically observe in two-dimensions, a “caging” transition at high densities where the active state becomes inactive though we cannot yet exclude the possibility that the transition occurs at full density in the infinite system limit as it does in, say, the Kob-Andersen model [50]. However, the caging here is different from the Kob-Anderson model in that it does not obey detailed balance. A uniform spontaneous deactivation rate helps keep the critical density below unity. We measured the usual scaling exponents, and the transition appears to belong to some new universality class other than conserved directed percolation. It would be very interesting to examine more fully the effect of this highly localized inactivation mechanism and better determine how robust this potentially new universality class is.

## Chapter 3

# Force network analysis of amorphous solids near the onset of rigidity

### 3.1 Background

The jamming phase diagram depicts a plausible scenario for a unified description of the phase change/crossover from a liquid to an amorphous solid in nonequilibrium systems ranging from granular particles to colloidal particles to molecular particles [57, 58]. These phase changes can be driven by temperature changes, packing fraction changes, and/or changes in applied shear stress. See Fig. 3.1. Whether or not the boundaries of the jamming phase diagram are sharp in the equivalent equilibrium sense is still a matter of debate, particularly for molecular particles in the presence of temperature changes [59]. However, numerical studies of repulsive, soft particles at zero-temperature indicate the potential of a transi-

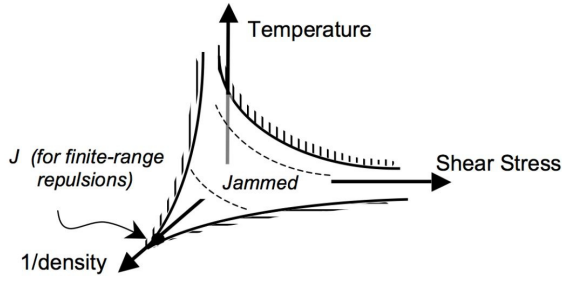


Figure 3.1: Jamming phase diagram. Adapted from Ref. [56]

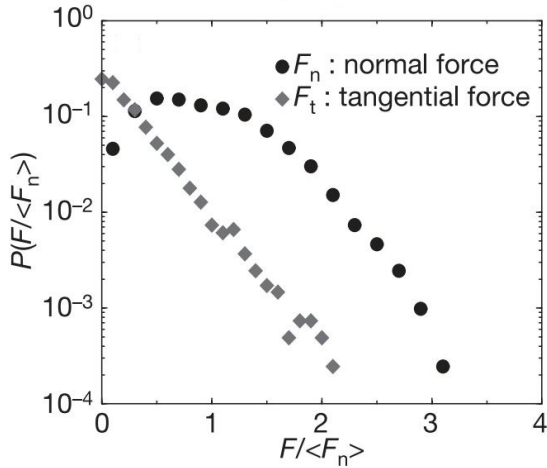


Figure 3.2: Contact force distribution in an experiment. Adapted from Ref. [83]

tion in the equivalent thermodynamic sense as the packing fraction of the system is increased [60, 61].

The numerics of the zero-temperature repulsive, soft particle system suggest that the transition from liquid to amorphous solid is somewhat of an unusual nature [60, 61, 62]. For example, the average coordination number jumps from zero to some finite value at the transition, followed by a square root increase as a function of distance from the transition, i.e.  $\phi - \phi_c$ , where  $\phi$  denotes the packing fraction and  $\phi_c$ , the critical packing fraction above which the system behaves as a solid. The square root behavior begs for a mean-field description. However, why would a two-dimensional amorphous solid near the onset of rigidity behave mean-field-like? Moreover, the jump in the average coordination number only depends on the

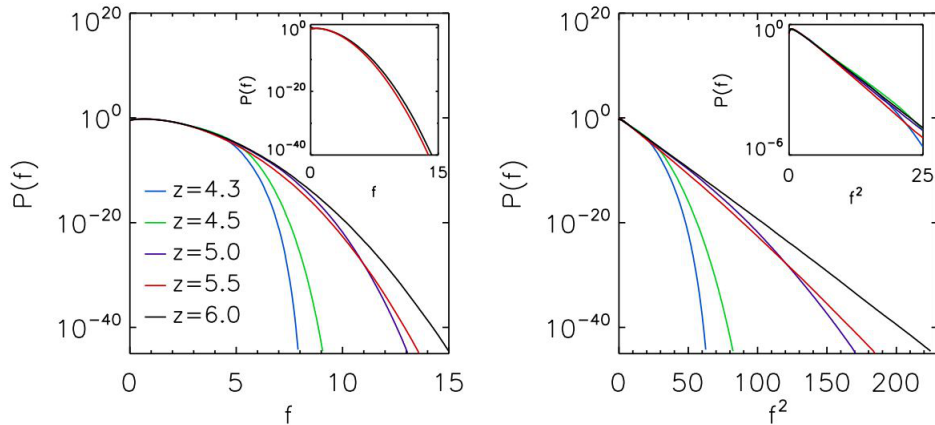


Figure 3.3: Contact force distribution from simulations. Adapted from Ref. [87]

dimension of the system. Both properties are observed in experiments [63]. The latter property is due to isostaticity where the number of contacts equals the number of degrees of freedom on average such that the system is not overconstrained or underconstrained, but minimally rigid in an average sense. The “universality” is the magnitude of the jump in the average coordination number is reminiscent of the universality of the value of the jump in the spin-wave stiffness in the two-dimensional Kosterlitz-Thouless transition [64]. While there exists a jump in a possible order parameter at the transition, the square root scaling demonstrates that the transition is not the typical first-order transition with no diverging correlation lengths. In fact, there are several diverging correlation lengths above and below the transition. For example, the fraction of jammed configurations as a function of  $\phi$  becomes increasingly sharper as the system size is increased. This sharpening can be tied to an increasing lengthscale below which the system acts as uncorrelated subsystems each with their respective critical packing fractions.

As for the jammed phase itself, it exhibits various interesting properties. While the scaling of the bulk modulus with packing fraction is the same as ordered elastic solids, the scaling of the shear modulus with packing fraction shows an anomalous response [60, 61]. In addition, the vibrational modes are of a “swirly” nature

and appear to be quasi-localized as the jamming transition is approached from the solid side [65, 66]. Similar behavior has been observed in other amorphous solids [67, 68, 69, 70]. Both of these observations may be related to the non-affine displacements of the particles, which become more pronounced near the jamming transition. There is also an excess in the vibrational density of states beyond the Debye prediction at the transition. This excess has been likened to the Boson peak [71, 72, 73] in glassy systems.

## 3.2 Inquiry

There have been a number of approaches to understand some of the above properties, including a statistical mechanics approach [74], a field theoretic approach [75], and a phenomenological approach [76, 77, 78]. The phenomenological approach examines the consequences of the isostatic nature of the transition by establishing a lengthscale below which the system behaves as an isostatic solid and above which the system behaves as an ordinary elastic solid. This lengthscale has been inferred from the numerical simulations by relating the frequency below which there exists an excess in the density of states (beyond the Debye prediction) to a lengthscale via a linear dispersion relation [79]. However, a direct measurement of the elasticity of the system via a local perturbation shows the system to respond on average as an ordinary elastic solid at all lengthscales at the jamming transition [80, 81]. On the other hand, the study of fluctuations in the response of all contacts some radial distance from the local perturbation demonstrates a clear crossover lengthscale where the root-mean-squared fluctuations go from one type of power-law dependence on radial distance to another type further away from the perturbation. This crossover lengthscale appears to scale with distance from the transition.

---

One would like to understand, for example, why the averaged response of the system behaves as ordinary two-dimensional elastic solid at the transition and why a potential isostatic lengthscale may be showing up only in fluctuations to a response in position space. The two-dimensional averaged elastic behavior is also counter to the mean-field behavior observed in the contact geometry near jamming. To begin to investigate such mysteries, we numerically study the contact force network of a two-dimensional system of repulsive, soft particles as the jamming transition is approached from above. The contact force network, with its forces and its contact geometry, dictates the properties of an amorphous solid.

Until now, most numerical studies using repulsive soft spheres (the standard one now used to simulate jamming) have focused on the distribution of forces without regard to their spatial location. This is because the contact forces in highly packed granular material are rather heterogeneous. The heterogeneity is mostly studied in terms of the probability distribution of the contact force magnitude  $p(f)$ . There has been some controversy about the shape of  $p(f)$ . Does it have an exponential tail or a Gaussian tail? An initial experiment measuring the forces on the boundary of a granular system obtained an exponential decay in  $p(f)$  for large forces [82], while later experiments producing bulk measurements suggested that  $p(f)$  has a closer to Gaussian tail [83]. See Fig. 3.2. The difference between measurements done in bulk and on the boundaries is not yet understood. Computer simulations on frictionless repulsive soft sphere systems confirm the Gaussian tail  $p(f) \sim \exp\{-f^2\}$  in two-dimensions (see Fig. 3.3) and a tail slightly different from Gaussian in the three-dimensions since  $p(f) \sim \exp\{-f^{1.7}\}$  [87]. Given the previous focus on  $p(f)$ , we will look for spatial correlations in the magnitude of the forces in the contact force network.

In addition, we will also analyze the contact geometry, the second important ingredient of the force contact network, in a novel way. We propose a mapping

of the contact/coordination number to a spin state in order to potentially better understand some of the properties of the jammed solid from what will turn out to be a spin glass perspective. Therefore, we will be able to draw direct links between spin glasses and amorphous solids. Our mapping should further open the door for other amenable analytical techniques used in spin glasses with quenched disorder for studying amorphous solids where the disorder is not quenched. We note that there exists very interesting work on a replica-inspired approach to the glass transition for hard spheres as approached from the liquid side (as opposed to the solid side) [85].

### 3.3 Force bonds and spatial correlations

To study the force network of a two-dimensional jammed solid of repulsive, soft particles, jammed configurations are generated using the algorithm introduced by O’Hern and collaborators [60, 61]. More specifically, the system consists of 50:50 mixture of  $N$  particles with a diameter,  $\sigma$ , ratio of 1.4. The packing fraction sets the radii for a system of length unity. The particles interact via the following two-body potential:

$$V(r_{ij}) = \frac{\epsilon}{\lambda} \left(1 - \frac{r_{ij}}{\sigma_{ij}}\right)^\lambda \Theta\left(1 - \frac{r_{ij}}{\sigma_{ij}}\right), \quad (3.1)$$

where  $r_{ij}$  is the distance between the centers of the two particles  $i$  and  $j$ ,  $\sigma_{ij} = (\sigma_i + \sigma_j)/2$ , and  $\epsilon$  sets the energy scale for the system. The particles are placed randomly in the system with periodic boundary conditions and the conjugate gradient algorithm is invoked until the system reaches its nearest local minimum. We use an energy tolerance per particle of  $10^{-16}$  in units of  $\epsilon$ .

In the repulsive, soft particle system, there are several known properties of the forces between overlapping particles: (1) the shape of the distribution of forces [86,



87] and (2) the distribution of forces demonstrates a lack of self-averaging [60, 61]. As for the shape of the distribution, the distribution is not long-tailed. Recent simulations in two- and three-dimensions have determined the shape of the tail down to normalized force values of  $10^{-45}$  [87]. In two-dimensions, the tail is Gaussian. In three-dimensions, the tail falls off slightly more slowly than Gaussian, i.e.  $P(f) \sim e^{-f^{1.7(1)}}$ , where  $f$  is the magnitude of the force between two overlapping particles. As for the lack of self-averaging, the distribution of forces takes on one form if the forces in each sample are normalized via the average force per sample or if the forces from all samples are pulled and normalized by the average force from all samples. Therefore, one cannot consider a large sample to be comprised of many smaller samples. A lack of self-averaging is also found in configurations of spin glasses.

While the distribution of forces is a very useful quantity, it does not encode any spatial information. Motivated by the recent work of Zhou and Dinsmore [88], we search for spatial correlations in the magnitude of forces. To do this, we measure the angle between *any* two force bonds emanating from a particle in the jammed packing at a particular packing fraction,  $\phi$ . We denote this angle as  $\theta$ . See the schematic in Figure 3.4. The probability distribution for  $\theta$ ,  $P(\theta)$ , is plotted in Figure 3.4 for all coordination numbers greater than 2 for  $\phi = 0.841$  with  $\lambda = 3/2$  and  $N = 512$ . The lower bound on the coordination number is determined by the principle of local mechanical stability. For this particular  $\phi$  and system size, the average coordination of the jammed configurations,  $\langle z(\phi) \rangle = 4.076(2)$  such that we are not far from the jamming transition where  $\langle z(\phi) \rangle \approx 4$  in two-dimensions. Also, the fraction of jammed configurations is approximately two-thirds. So we are in the jammed phase. We should point out that earlier work extrapolated to a critical value of  $\phi_c$  in the infinite system limit of approximately 0.842. However, there exists a body of recent work suggesting that  $\phi_c$  depends on the protocol

for obtaining jammed configurations such that “Point J” should be modified to “Segment J” [89, 90, 91, 92]. Implications of these findings have not been fully fleshed out to date. Figure 3.4 also depicts  $P(\theta)$  for a particular  $z$ , or  $P_{z=4}(\theta)$ .

We then compare  $P(\theta)$  with  $P(\theta_{lg})$ , where  $\theta_{lg}$  is the angle between the two largest force bonds on a particle. We observe that the probability distribution in the latter case is more heavily biased towards the larger angles. In other words, there exists a suppression of the smaller angles between the two largest force bonds on a particle giving rise to chain-like correlations in the locally largest force bonds. Defining  $W = \int_{120^\circ}^{180^\circ} (P(\theta_{lg}) - P(\theta))d\theta$  as a measure of the bias,  $W = 0.434(1)$  for  $\phi = 0.841$  and  $N = 512$ .

Let us compare  $P(\theta)$  and  $P(\theta_{lg})$  with the equivalent distributions for a more ordered packing. To do this, we use a monodisperse distribution of repulsive, soft particles in two-dimensions at a higher packing fraction. For a hexagonal packing of hard particles in two-dimensions, the packing fraction is equal to approximately 0.907. We choose a slightly larger packing fraction to ensure overlaps. See Figure 3.5. We observe three dominant peaks at  $60^\circ$ ,  $120^\circ$ , and  $180^\circ$  degrees indicating a hexagonal packing. We also note a bias in  $P(\theta_{lg})$  towards the larger angles for the ordered case as well.

In the disordered case, there are a number of dominant peaks in  $P(\theta)$  at  $\theta = 54^\circ, 60^\circ, 64^\circ$ , and  $70^\circ$ . There are also some subdominant peaks, many of them separated by intervals of  $6^\circ$ . See, for example, the range of  $\theta = 102^\circ$  to  $\theta = 114^\circ$ . These subdominant peaks are due to the bidispersity in particle radii. If the 1.4 ratio is increased, the spacings between the subdominant peaks increases. To see this, consider a particle surrounded by all “small” particles. If we replace one of the small particles by a larger particle, the larger particles will push its neighbors away due to insufficient space and therefore change the contact angle. We can calculate this change given the ratio between the two different radii in

the just-touching case. For a radius ratio of 1.4, the change in contact angle is approximately  $5.4^\circ$ , the interval between the subdominant peaks.

For  $N = 512$  and  $\lambda = 3/2$ , as  $\phi$  is increased from  $\phi = 0.841$  to  $\phi = 0.843$ , the bias towards the larger angles remains robust. More specifically,  $W$  remains constant. See Figure 3.6. For even larger  $\phi$ ,  $W$  decreases. For example,  $W = 0.424(2)$  for  $\phi = 0.846$ . This trend also agrees with the findings of Zhou and Dinsmore [88] where larger  $z$  suppresses chain formation. Since  $\langle z(\phi) \rangle$  increases with  $\phi$ , this trend is expected. Figure 3.7 also demonstrates this effect where  $P_{z=3,4,5}(\theta_{lg})$  are plotted individually for  $\phi = 0.843$ . As  $z$  is increased from 4 to 5,  $W$  decreases from  $0.454(2)$  to  $0.413(2)$ . Finally, the trend of the suppression of smaller contact angles for larger force bonds persists for larger system sizes indicating that the suppression is not a finite system effect. We have also checked that the suppression persists for  $\lambda = 5/2$  and  $\lambda = 2$  as well, the more studied cases.

To contrast our results with those of Zhou and Dinsmore [88], we do not observe a peak in  $P_z(\theta_{lg})$  at 180 degrees for all  $z$ . Rather the peak in  $P_z(\theta_{lg})$  for  $z = 3$ , for example, is closer to  $160^\circ$ . Only for  $z = 4$ , is the peak at  $180^\circ$ . Therefore, the large force bond propagation is not as “straight” as in Zhou and Dinsmore [88] simulations where a peak at  $180^\circ$  is observed for all  $z$ . Their protocol generates stable configurations by demanding force balance on each particle given that some of the forces on each particle are randomly generated. Zhou and Dinsmore argue that the finding of chain-like correlations is simply a consequence of Newton’s third law. The peaks in their  $P_z(\theta_{lg})$  may be an indication of this. However, since our equivalent distributions are not all peaked at 180 degrees, a more complicated mechanism may be at work.

Our results suggest a possible spatial correlation in the force bond strength. Given that larger angles between the locally largest forces persist, perhaps locally

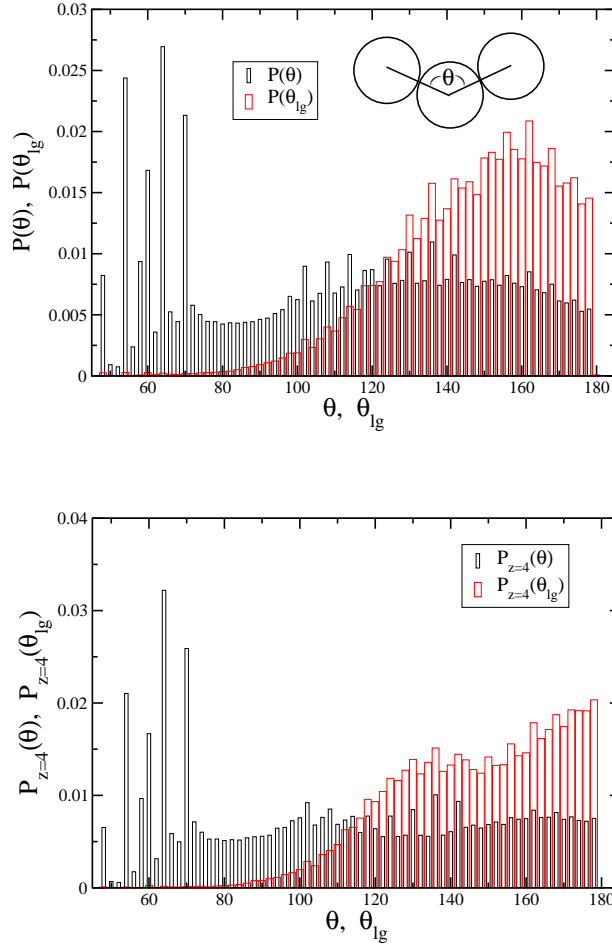


Figure 3.4: Top:  $P(\theta)$  and  $P(\theta_{lg})$  for  $\phi = 0.841$ ,  $N = 512$ , and  $\lambda = 3/2$ . Bottom:  $P_{z=4}(\theta)$  and  $P_{z=4}(\theta_{lg})$  for the same parameters. The bin size is  $2^\circ$ .

large force bonds can persist/percolate across the sample. To test for this, we construct a force chain by traversing along largest and second largest local force bonds and determining whether the chain of particles spans the system or not. The algorithm for this task is the following:

- (1) Identify the largest force bond in the system.
- (2) Traverse from one of the particles on either side of the largest force bond to the another overlapping particle along the second largest force bond.
- (3) Traverse to the next overlapping particle along either the largest force bond

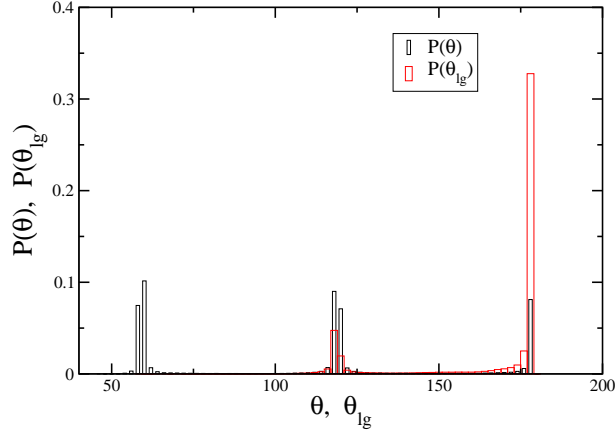


Figure 3.5:  $P(\theta)$  and  $P(\theta_{lg})$  for  $\phi = 0.91$ ,  $N = 512$ , and  $\lambda = 3/2$  for a monodisperse system.

or the second largest force bond (if the largest force bond has already been traversed).

(4) Repeat (3) until reaching an overlapping particle where both the largest and second largest force bonds have already been traversed.

(5) Go back to the largest force bond in the system. Pick the other particle not initially chosen. If its second largest force bond has not been traversed, repeat steps (4) and (5).

Note that the largest force bond of one particle is not necessarily the largest force bond of the other particle associated with the bond. This algorithm constructs the largest force chain in the sample. We also construct the weakest force chain in the sample by replacing largest with smallest, etc. Finally, we also study force chains beginning from any force bond in the system.

In Figure 3.8 we present an example of the largest force chain. Loops make up some fraction of the “chain”. This is due to fluctuations in the forces. The larger force bonds exhibit chain-like structures, while smaller force bonds form local loops. We have checked this in the simulations by constructing the equivalent

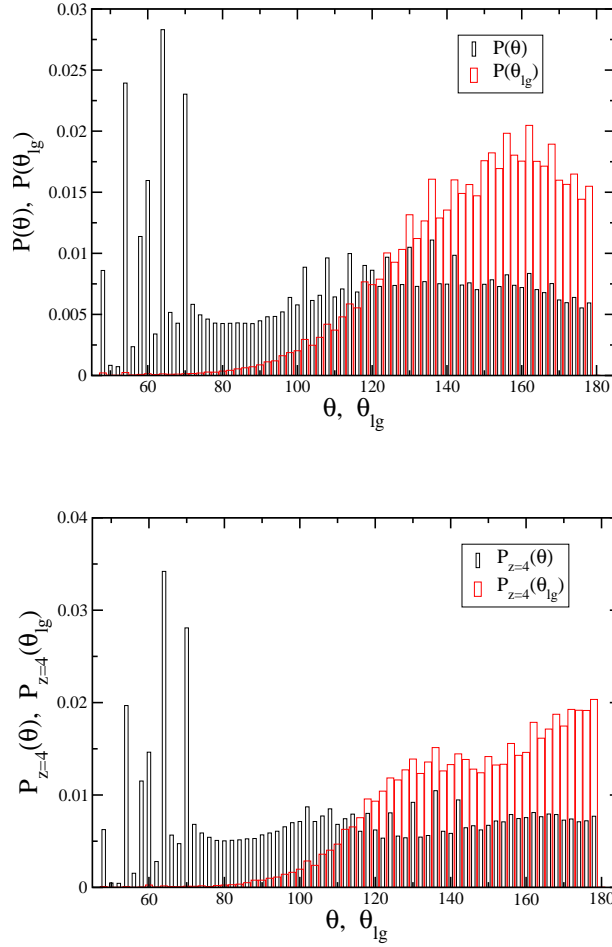


Figure 3.6: Top:  $P(\theta)$  and  $P(\theta_{lg})$  for  $\phi = 0.843$ ,  $N = 512$ , and  $\lambda = 3/2$ . Bottom:  $P_{z=4}(\theta)$  and  $P_{z=4}(\theta_{lg})$  for the same parameters.

weakest force chain. Since the largest local force bond between two particles may be one of the smaller force bonds, as compared to the rest of the force bonds in the system, chains can end in loops. Note that, at least for this example, the largest force chain spans the system in the vertical direction.

How typical is this spanning for the largest force chains? Figure 3.9 shows the probability of spanning in either direction,  $P_s$ , as a function of  $N$  for a particular  $\phi$ . We see that  $P_s$  decreases with increasing  $N$ . While for small  $N$ ,  $P_s$  appears to decay linearly with  $N$ , the larger particle number data makes this candidate

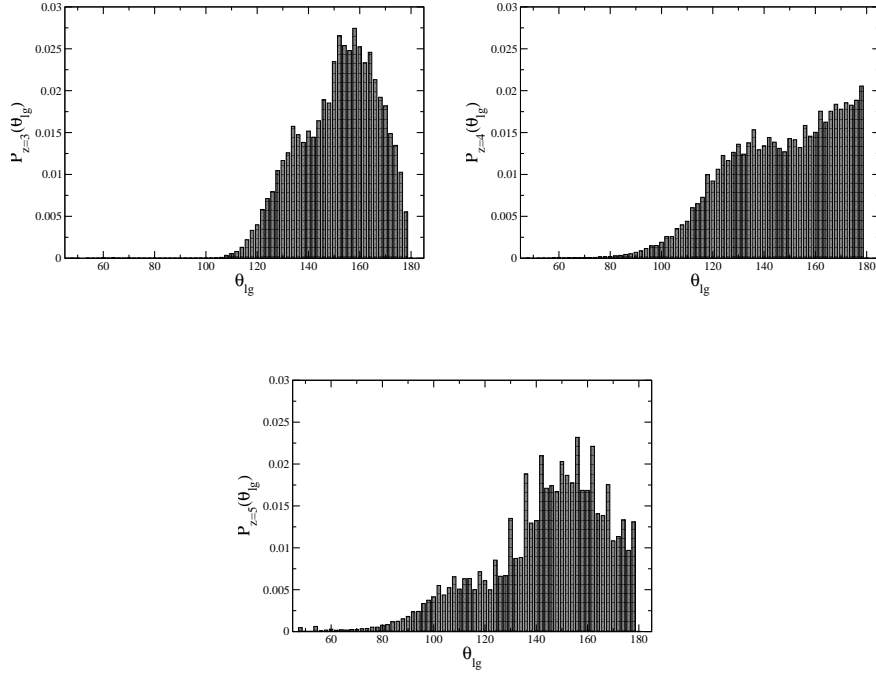


Figure 3.7: Left:  $P_{z=3}(\theta_{lg})$  for  $\phi = 0.843$ ,  $N = 512$ , and  $\lambda = 3/2$ . Right:  $P_{z=4}(\theta_{lg})$  for the same parameters. Bottom:  $P_{z=5}(\theta_{lg})$  for the same parameters.

function less likely. We also observe that  $P_s$  increases as  $\phi \rightarrow \phi_c$ , particularly for the largest particle number data, which is consistent with the increase in small angle suppression as  $\phi \rightarrow \phi_c$  for the locally largest forces. As for the infinite system limit, it may be that the conditions to generate spanning chains need to be relaxed to generate spanning chains with nonzero probability. Also, if we start from any force bond in the system and generate a force chain moving along the locally largest two force bonds for each particle, the probability for spanning decreases. To be specific, for  $\phi = 0.841$ ,  $N = 1024$ , and  $\lambda = 3/2$ ,  $P_s \approx 0.563$  starting at any force bond as compared to the largest force chain spanning of probability, where  $P_s \approx 0.688$ .

At this point, we must comment on the relation of our results to those of Makse and collaborators [93] performing dynamical simulations of deformable grains. They construct spanning force chains by starting with a grain at one end of the

system and traversing the maximum force bond at every particle such that they reach the other side of the system. They find fewer spanning force chains closer to the transition than further away. They argue that this observation is due to an increasingly homogeneous distribution of forces far away from the transition. We should also contrast our results with work by Ostojic and collaborators [94]. They study the spatial extent of force bonds exceeding some threshold force. The threshold force is lowered until the force bonds exceeding the threshold force span the system. They observe a percolation transition of a new universality class. We, instead, investigate the local, largest forces. Also, we do not have spanning as a criterion, but rather as an “afterthought”.

To better understand the spatial properties of the largest force chain, we measure its fractal dimension. Presumably, the fractal dimension is unity, though one should check this. To do so, we count the number of particles participating in the largest force chain. To relate this number with a length, in two-dimensions,  $L \sim \sqrt{N}$ . Figure 3.10 plots the average number of particles participating in the largest force chain,  $N_{FC}$ , as a function of system size,  $N$ . On the log-log scale, there is some curvature to the data. If we assume a fractal form, for  $\lambda = 3/2$  and  $\phi = 0.843$ , we measure a fractal dimension of 1.10(5)—very close to unity. Comparing our largest force chain data to the Ostojic formulation [94], we measure the number of particles participating in the largest force spanning cluster,  $N_{LF}$ . The fractal dimension of the spanning cluster of largest forces is 1.62(2). We then measure the number of particles participating in the smallest force spanning cluster,  $N_{SF}$ , where we replace “exceeding a threshold force” in the Ostojic formulation [94] with “below a threshold force”, the fractal dimension is 1.68(2). The fractal dimension of the spanning cluster at the ordinary percolation transition is about 1.89 [42], which is somewhat larger than the value measured for the spanning cluster of largest forces (and smallest forces). This discrepancy may



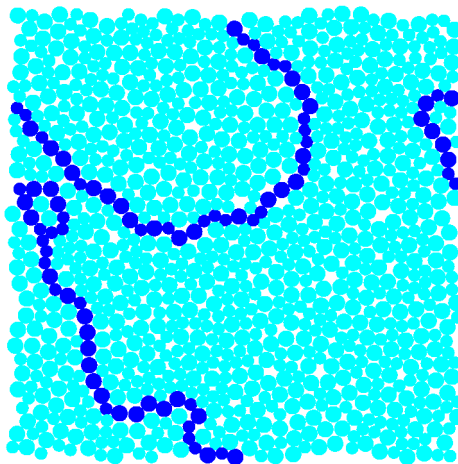


Figure 3.8: Jammed configuration for  $\phi = 0.841$ ,  $N = 1024$ . The particles participating along the largest force chain (dark blue) as distinguished from the other particles (light blue).

be due to the chain-like correlations in the largest, local force bonds, though one cannot discount the possibility of an eventual crossover to ordinary percolation.

### 3.4 Contact number and spins

The forces are not the only information encoded in the force network. The contact, or coordination, number is another piece of information. Figure 3.11 is the same jammed configuration as depicted in Figure 3.8. Each color now represents a different coordination number. If all pairs of neighboring particles were of different colors, the graph would represent a proper vertex coloring. However, note that there are some vertices sharing an edge that do have the same color. So Figure 3.8 does not represent a proper vertex coloring.

But let us, for the moment, address proper vertex colorings. A proper vertex coloring using at most  $p$  colors exists if there exists a zero energy solution of zero-temperature antiferromagnetic Potts model with  $p$  states. In other words, the

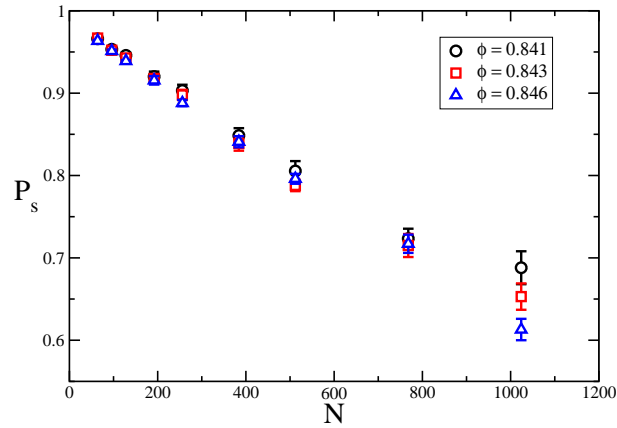


Figure 3.9: The probability of spanning in either direction,  $P_s$ , for the largest force chain.

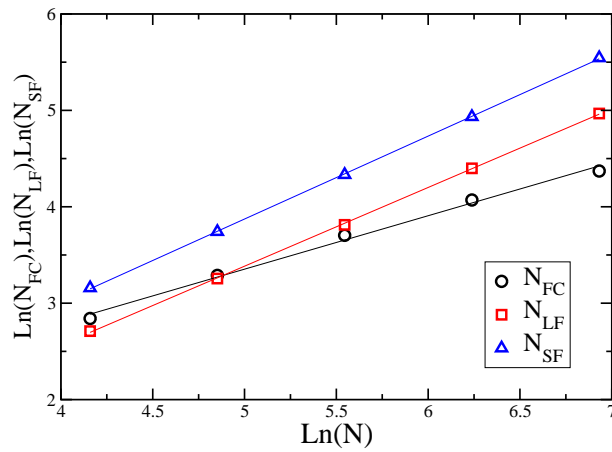


Figure 3.10: Log-log plot of the average number of particles in the largest force chain that span,  $N_{FC}$ , the average number of particles in the largest force spanning cluster,  $N_{LF}$ , and the average number of particles in the smallest force spanning cluster,  $N_{SF}$ , as a function of  $N$ . The error bars are smaller than the symbols. The straight lines are fits to the data. Here,  $\phi = 0.843$  and  $\lambda = 3/2$ .

$p$ -coloring problem maps to a zero-temperature antiferromagnetic Potts model with  $p$  states. Now, if one were to consider the jamming problem, the number of possible colors participating in the jammed clusters is 5 ( $z = 3$  through  $z = 7$ , for this particular two-dimensional bidisperse system) which leads to a  $p = 5$  state Potts model. At  $\phi = \phi_c$ , the isostatic condition would bias one of the colors—for example, the color associated with coordination number four dominates for two-dimensional frictionless discs. This bias can be encoded via a magnetic field. The isostatic condition also imposes other weights on the other colors as well such that the average coordination number is four. In particular, recent work shows that at the jamming transition in two-dimensions, the coordination numbers range from 3 to 5 such that  $z = 4$  particles make up about half the system and  $z = 3, 5$  particles make up the other half [95]. As the packing fraction increases, the weights for each color changes. For a hexagonal packing, all couplings are ferromagnetic.

Both the antiferromagnetism and the competing magnetic field (to account for the average coordination number of four in two-dimensions) contribute to frustration of the spin system. Moreover, there exists randomness in the system due to (1) the fact that not all particles are participating in the jammed configuration and (2) the randomness of the forces. The combination of frustration and disorder should lead to a spin glass phase [96, 97]—a spin glass phase with no quenched disorder. In fact, the couplings and dilutions (particles not participating in the jammed configurations) are dynamically generated. However, the lack of self-averaging in the forces is characteristic of quenched disordered system. Indeed, there are systems with no disorder that can be mapped to quenched disorder and there are systems with unquenched disorder that can also be mapped to quenched disorder. For the former, consider an Ising spin system whose interaction fluctuates in sign with distance between sites [98]. For the latter, consider a liquid of hard spheres as described by hypernetted chain equations [85].

The potential for a jamming-spin glass correspondence provides motivation to analyze the jamming system in terms of a spin glass. If we compute the ratio of antiferromagnetic couplings (different coordination numbers (colors) between contacts) to ferromagnetic couplings (same coordination numbers (colors) between contacts), for  $\phi = 0.841$ ,  $N = 1024$ , for example, the ratio is approximately 2.5. We could ignore the random variation in the magnitude of the forces (interactions between spins) and set the coupling to be a constant using the measured ratio of antiferromagnetic spins to ferromagnetic spins to simulate a two-dimensional  $p = 5$  Potts glass system at zero-temperature. While there exists a number of ground state algorithms for two-dimensional Ising spin glasses [99, 100, 101], we do not know of an exact ground state algorithm for the 5-state Potts glass and so we leave this avenue for future work.

Instead, to further the possible connection between jammed solids and spin glasses, we compute the spin glass equivalent of bond chaos in the repulsive, soft particle system [102]. Chaos in mean-field spin glasses is presumably due to the fact that the spin glass phase is a marginal phase such that a perturbation in the energy of the system is sufficient to alter the weights of different equilibrium configurations [103]. More specifically, in mean-field, the Hessian associated with Parisi's ansatz for the structure of the matrix order parameter contains all non-negative eigenvalues [104]. In finite-dimensions, the marginality is presumably due to the slowly decaying correlation functions [105]. It is interesting to note that jammed solids at the jamming transition are marginally rigid and, therefore, may also exhibit similar chaotic features.

So, we use this notion of chaos in spin glasses to look for a quantitative measure of chaos in the jamming system. To do this, we first assign a list of random numbers as the initial position of particles in a system and use conjugate gradient algorithm to generate a jammed state. Next, we use the same initial positions

and perturb them by a given strength, then apply the same conjugate gradient algorithm to generate another jammed state. Specifically, for particle  $i$  with initial position  $(x_i, y_i)$  in the unperturbed system, the corresponding particle  $i$  in the perturbed system has an initial position of

$$\begin{aligned} x'_i &= x_i + \delta c_i \\ y'_i &= y_i + \delta d_i, \end{aligned} \tag{3.2}$$

where  $\delta$  is the magnitude of perturbation strength, and  $c_i$  and  $d_i$  are randomly generated numbers chosen from the same distribution used to generate  $x_i$  and  $y_i$ .

If the two sets of initial positions both lead to a jammed state, we calculate the overlap between the two states as defined by

$$r(\delta, N, \phi) = \left\langle \frac{\sum_{j=1}^M \cos^2(S_j - S'_j)}{M^2} \right\rangle, \tag{3.3}$$

where  $S_j$  is the spin state of the unperturbed system (using the Domb representation),  $S'_j$  is the spin state of the perturbed system, and  $M$  is the number of spins in both systems with  $z > 2$ , which grows with  $N$ . The brackets denote ensemble averaging. For  $\delta = 0$ ,  $r = 1$ . The system is chaotic when

$$\lim_{\delta \rightarrow 0} \lim_{N \rightarrow \infty} r(\delta, N, \phi) < 1. \tag{3.4}$$

It may be that the limit of  $\phi \rightarrow \phi_c$  may also have to be taken to observe chaos given that only at the jamming transition is the system marginally rigid.

In Figure 3.12 we present results for  $r$  as a function of  $N$  for different values of  $\delta$  and  $\phi$ . For fixed  $\phi$ , we observe that  $r$  initially decreases with increasing  $N$  and then begins to level off (though one cannot rule out a small increase in  $r$  for the largest  $N$  studied). Moreover,  $r$  increases with decreasing  $\delta$  for fixed  $N$ , as

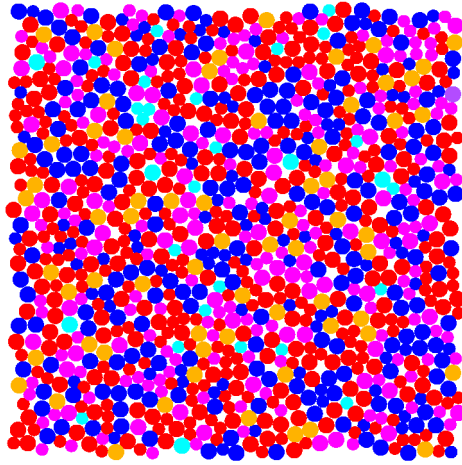


Figure 3.11: Jammed configuration (same as above) colored via coordination number. Light blue denotes  $z = 0$ , magenta denotes  $z = 3$ , red denotes  $z = 4$ , blue depicts  $z = 5$ , orange depicts  $z = 6$ , and purple denotes  $z = 7$  (possible for 1.4 diameter ratio bidisperse system).

expected. Since it is not clear that  $r$  reaches a limit as a function of  $N$  for fixed  $\delta$ , we cannot easily extrapolate to the zero perturbation limit. However, it is clear from the data that as  $\phi$  decreases towards unjamming,  $r$  decreases, indicating that as the jamming transition is approached from above, the system is becoming increasingly chaotic.

### 3.5 Jammed solids, spin glasses, and some speculation

Let us summarize our numerical findings:

- (0) There is a suppression of the smaller angles subtending locally larger force bonds. This suppression increases as  $\phi_c$  is approached from above.
- (1) The probability for spanning of the largest force chain increases as  $\phi_c$  is ap-

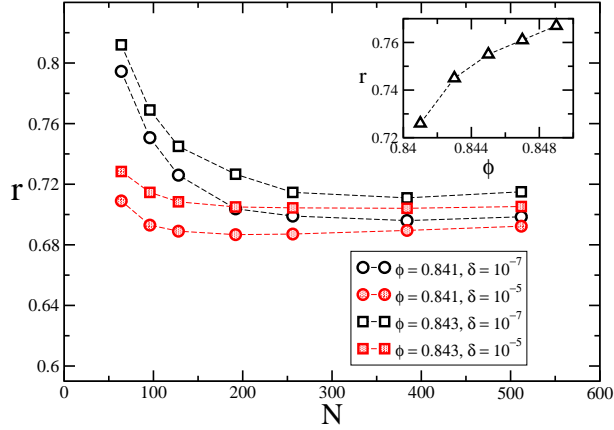


Figure 3.12: Plot of  $r$  as a function of  $N$  for several  $\delta$ s. Inset: Plot of  $r$  for  $N = 128$  as a function of  $\delta$ . The error bars are smaller than the symbols.

proached from above.

(2) The coordination number-spin state mapping suggests that the jammed solid becomes increasingly chaotic as  $\phi_c$  is approached from above.

Keeping the above findings in mind, we recall one of the traditional models of an amorphous solid via a randomly dilute network of springs with probability  $p$ , the model otherwise known as rigidity percolation [106]. While the nature of the rigidity percolation transition remains contentious [107, 108], an important concept has emerged in terms of constraint counting, a concept initially presented by Maxwell back in 1864 [109]. Below the rigidity percolation threshold, there are only underconstrained bonds, above the threshold, there exists overconstrained bonds. At the transition, on average, the system is not overconstrained or underconstrained—it is isostatic. This condition should then determine the location of the transition. For central force interactions,  $p_r = 2d/z$ , where  $d$  is the dimension of the system and  $p_r$  is the occupation probability above which the system is rigid. For the triangular lattice,  $p_r = 2/3$ . Numerical studies find a result close to this estimate. However, the Maxwell argument does not take into

account redundant bonds and the possibility of a fractal set of overconstrained bonds participating in a rigid cluster.

Jacobs and Thorpe have numerically extended Maxwell's argument by identifying those overconstrained bonds via an algorithm implemented on a two-dimensional bar-joint network [110], which makes use of a theorem from Laman [111]. They demonstrate that at the transition, the overconstrained bars make up a fractal subset of the bonds. As more bars are added, the fraction of overconstrained bars increases such that they make up a finite fraction of the bars. It turns out that the fraction of overconstrained bars can be viewed as the order parameter for the rigidity percolation transition.

Indeed, it would be interesting to extend some of these ideas of rigidity percolation more concretely to the repulsive, soft particle system, such as trying to identify the overconstrained bonds via use of the pebble game algorithm. However, use of the pebble algorithm takes into account only fixed connectivity information and it does not take into account the force information. Of course, there have been several recent works drawing a more intimate connection between rigidity percolation and jamming. Ellenbroek and collaborators map the jammed solid to a network of stretched springs [112]. Study of the stretched spring network demonstrates anomalous scaling of the bulk modulus as opposed to the shear modulus. Even more recent work investigates a square lattice occupied by springs [113]. Such a lattice is isostatic with a frequency-independent density of states. As next-nearest springs are occupied, the system undergoes a rigidity percolation transition for an infinitesimal occupation of next-nearest neighbor springs. This system exhibits the kind of transition proposed by the phenomenological framework put forth by Wyart and collaborators [76, 77, 78]. There exists a clear lengthscale below which the system behaves isostatically and above which it does not, which is not so readily apparent in the disordered packing, at least in terms of a direct measurement.



While working within the more traditional spring framework is certainly useful, coupling the coordination number-spin state mapping with the force information via interaction strengths between the spins and the dilution information provides one with an alternate description of a jammed solid—a spin description to be compared to the traditional framework. For example, overconstrained bonds in rigidity percolation may correspond to frozen spins—spins that take on the same state in every configuration—in the spin picture. From the numerical information obtained so far, there are more antiferromagnetic interactions than ferromagnetic interactions. As for the magnitude of the interactions between the spins, recall the chain-like correlations observed in the locally larger force bonds. This information can be also be encoded into a Potts spin Hamiltonian via chain-like correlations in the spin interaction strengths.

How does the Potts spin Hamiltonian change with increasing packing fraction? The amount of dilution decreases. Moreover, the ratio of antiferromagnetic to ferromagnetic interactions also decreases. What about the force information? We observe that the probability of spanning increases with decreasing  $\phi$  for the largest system sizes. Based on this observation, the chain-like correlations in the spin interaction strengths decrease as the packing fraction increases. All of these properties can be encoded into a Potts spin Hamiltonian.

Given the interplay of frustration and randomness, we conjecture that a Potts spin analog of the jammed solid should exhibit spin glass behavior. A possible spin glass/jammed solid correspondence may help to explain the ordinary elasticity findings of Ellenbroek and collaborators at all lengthscales when measuring the system’s averaged response to inflation of a central particle [80, 81]. For both the paramagnet and the spin glass, the average magnetization is zero, i.e. one cannot distinguish between the two phases. To observe the spin glass phase, one must measure higher order quantities such the Edwards-Anderson order parameter. El-

lenbroek and collaborators did observe a deviation from ordinary elasticity when measuring fluctuations in the forces averaged over all contacts within a distance from the perturbation [80, 81]. The lengthscale beyond which the fluctuations level off may correspond to a finite-dimensional spin glass phase, which exhibits very different properties than a mean-field spin glass. The replica, or mean-field, scenario [114, 115] gives evidence for infinite number of pure thermodynamic states, while the low-dimensional, or droplet scenario [116, 117], at least in the Ising case, argues for two groundstates, the same ones occurring in the Ising ferromagnet—all spins up or all spins down. In the droplet picture, an applied magnetic field is a relevant perturbation driving the system to a ferromagnetic phase, while in the replica scenario, an infinitesimally applied magnetic field does not destroy the spin glass phase. How such a lengthscale separating mean-field and low-dimensional behavior could come about is demonstrated in a somewhat technical calculation that we have placed in Appendix A.

## 3.6 Discussion

The existence of force chains have been demonstrated both experimentally [118] and numerically [93]. We numerically demonstrate the existence of chain-like correlations in the locally large forces in the repulsive, soft particle system. This finding may call for an updated effective force chain description with the non-force chain particles providing for long-range interactions along the force chains as the basis of the description. One can test for these long-range interactions by perturbing a force chain locally and observing the response further along the force chain.

Experiments by Majumdar and Behringer [119] have shown an ordering of force chains in the presence of shear. In the absence of shear, the network of locally large

---

force chains is isotropic. In the presence of shear, the force chains align along the shear direction. A reordering of the force chain network structure via non-affine displacements such that the system is inherently anisotropic may account for the anomalous shear modulus exponent found in the repulsive, soft particle system. One can test for this reordering in the repulsive, soft particle system by checking for spanning of the locally large forces in the direction along and perpendicular to the shear separately.

We also propose a coordination number-spin state mapping. With this mapping, we find that the repulsive, soft particle system becomes increasingly chaotic as the the jamming transition is approached from above. More testing of this mapping is needed. For example, one can investigate the response of the system to shear and see how the coordination number changes throughout the system. A changing coordination number corresponds to a changing spin state. It may be that the framework of random spin wave theory (or some alteration thereof) can be used to understand the response of the jammed solid to various perturbations.

Based on the fact that jamming and glass transition share some commonalities, via transitivity, one suspects that the spin glass transition should be related to the jamming transition. A particle (graph) coloring with non-trivial biasing to enforce the isostaticity condition at the onset of jamming may provide us with the third missing link. Whether or not the equivalent spin glass is mean-field or low-dimensional remains to be seen. Of course, both the marginality and the massless, or replicon, modes found in mean-field spin glasses make for a tantalizing match [120, 121]. A link between jammed solids and spin glasses also provides a connection to constraint satisfaction problems. This connection has recently been explored by Mailman and Chakraborty [122] and also by Krazkala and Kurchan [123, 124]. Constraint satisfaction problems are at the heart of attempting to understand what makes problems solvable.

While the phenomenological isostatic framework provides insight into the jamming transition, its success hinges on the measured exponents for system sizes ranging up to approximately 10000 particles currently. History teaches us that the reliance on numerical results for support may ultimately reveal oversimplified assumptions [125]. Hence, the importance of constructing well-defined, calculable toy models of jamming transition cannot be underestimated. Such is the case for  $k$ -core percolation, the simplest model of rigidity percolation [126]. If one allows the  $k$ -core percolation transition to take place as soon as a non-zero spanning  $k$ -core cluster is allowed, i.e. minimal rigidity, then the mean-field exponents are presumably in the same category as those measured for the finite-dimensional repulsive, soft sphere system. Note that minimal rigidity here does not translate to an average bond occupation of four per site. While the  $k$ -core constraint is indeed a local one, it contains the nonlocal feature of rigidity percolation—that the removal of a single bond can trigger the removal of an entire occupied cluster. Other spin systems, such as the dilute 3-state Potts antiferromagnet on the triangular lattice, also exhibit a similar nonlocal property [127]. There exists other work towards calculable models of jammed solids that should be pursued further. For example, see Refs. [128, 129, 130].

In closing, given the connection between spin systems and repulsive, soft particle systems, we expect that construction and study of new spin models with constraints inspired by jamming will pave the way for further insights into the mysteries of jammed solids.

# Chapter 4

## On the non-locality of the fractional Schrödinger equation

### 4.1 Background

A wide variety of stochastic processes are more general than the familiar Brownian motion, but presumably can still be described by modifying the diffusion equation using a fractional Laplacian operator [131, 132]. Such “fractional diffusion” is now a large and active field, and a number of books have been written on the mathematics and physics of fractional diffusion operators [36, 133, 134]. As mentioned in Chapter 1, stochastic processes such as fractional diffusion can be described by Lévy flights. More specifically, the diffusion equation can be modified by replacing the ordinary Laplacian with the fractional Laplacian. The fractional Laplacian generates non-local effects as observed in Lévy flights. The suitable

fractional Laplacian, the Feller-Riesz derivative operator, is defined as

$$\nabla^\alpha f(x, t) = -\frac{1}{2\pi} \int_{-\infty}^{\infty} dk e^{ikx} |k|^\alpha \tilde{f}(k, t), \quad (4.1)$$

where  $\alpha$  is the fractional index and  $\tilde{f}(k, t)$  is the Fourier transform of  $f(x, t)$ . It is easy to see that when  $\alpha = 2$ , the Feller-Riesz derivative operator is equivalent to the ordinary Laplacian. Note that the Lévy index denoted by  $\mu$  in Chapter 1 is now denoted by  $\alpha$  for this chapter.

It is well established that the diffusion process is related to quantum mechanics through the path integral representation where the Schrödinger equation is derived via an integral over Brownian paths. Given the generalization of anomalous diffusion or Lévy paths, N. Laskin extended the idea of the path integral to Lévy paths and, thus, formulated fractional quantum mechanics [135, 136, 137]. By using the quantum Feller-Riesz derivative,

$$(-\hbar^2 \Delta)^{\alpha/2} \psi(x, t) \equiv \frac{1}{2\pi\hbar} \int_{-\infty}^{\infty} dp e^{ipx/\hbar} |p|^\alpha \phi(p, t), \quad (4.2)$$

where  $\phi(p, t) = \int dx \psi(x, t) e^{-ipx/\hbar}$  is the Fourier-transformed wavefunction, Laskin derived the fractional Schrödinger equation as ( $D_\alpha$  is the corresponding "diffusion" constant)

$$i\hbar \frac{\partial \psi(x, t)}{\partial t} = D_\alpha (-\hbar^2 \Delta)^{\alpha/2} \psi(x, t) + V(x, t) \psi(x, t). \quad (4.3)$$

Since then, mathematical physicists have constructed solutions to this equation for various potentials. In particular, a number of familiar potentials, including the free particle, the harmonic oscillator, the delta potential and the infinite square well, have been revisited and exact solutions were claimed to be obtained. In these works, the traditional boundary-matching technique in solving piecewise potentials in ordinary quantum mechanics was applied despite the fact that the quantum

Feller-Riesz derivative, or the fractional Schrödinger operator, is highly non-local thereby invalidating the boundary-matching technique. We have explicitly proved this and will discuss it later. Meanwhile, the free particle solution and delta potential solution are valid and are obtained as follows.

#### 4.1.1 Free particle

The fractional Schrödinger equation for a free particle is

$$i\hbar \frac{\partial \psi(x, t)}{\partial t} = D_\alpha (-\hbar^2 \Delta)^{\alpha/2} \psi(x, t). \quad (4.4)$$

The Fourier transform yields

$$i\hbar \frac{\partial \phi(p, t)}{\partial t} = D_\alpha |p|^\alpha \phi(p, t), \quad (4.5)$$

and this equation is solved via plane waves, or

$$\phi(p, t) = C e^{-iD_\alpha |p|^\alpha t / \hbar}, \quad (4.6)$$

where  $C$  is a constant. This solution mimics the solution of the ordinary free particle Schrodinger equation. From this solution, Laskin derived the uncertainty relation for fractional quantum mechanics, which is expressed as

$$\langle |\Delta x|^\mu \rangle^{1/\mu} \langle |\Delta p|^\mu \rangle^{1/\mu} > \frac{\hbar}{(2\alpha)^{1/\mu}}, \quad (4.7)$$

for  $\mu < \alpha$  and  $1 < \alpha \leq 2$ .

### 4.1.2 Dirac $\delta$ potential

The attractive Dirac  $\delta$  potential is given by  $V(x) = -\gamma\delta(x)$ . The fractional Schrödinger equation is, therefore,

$$i\hbar\frac{\partial\psi(x,t)}{\partial t} = D_\alpha(-\hbar^2\Delta)^{\alpha/2}\psi(x,t) - \gamma\delta(x)\psi(x,t). \quad (4.8)$$

The steady state equation would be (with system energy,  $E$ )

$$D_\alpha(-\hbar^2\Delta)^{\alpha/2}\psi(x) - \gamma\delta(x)\psi(x) = E\psi(x). \quad (4.9)$$

Its Fourier transform is

$$D_\alpha|p|^\alpha\phi(p) - \frac{\gamma}{2\pi\hbar}\int_{-\infty}^{\infty} dp\phi(p) = E\phi(p). \quad (4.10)$$

Let  $\int dp\phi(p) = C$  be a constant and the solution is in the form of

$$\phi(p) = \frac{\gamma}{2\pi\hbar}\frac{C}{D_\alpha|p|^\alpha - E}. \quad (4.11)$$

An inverse Fourier transform yields the solution in real space.

## 4.2 Inquiry

In 2000, Laskin introduced the fractional Schrödinger equation, in which the normal Schrödinger equation is modified in analogy with fractional diffusion [135, 136, 137]. Laskin claimed to exactly solve this equation in the case of the one-dimensional infinite square well [135]. A more recent (2006) work claimed to find solutions again for the infinite one-dimensional square well (agreeing with Laskin's original solution), and for one-dimensional scattering off of a barrier po-



tential [138]. A 2007 work used a different method of analysis to claim solutions for the linear, delta function, and Coulomb potentials in one dimension [139]. Laskin also recently built on the same claimed solution to derive properties of the quantum kernel [140]. Laskin [135, 136, 137] has conjectured that physical realizations of Levy quantum mechanics may be limited to  $1 < \alpha < 2$  where averaged quantities are finite. One could have made a similar conjecture in the classical case, however, there are indeed physical realizations of Levy classical mechanics with  $0 < \alpha \leq 1$ . Therefore, we consider  $0 < \alpha < 2$  in analogy with the classical case.

The purpose of this chapter is to point out that of the many purported exact solutions presented in the literature, only the one for the delta function potential is correct.

We focus on the case where the potential is independent of time, so we are interested in solutions of the following equation:

$$D_\alpha (-\hbar^2 \Delta)^{\alpha/2} \psi(x) + V(x) \psi(x) = E\psi(x). \quad (4.12)$$

The fractional diffusion operator is a *nonlocal* operator except when  $\alpha = 0, 2, 4, \dots$ . This means that  $(-\hbar^2 \Delta)^{\alpha/2} \psi(x)$  depends not just on  $\psi(y)$  for  $y$  near  $x$ , but on  $\psi(y)$  for all  $y$ . This nonlocality, in turn, means that when solving Eq. (4.12), the form of the wavefunction in a given region depends not just on the potential in that region, but on the potential everywhere. Because of this, for a piecewise-defined potential, we cannot follow the normal strategy of solving separately for the wavefunction in each piecewise region, and then using conditions of continuity and differentiability to match up the solutions. However, this is precisely the strategy used in the papers cited above, and the solutions obtained in those papers are thus invalid. We illustrate the problem by looking in some detail at the case

of the one-dimensional infinite square well in Sec. 4.2. The problems with the purported solutions for other potentials are similar, and are discussed in Sec. 4.3. Section 4.4 presents an exact solution for the one-dimensional fractional harmonic oscillator with  $\alpha = 1$ , followed by discussion in Sec. 4.5.

### 4.3 Infinite one-dimensional square well

Consider Eq. (4.12) in the limit of the potential becoming an infinite square well

$$V(x) = \begin{cases} 0 & \text{if } |x| < a \\ \infty & \text{if } |x| \geq a. \end{cases} \quad (4.13)$$

We first note that for the case of free space, where the potential  $V$  is zero *everywhere*, it is easy to see that plane waves are eigenfunctions of the quantum fractional Hamiltonian:

$$(-\hbar^2 \Delta)^{\alpha/2} e^{ipx/\hbar} = |p|^\alpha e^{ipx/\hbar}. \quad (4.14)$$

However, Eq. (4.14) is only valid if the function operated on is  $e^{ipx/\hbar}$  *everywhere*; it is not a local equation that can be applied just in a restricted region. Because the quantum Riesz fractional derivative is a nonlocal operator, the wavefunction in the well knows about the wavefunction and potential outside of the well. Previous works looking at the one-dimensional infinite square well incorrectly applied Eq. (4.14) only inside the well, and concluded that the solution inside the well would be a simple linear superposition of left- and right-moving plane waves of the same energy [135, 138].

Although these papers use an invalid assumption, could their end results be correct nevertheless? Both papers claim that the solutions for the one-dimensional

square well are the same for the fractional case as for the standard non-fractional case, only with modified energies. So, they obtain for the ground state

$$\psi_0(x) = \begin{cases} A \cos\left(\frac{\pi x}{2a}\right) & \text{for } |x| \leq a \\ 0 & \text{otherwise.} \end{cases} \quad (4.15)$$

The Fourier transform of this is

$$\begin{aligned} \phi_0(p) &:= \int_{-\infty}^{+\infty} dx e^{-ipx/\hbar} \psi_0(x), \\ &= -\frac{A\pi\hbar^2}{a} \frac{\cos(ap/\hbar)}{p^2 - (\pi\hbar/2a)^2}. \end{aligned} \quad (4.16)$$

From  $\phi_0(p)$  we can calculate the fractional Riesz derivative:

$$(-\hbar^2\Delta)^{\alpha/2} \psi_0(x) = -\frac{2A}{\pi} \left(\frac{\pi\hbar}{2a}\right)^\alpha \int_0^\infty dp \frac{p^\alpha}{p^2 - 1} \cos\left(\frac{1}{2}\pi p\right) \cos\left(\frac{\pi p x}{2a}\right). \quad (4.17)$$

We see here how the nonlocality manifests itself in the mathematics. If we only looked at the wavefunction inside the square well, then  $\psi_0(x)$  would appear to consist of plane waves of just two wavevectors,  $\pm\pi/(2a)$ . However, in reality,  $\psi_0(x)$  is 0 outside the well, making it a wave packet, rather than just a combination of two plane waves, and so it contains a continuous range of wavevectors, as seen in Eq. (4.16). The fractional Riesz derivative thus sees all these wavevectors.

Now we shall show that  $\psi_0(x)$  is not a solution of the infinite square well via a proof by contradiction. First, assume that  $\psi_0(x)$  is a solution of the fractional Schrödinger equation. Then the fractional Riesz derivative  $(-\hbar^2\Delta)^{\alpha/2} \psi_0(x)$  must be proportional to  $\psi_0(x)$  on the open interval,  $|x| < a$ , where  $V(x) = 0$ . Since,  $\psi_0(x)$  is continuous and  $\psi_0(a) = 0$ , this implies that the limit  $x \rightarrow a^-$  of (4.17) should also vanish. However, this condition is *not* equivalent to (4.17) vanishing at  $x = a$  because the Hamiltonian includes the potential and so we cannot rely on

continuity of  $\psi_0(x)$  at  $x = a$ .

A Fourier transform such as (4.17) is continuous if the integral is absolutely convergent. The integrand in (4.17) is bounded by  $p^\alpha$  for small  $p$  and by  $(1+\epsilon)p^{\alpha-2}$  for large  $p$ . Therefore, (4.17) is indeed a continuous function for all  $x$  for  $-1 < \alpha < 1$ . Thus, for  $-1 < \alpha < 1$ , we can take the limit  $x \rightarrow a^-$  (4.17) by setting  $x = a$ , and if  $\psi_0(x)$  is a solution, this should give zero:

$$f(\alpha) := \int_0^\infty dp \frac{p^\alpha}{p^2 - 1} \cos^2\left(\frac{1}{2}\pi p\right) = 0. \quad (4.18)$$

Taking the derivative with respect to  $\alpha$ , we see

$$\frac{df}{d\alpha} = \int_0^\infty dp \frac{p^\alpha \ln p}{p^2 - 1} \cos^2\left(\frac{1}{2}\pi p\right). \quad (4.19)$$

The integrand in Eq. (4.19) is everywhere positive, so  $df/d\alpha > 0$ , and we cannot have  $f(\alpha) = 0$  for all  $\alpha$ . The ground state (4.15) claimed in Refs. [135] and [138] thus cannot be an solution of the fractional Schrödinger equation for all  $\alpha$ . It can only be a solution once in the interval  $-1 < \alpha < 1$ —namely when  $\alpha = 0$ .

The above argument does not hold for  $1 \leq |\alpha|$  and in fact for some values of  $\alpha$ , (4.17) is not continuous at  $x = a$ . However, a related argument to one presented above shows that this  $\psi_0$  cannot be a solution at least for  $1 < \alpha < 2$ . For  $\alpha = 2$ , on the other hand,  $\psi_0(x)$  actually *is* a solution. Indeed it is a solution whenever the fractional Riesz derivative is an ordinary derivative—that is, for  $\alpha = 0, 2, 4, \dots$

It may seem counterintuitive that Eq. (4.15) is not the correct ground state. The standard ( $\alpha = 2$ ) Schrödinger equation for an infinite potential well is equivalent to the Schrödinger equation on an interval with the Dirichlet boundary conditions  $\psi(-a) = \psi(a) = 0$ . By raising that Hamiltonian to the power  $\alpha/2$  we get a plausible fractional Laplacian and Eq. (4.15) is indeed a solution. However, this is *not* the Riesz fractional derivative. In other words, the fractional Schrödinger

equation for an infinite potential well is not equivalent to the fractional Schrödinger equation on an interval.

At this point, we do not know what the true solutions are for values of  $\alpha$  other than 0, 2, 4, . . . . In Ref. [141], Zoia *et al.* find numerical solutions for the ground state. The solutions depend on  $\alpha$  and differ from the simple sine wave solution in Eq. (4.15).

## 4.4 Other systems

While we have only discussed the infinite one-dimensional square well in detail, the comments here equally invalidate the other claimed solutions of the fractional Schrödinger equation. For example, in Section II of Ref. [139], the linear potential,

$$V(x) = \begin{cases} Fx & \text{if } x \geq 0 \\ \infty & \text{if } x < 0 \end{cases}, \quad (4.20)$$

is studied. The authors of Ref. [139] treat this equation in a piecewise approach by solving the equation for the potential  $V(x) = Fx$  and applying a boundary condition at  $x = 0$ . This is invalid for the same reasons stated above for the square well potential. Similar comments apply to the analysis of the Coulomb potential in section IV of that same paper.

Our comments, however, do not invalidate the analysis of the delta function potential in Section III of Ref. [139], which did not implement a piecewise approach, but instead worked with the Fourier transform of the delta function potential. However, the authors of Ref. [139] fail to note that the bound state for the delta function potential is valid only for  $\alpha \geq 1$ . For  $\alpha \leq 1$ , there is no bound state since the integral in Eq. 33 of Ref. [139] diverges. In more recent work, Dong and Xu [142] attempt to solve the same problem again, using a piecewise approach.

They then compare this to their initial correct solution and derive an incorrect identity for the H-function.

## 4.5 The fractional harmonic oscillator

Consider the fractional Schrödinger equation with the potential

$$V(x) = \frac{1}{2}kx^2. \quad (4.21)$$

Fourier transforming Eq. (4.12) gives

$$\frac{1}{2}k\hbar^2 \frac{d^2\phi}{dp^2} = (D_\alpha |p|^\alpha - E)\phi(p). \quad (4.22)$$

In momentum space, the equation maps to the ordinary Schrödinger equation with a positive  $\alpha$  power law potential and  $k = 1/m$ . In other words, the kinetic and potential energies have reversed roles.

### 4.5.1 WKB approximation

Given the mapping to ordinary quantum mechanics, in the limit  $\hbar \rightarrow 0$ , one can use the WKB approximation in momentum space to approximate the energy eigenvalues, with  $p$  replacing  $x$ . The quantization condition in momentum space is

$$\int_{p_1}^{p_2} \lambda(p) dp = (n + \frac{1}{2})\pi\hbar, \quad n \in \{0\} \cup \mathcal{Z}^+, \quad (4.23)$$

where  $\lambda(p) = \sqrt{\frac{2}{k}(E - D_\alpha |p|^\alpha)}$ , and  $p_1$  and  $p_2$  are the classical turning points, i.e.

$p_{1,2} = \pm(E/D_\alpha)^{1/\alpha}$ . The above condition leads to

$$E_n = \left( \frac{(n + \frac{1}{2})\hbar\pi\sqrt{k}(D_\alpha)^{1/\alpha}\Gamma(\frac{3}{2} + \frac{1}{\alpha})}{2\sqrt{2}\Gamma(\frac{3}{2})\Gamma(1 + \frac{1}{\alpha})} \right)^{\frac{2\alpha}{2+\alpha}}. \quad (4.24)$$

This agrees with Laskin's more general WKB result [143] for an arbitrary power-law potential. However, by the argument we have just given, this special case is better justified than Laskin's general claim. It is unclear whether there is any reason to believe the WKB approximation to be valid for systems other than the harmonic oscillator, since for other potentials, the Fourier transform of the fractional Schrödinger equation will not be an ordinary Schrödinger equation.

#### 4.5.2 An exact solution for $\alpha = 1$

When  $\alpha = 1$ , Eq. (4.22) becomes

$$\frac{1}{2}k\hbar^2\frac{d^2\phi}{dp^2} = (D_1|p| - E)\phi(p). \quad (4.25)$$

Restricting to  $p > 0$  or  $p < 0$ , this differential equation is equivalent to the Airy equation (by a rescaling transformation). For a normalizable wavefunction, we must have  $\phi(p = \infty) = \phi(p = -\infty) = 0$ . This condition rules out Airy functions of the second kind ( $\text{Bi}(z)$ ) as solutions. Because of the symmetry of the potential, the solutions are alternately symmetric or antisymmetric. More precisely,

$$\phi(p) = (\text{sgn } p)^n \text{Ai}(\kappa|p| - r_n), \quad (4.26)$$

where  $\kappa \equiv (2D_1/(k\hbar^2))^{1/3}$ , and the  $r_n$ 's are the successive roots of  $\text{Ai}'$  (for  $n$  even), or of  $\text{Ai}$  (for  $n$  odd). The energy eigenvalues are

$$E_n = - \left( \frac{k}{2}\hbar^2 D_1^2 \right)^{1/3} r_n. \quad (4.27)$$

Note that  $r_n < 0$ , so  $E_n > 0$ .

Using the asymptotic expansion of the Airy function, we find that the roots are well approximated by

$$r_n \approx - \left( \frac{3\pi}{4} \left( n + \frac{1}{2} \right) \right)^{2/3}, \quad n \in \{0\} \cup \mathcal{Z}^+ \quad (4.28)$$

in the limit of large  $n$ . This approximation reproduces the result of the WKB approximation above. This approximate formula is off by 8.7% for  $n = 0$ , 0.77% for  $n = 1$ , and 0.41% for  $n = 2$ , and rapidly becomes more accurate for larger  $n$ . Inserting Eq. (4.28) into Eq. (4.27) thus gives a very good approximate formula for the energies of the simple harmonic oscillator for  $\alpha = 1$ .

## 4.6 Discussion

It would be useful to know the correct groundstate of the one-dimensional infinite square well or harmonic oscillator for general  $\alpha$ , but this is a difficult problem. In Ref. [144], Bañuelos *et al.* needed a lengthy proof merely to show that the groundstate solution for the infinite square well in the region  $(-1, 1)$  is concave on the interval  $(-\frac{1}{2}, +\frac{1}{2})$ .

Similar technical issues regarding nonlocality have arisen in the statistical mechanics community as well. For example, in Ref. [145], the authors claimed to analytically determine the mean first passage time for a Lévy flight with absorbing boundary conditions on the interval  $[0, 1]$ . They did so by imposing the standard absorbing boundary conditions for the probability density at  $x = 0$  and  $x = L$ . However, a subsequent publication [146] pointed out that due to the nonlocal nature of the Lévy flight, the correct boundary condition is for the probability density to vanish for all  $x \leq 0$ , and for all  $x \geq L$ , rendering the analysis in Ref. [145] invalid.



Finally, one must also ask about possible physical realizations of the fractional Schrödinger equation. In Ref. [141], Zoia, Rosso, and Kardar constructed a lattice model whose continuum limit is described by fractional diffusion using symmetric Toeplitz matrices. A quantum representation of this model via a mesoscopic network of long range connections whose hopping amplitudes are described by the entries of these matrices may be a realization of the fractional Schrödinger equation. Further modification could lead to experimental tests of the problems we have discussed here.

# Appendix A

## Long-range, one-dimensional Potts glass

Here we analyze the one-dimensional, long-range interacting  $p$ -state Potts glass with Gaussian distributed quenched bond randomness. There exists previous analysis of the one-dimensional, long-range interacting Ising spin glass. In light of our coordination number-spin state mapping, we extend these results to the Potts glass case.

Why study a model with long-range interactions? The chain-like correlations in the forces may call for an effective theory centered on these chains with the non-force chain bonds providing for long-range forces along the chain. In fact, the existence of these chain-like correlations is reminiscent of a picture proposed earlier by Cates and collaborators [147] where the jammed solid is comprised of linear force chains and a sea of spectator particles modeled as an incompressible solvent. Instead of considering the force chain as a linear object supporting loads only along its own axis, consider the force chain as a polymer—a polymer embedded in solution, i.e. the other particles. Just as the hydrodynamics of the solution couple one

part of the polymer with a distant part, resulting in long-range interactions along the polymer, the force chain would also experience long-range interactions [148]. We note that the polymer-in-solution analogy has its shortcomings. A more accurate analogy might be a polymer embedded in another polymer-type medium. Also, presumably the particles participating in the largest force chain would no longer be part of the largest force chain upon shearing or other perturbations. In other words, there is particle conversion between the force chain and non-force chain particles.

How would this effective force chain framework depend on the packing fraction? At the onset of jamming, presumably there exists an isotropic, fractal network of larger force spanning chains. As the packing fraction is increased, the larger force chains become shorter such that eventually there is no distinction between the chains and the other particles since the definition of a force chain would have to be relaxed in order to achieve spanning. So the lengthscale of the chain lattice shrinks as packing fraction is increased and the long-ranged interactions become screened out just in the case of many polymers in solution. At a particular packing fraction; while for lengthscales smaller than “chain” lattice, the system behaves long-ranged, or mean-field-like; for lengthscales larger than “chain” lattice, the long-range interactions are screened out and the system behaves as a low-dimensional system. Therefore, within one system, one can interpolate between mean-field and finite-dimensions due to the correlated heterogeneity in the forces/interactions.

While a precise formulation of an effective force chain theory is not yet within reach, we discuss the possible ramifications of long-range interactions in a conventional spin glass system. We begin with the  $p$ -state Potts glass Hamiltonian in  $d$ -dimensions,

$$H = - \sum_{i,j} \frac{J_{ij}}{|i-j|^\sigma} \sum_{a=1}^{p-1} S_{ia} S_{ja}, \quad (\text{A.1})$$

where  $\mathbf{S}_i$  is a  $p$ -state Potts spin in the simplex representation [149] at site  $i$  and  $\sigma$  denotes the interaction range. The distribution of the coupling constant  $J_{ij}$  is given by

$$P(J_{ij}) = \frac{1}{\sqrt{2\pi}J^2} e^{-(J_{ij}-J_0)^2/2J^2}.$$

The replica trick is applied to the Hamiltonian to compute the free energy averaged over disorder by considering  $n$  identical replicas of the original system. The averaged free energy,  $F$ , is then given by

$$F = -k_B T \lim_{n \rightarrow 0} \frac{\overline{Z^n} - 1}{n}, \quad (\text{A.2})$$

where

$$\overline{Z^n} = \int \left( \prod_{i,j} P(J_{ij}) dJ_{ij} \right) \text{Tr}_{\{S_i^\alpha\}} \exp \left\{ \sum_{\alpha=1}^n \sum_{i,j} \frac{J_{ij}}{k_B T |i-j|^\sigma} \sum_{a=1}^{p-1} S_{ia}^\alpha S_{ja}^\alpha \right\}.$$

After integrating over the disorder and applying the Hubbard-Stratonovich transformation,

$$\overline{Z^n} = \int \prod_{\substack{\alpha \neq \beta \\ a,b}} dQ_{i,ab}^{\alpha\beta} \exp \left\{ -\frac{1}{2} K_{ij}^{-1} Q_{i,ab}^{\alpha\beta} Q_{j,ab}^{\alpha\beta} \right\} \text{Tr}_{\{S_i^\alpha\}} \exp \left\{ S_{ia}^\alpha S_{ib}^\beta Q_{i,ab}^{\alpha\beta} \right\}, \quad (\text{A.3})$$

where the matrix  $K$  is defined by

$$K_{ij} = \frac{J^2}{(k_B T)^2} \frac{1}{|i-j|^{2\sigma}} \quad (\text{A.4})$$

and  $\frac{J_0}{J} < \frac{4-p}{2}$  with  $J = k_B T_g$  such that we set the ferromagnetic order parameter to zero.

To perform the trace over the spins, we recall that the simplex representation of the  $p$ -state Potts model requires

$$\begin{aligned}
\sum_s e_a^s e_b^s &= p\delta_{ab}, \\
\sum_a e_a^s e_a^{s'} &= p\delta_{ss'} - 1, \\
\sum_s e_a^s &= 0,
\end{aligned} \tag{A.5}$$

where in the replicated partition function each  $S_{ia}$  is represented by one of the  $e_a$ 's. We also define  $v_{abc} = \sum_s e_a^s e_b^s e_c^s$  for convenience [150]. We expand the second exponential term in Eq. 7 to order  $Q^3$ , and after computing the trace and re-exponentiation, we obtain

$$\begin{aligned}
Tr_{\{S_i^\alpha\}} \exp \left\{ S_{ia}^\alpha S_{ib}^\beta Q_{i,ab}^{\alpha\beta} \right\} &= \frac{1}{4} \sum_{\alpha \neq \beta} (Q_{i,ab}^{\alpha\beta})^2 + \frac{1}{6} \sum_{\alpha \neq \beta \neq \gamma} Q_{i,ab}^{\alpha\beta} Q_{i,bc}^{\beta\gamma} Q_{i,ca}^{\gamma\alpha} \\
&+ \frac{1}{12} \sum_{\alpha \neq \beta} \frac{v_{abc} v_{def}}{p^2} Q_{i,ad}^{\alpha\beta} Q_{i,be}^{\alpha\beta} Q_{i,cf}^{\alpha\beta} + \mathcal{O}((Q_{i,ab}^{\alpha\beta})^4).
\end{aligned} \tag{A.6}$$

After taking the continuum limit, we rewrite  $\overline{Z}^n$  in momentum space as

$$\overline{Z}^n = \int \prod_{\substack{(\alpha,\beta) \\ a,b}} dQ_{ab}^{\alpha\beta}(\vec{q}) \exp\left(-\int d^d \vec{q} H\{Q_{ab}^{\alpha\beta}(\vec{q})\}\right) \tag{A.7}$$

with

$$\begin{aligned}
H &= \frac{1}{4} \int_q \sum_{\alpha \neq \beta} (r + q^{2\sigma-d}) Q_{ab}^{\alpha\beta}(\vec{q}) Q_{ab}^{\alpha\beta}(-\vec{q}) \\
&- \frac{1}{6} v \int_{q_1 q_2 q_3} \sum_{\alpha \neq \beta \neq \gamma} (2\pi)^d \delta(\vec{q}_1 + \vec{q}_2 + \vec{q}_3) Q_{ab}^{\alpha\beta}(\vec{q}_1) Q_{bc}^{\beta\gamma}(\vec{q}_2) Q_{ca}^{\gamma\alpha}(\vec{q}_3) \\
&- \frac{1}{2} u \int_{q_1 q_2 q_3} \sum_{\alpha \neq \beta} (2\pi)^d \delta(\vec{q}_1 + \vec{q}_2 + \vec{q}_3) Q_{ad}^{\alpha\beta}(\vec{q}_1) Q_{be}^{\alpha\beta}(\vec{q}_2) Q_{cf}^{\alpha\beta}(\vec{q}_3) v_{abc}^\alpha v_{def}^\beta,
\end{aligned} \tag{A.8}$$

where  $r$ ,  $u$ , and  $v$  are the coupling constants and  $\int_q = \int \frac{d^d \vec{q}}{(2\pi)^d}$ . We have omitted a

$q^2 Q_{ab}^{\alpha\beta}(\vec{q}) Q_{ab}^{\alpha\beta}(-\vec{q})$  term.

Performing the momentum shell renormalization group with one-loop corrections using the usual notation [151], we obtain

$$\begin{aligned}
 r' &= \zeta^2 b^{-d} (r - (-2(p-1)v^2 + 18p^4(p-2)^2 u^2) C(b)) \\
 v' &= \zeta^3 b^{-2d} (v + (-3p+4)v^3 D(b)) \\
 u' &= \zeta^3 b^{-2d} (u + 36u^3 p^4 (p-3)^2 D(b)) \\
 \zeta &= b^{1+d/2-\eta/2}
 \end{aligned} \tag{A.9}$$

where  $C(b) = \int_{1/b}^1 \frac{d^d \vec{q}}{(2\pi)^d (q^{2\sigma-d} + r)^2}$  and  $D(b) = \int_{1/b}^1 \frac{d^d \vec{q}}{(2\pi)^d q^{3(2\sigma-d)}}$ . Since the renormalization group does not generate new long-range terms,  $\eta = 2 + d - 2\sigma$  to all orders. Therefore, for  $\sigma < \frac{2d}{3}$ , both cubic couplings are irrelevant and the critical behaviour is mean-field [152] with Gaussian fluctuations. For  $\sigma > \frac{2d}{3}$ , the cubic terms become relevant and different critical behaviour is observed.

The modified value of  $\eta = 2 + d - 2\sigma$  is a general feature of long-range interactions. The  $v$  and  $u$  terms are irrelevant at  $\sigma < 2/3$  in the one-dimensional case. Thus, the system behaves mean-field-like when  $1/2 < \sigma < 2/3$ , where the lower bound  $\sigma < 1/2$  assures the convergence of free energy. This result is a simple generalization of the previous  $p = 2$  case [153, 154] and the short-range case [155]. Modifying the range of the interaction corresponds to modifying the effective spatial dimension of the system from low-dimensional to mean-field. This property has been numerically verified in the  $p = 2$  case and the 3-spin spin glass [156, 157]. In the jammed solid, the interaction range is presumably tuned by the presence of other spanning force chains (Potts chains). On lengthscales smaller than the chain lattice, the long-range interaction dominates and above this lengthscale, the short-range interaction dominates.

# Bibliography

- [1] T. E. Harris, "Contact interactions on a lattice", *Ann. Prob.*, **2**, 969 (1974).
- [2] T. M. Liggett, "Interacting Particle Systems" (Springer-Verlag, New York), (1985). Also see B. Derrida, E. Domany, and D. Mukamel, "An exact solution of the one dimensional asymmetric exclusion model with open boundaries", *J. Stat. Phys.* **69**, 667 (1992).
- [3] C. T. MacDonald and J. H. Gibbs, "Concerning the kinetics of polypeptide synthesis on polyribosomes", *Biopolymers* **7**, 707 (1969).
- [4] M. Mezard, G. Parisi, and A. Zee, "Spectra of euclidean random matrices", *Nuclear Physics B*, **559**, 689 (1999).
- [5] M. E. Fisher, "Walks, walls, wetting, and melting", *J. Stat. Phys.* **34**, 665 1984.
- [6] L. Corte, P. M. Chaikin, J. P. Gollub, and D. J. Pine, "Random organization in periodically driven systems", *Nature Physics*, **4**, 420 (2008).
- [7] D. A. Huse and M. E. Fisher, "Commensurate melting, domain walls, and dislocations", *Phys. Rev. B* **29**, 239 (1984).
- [8] P. J. Forrester, "Vicious random walkers in the limit of a large number of walkers", *J. Stat. Phys.* **46**, 767 (1989).

- 
- [9] F. J. Dyson, "A Brownian-motion model for the eigenvalues of a random matrix", *J. Math. Phys.* **3**, 1191 (1962).
- [10] J. Baik, "Random vicious walks and random matrices", *Commun. Pure Appl. Math.* **53**, 1385 (2000) .
- [11] J. W. Essam and A. J. Guttmann, "Vicious walkers and directed polymer networks in general dimensions" *Phys. Rev. E* **52**, 5849 (1995).
- [12] G. M. Viswanathan, V. Afanasyev, S. V. Buldyrev, E. J. Murphy, P. A. Prince, and H. E. Stanley, "Lévy flight search patterns of wandering albatrosses", *Nature* **381**, 413 (1996).
- [13] M. A. Lomholt, B. van den Broek, S.-M. J. Kalisch, G. J. L. Wuite, and R. Metzler, "Facilitated diffusion with DNA coiling", *PNAS* **106**, 8204 (2009).
- [14] B. Bergersen and Z. Racz, "Dynamical generation of long-range interactions: Random Lévy flights in the kinetic Ising and spherical models", *Phys. Rev. Lett.*, **67**, 3047 (1991).
- [15] P. Barthelemy, J. Bertolotti, and D. S. Wiersma, "A Lévy flight for light", *Nature*, **453**, 495 (2008).
- [16] T. Koren, M. A. Lomholt, A. V. Chechkin, J. Klafter, and R. Metzler, "Leapover Lengths and First Passage Time Statistics for Lévy Flights", *Phys. Rev. Lett.*, **99**, 160602 (2007).
- [17] M. E. Fisher and M. P. Gelfand, "The reunions of three dissimilar vicious walkers", *J. Stat. Phys.* **53**, 175 (1988).
- [18] K. Winkler and A. J. Bray, "Drowsy cheetah hunting antelopes: A diffusing predator seeking fleeing prey", *J. Stat. Mech.*, P02005, (2005).



- 
- [19] A. J. Bray and K. Winkler, "Vicious walkers in a potential", *J. Phys. A* **37**, 5394 (2004).
- [20] D. S. Lemons, *An introduction to stochastic processes in physics* (The Johns Hopkins University Press, Baltimore, 2002).
- [21] H. A. Kramers, "Brownian motion in a field of force and the diffusion model of chemical reactions", *Physica* **7**, 304 (1941).
- [22] R. Fukushima, A. Tanida, and K. Yano, "Non-Markovian property of certain eigenvalue processes analogous to Dyson's model", *Adv. Stud. Pure Math.* **57**, 119 (2010).
- [23] T. W. Burkhardt, "Semiflexible polymer in the half plane and statistics of the integral of a Brownian curve", *J. Phys. A: Math. Gen.* **26**, L1157 (1993).
- [24] A. C. Maggs, D. A. Huse and S. Leibler, "Unbinding Transitions of Semi-flexible Polymers", *Europhys. Lett.* **8**, 615 (1989).
- [25] T. W. Marshall and E. J. Watson, "A drop of ink falls from my pen. . . it comes to earth, I know not when", *J. Phys. A: Math. Gen.* **18**, 3531 (1985).
- [26] Y. G. Sinai, Distribution of some functionals of the integral of a random walk, *Theor. Math. Phys.* **90**, 219 (1992).
- [27] J. M. Schwarz and R. Maimon, First-passage-time exponent for higher-order random walks: Using Levy flights, *Phys. Rev. E* **64**, 016120 (2001).
- [28] E. Sparre Andersen, On the fluctuation of sums of random variables, *Math. Scand.* **1**, 263 (1953) .

- [29] W. Feller *An Introduction of Probability Theory and its Applications*, (Wiley, New York), (1966).
- [30] S. N. Majumdar, A. Comtet, and R. M. Ziff, "Unified solution of the expected maximum of a discrete time random walk and the discrete flux to a spherical trap", *J. Stat. Phys.* **122**, 833 (2006).
- [31] P. Grassberger and W. Nadler, "Go with the winners' simulations", in: K. H. Hoffman, M. Schreiber (eds.), *Computational Statistical Physics - From Billiards to Monte Carlo* (Springer, Berlin) (2002), pp. 169-190.
- [32] S. Redner, *A guide to first-passage processes* (Cambridge University Press, New York) (2001).
- [33] D. J. Bicout and T. W. Burkhardt, "Absorption of a randomly accelerated Particle: Gambler's ruin in a different game", *J. Phys. A* **33**, 6835 (2000).
- [34] P. Cizeau and J. P. Bouchaud, "Theory of Levy matrices", *Phys. Rev. E* **50**, 1810 (1994).
- [35] I. Goncharenko and A. Gopinathan, "Vicious Levy Flights", *Phys. Rev. Lett.* **105**, 190601 (2010).
- [36] I. Podlubny, *Fractional Differential Equations* (Academic Press, London, 1999).
- [37] S. S. Samko, A. A. Kilbas, and O. I. Martichev, *Fractional Integral and Derivatives* (Gordon and Breach, New York, 1993).
- [38] R. A. Mantegna and H. E. Stanley, "Stochastic process with ultraslow convergence to a Gaussian: The truncated Lévy flight", *Phys. Rev. Lett.* **73**, 2946 (1994).

- 
- [39] A. N. Kolmogorov, *Dokl. Acad. Sci. USSR***36**, 115 (1940).
- [40] J.-H. Jeon, A. V. Chechkin, and R. Metzler, "First passage behaviour of fractional Brownian motion in two-dimensional wedge domains", *Eur. Phys. Lett.* **94**, 20008 (2011).
- [41] D. ben-Avraham, B. M. Johnson, C. A. Monaco, P. L. Krapivsky, and S. Redner, "Ordering of random walks: The Leader and the Laggard", *J. Phys. A: Math. Gen.* **36**, 1789 (2003).
- [42] D. Stauffer and A. Aharony, *Introduction to percolation theory, 2nd ed.*, Taylor and Francis, New York (1992).
- [43] H. Hinrichsen, "Nonequilibrium Critical Phenomena and Phase Transitions into Absorbing States", *Adv.Phys.* **49**, 815 (2000).
- [44] H.-K. Janssen, "On the nonequilibrium phase transition in reaction-diffusion systems with an absorbing stationary state", *Z. Phys., B* **42**, 151 (1981).
- [45] S. S. Manna, "Two-state model of self-organized criticality", *J. Phys. A: Math. Gen.*,**24**, L363 (1991).
- [46] M. Rossi, R. Pastor-Satorras, and A. Vespignani, "Universality Class of Absorbing Phase Transitions with a Conserved Field", *Phys. Rev. Lett.*,**85**, 1803 (2000).
- [47] R. Pastor-Satorras, and A. Vespignani, "Field theory of absorbing phase transitions with a non-diffusive conserved field", *Physical Review E*,**62**, 5875 (2000).

- [48] E. R. Weeks, J. C. Crocker, A. C. Levitt, A. Schofield, and D. A. Weitz, "Three-dimensional direct imaging of structural relaxation near the colloidal glass transition", *Science* **287**, 627 (2000).
- [49] W. Kob and H. C. Andersen, "Kinetic lattice-gas model of cage effects in high-density liquids and a test of mode-coupling theory of the ideal-glass transition", *Phys. Rev. E*, **48**, 4364 (1993).
- [50] C. Toninelli, G. Biroli, and D. S. Fisher, "Spatial Structures and Dynamics of Kinetically Constrained Models of Glasses", *Phys. Rev. Lett.* **92**, 185504 (2004) .
- [51] G. H. Fredrickson and H. C. Andersen, "Kinetic Ising Model of the Glass Transition", *Phys. Rev. Lett.* **53**, 1244 (1984).
- [52] F. van Wijland, K. Oerding, and H. J. Hilhorst, "Wilson renormalization of a reaction-diffusion process", *Physica A*, **251**, 179 (1998).
- [53] D. Blankschtein and A. Aharony, "Crossover from fluctuation-driven continuous transitions to first-order transitions", *Phys. Rev. Lett.* **47**, 439 (1981).
- [54] S. B. Lee and S. -G. Lee, "Validity of scaling relations in absorbing phase transitions with a conserved field", *Phys. Rev. E*, **78**, 040103(R) (2008).
- [55] A. Gabel, P. L. Krapivsky, and S. Redner, "Facilitated asymmetric exclusion", *Phys. Rev. Lett.* **105**, 210603 (2010).
- [56] A. J. Liu, S. R. Nagel, W. van Saarloos, and M. Wyart, "The jamming scenario - an introduction and outlook", Chapter in Dynamical heterogeneities in glasses, colloids, and granular media, Editors: L.

- Berthier, G. Biroli, J-P Bouchaud, L. Cipeletti and W. van Saarloos, (Oxford University Press), 2010.
- [57] A. J. Liu and S. R. Nagel, “Nonlinear dynamics - Jamming is not just cool anymore”, *Nature* **396**, 21 (1998).
- [58] A. J. Liu and S. R. Nagel, eds. *Jamming and rheology: Constrained dynamics on microscopic and macroscopic scales*, Taylor and Francis, New York (2001).
- [59] E. Donth, *The glass transition*, Springer, New York (2001).
- [60] C. S. O’Hern, S. A. Langer, A. J. Liu, and S. R. Nagel, “Random packings of frictionless particles”, *Phys. Rev. Lett.* **88**, 075507 (2002).
- [61] C. S. O’Hern, L. E. Silbert, A. J. Liu, and S. R. Nagel, “Jamming at zero temperature and zero applied stress: The epitome of disorder”, *Phys. Rev. E* **68**, 011306 (2003).
- [62] D. J. Durian, “Foam mechanics at the bubble scale”, *Phys. Rev. Lett.* **75**, 4780 (1995).
- [63] T. S. Majmudar, M. Sperl, S. Luding, and R. P. Behringer, ”The Jamming Transition in Granular Systems”, *Phys. Rev. Lett.* **98**, 058001 (2007).
- [64] J. M. Kosterlitz and D. J. Thouless, “Ordering, metastability and phase transitions in two-dimensional systems”, *J. Phys. C* **6**, 181 (1973).
- [65] Z. Zeravcic, W. van Saarloos, and D. R. Nelson, “Localization behavior of vibrational modes in granular packings”, *Eur. Phys. Lett.* **83**, 44001 (2008).
- [66] L. E. Silbert, A. J. Liu, and S. R. Nagel, “Normal modes in model jammed systems in three dimensions”, *Phys. Rev. E* **79**, 021308 (2009).

- 
- [67] B. B. Laird and H. R. Schober, “Localized low-frequency vibrational modes in a simple model glass”, *Phys. Rev. Lett.* **66**, 636 (1991).
- [68] J. Fabian and P. B. Allen, “Thermal expansion and Gruneisen parameters of amorphous silicon: A realistic model calculation”, *Phys. Rev. Lett.* **79**, 1885 (1997).
- [69] A. Widmer-Cooper, H. Perry, P. Harrowell, and D. R. Reichman, “Irreversible reorganization in a supercooled liquid originates from localized soft modes”, *Nat. Phys.* **4**, 711 (2008).
- [70] V. K. de Souza and P. Harrowell, “Rigidity percolation and the spatial heterogeneity of soft modes in disordered materials”, *Proc. Natl. Acad. Sci.* **106**, 15136 (2009).
- [71] R. C. Zeller and R. O. Pohl, “Thermal conductivity and specific heat of noncrystalline solids”, *Phys. Rev. B* **4**, 2029 (1971).
- [72] M. D. Ediger, C. A. Angell, and S. R. Nagel, “Supercooled liquids and glasses”, *J. Phys. Chem.* **100**, 13200 (1996)
- [73] T. Nakayama, “Boson peak and terahertz frequency dynamics of vitreous silica”, *Rep. Prog. Phys.* **65**, 1195 (2002).
- [74] S. Henkes, C. S. O’Hern, and B. Chakraborty, “Entropy and temperature of a static granular assembly: An ab initio approach”, *Phys. Rev. Lett.* **99**, 038002 (2007).
- [75] S. Henkes and B. Chakraborty, “Jamming as a critical phenomenon: A field theory of zero-temperature grain packings”, *Phys. Rev. Lett.* **95**, 198002 (2005).

- [76] M. Wyart, S. R. Nagel, and T. A. Witten, “Geometric origin of excess low-frequency vibrational modes in weakly connected amorphous solids”, *Eur. Phys. Lett.* **72**, 486 (2005).
- [77] M. Wyart, L. E. Silbert, S. R. Nagel, and T. A. Witten, “Effects of compression on the vibrational modes of marginally jammed solids”, *Phys. Rev. E*, **72**, 051306 (2005).
- [78] A. J. Liu, M. Wyart, W. van Saarloos, and S. R. Nagel, “The jamming scenario – an introduction and outlook”, submitted to a book on Dynamical Heterogeneities and Glasses, edited by L. Cipeletti *et al.* (February 2010).
- [79] L. E. Silbert, A. J. Liu, and S. R. Nagel, “Vibrations and diverging length scales near the unjamming transition”, *Phys. Rev. Lett.* **95**, 098301 (2005).
- [80] W. G. Ellenbroek, E. Somfai, M. van Hecke, and W. van Saarloos, “Critical scaling in linear response of frictionless granular packings near jamming”, *Phys. Rev. Lett.* **97**, 258001 (2006).
- [81] W. G. Ellenbroek, M. van Hecke, and W. van Saarloos, “Jammed frictionless disks: Connecting local and global response”, *Phys. Rev. E* **80**, 061307 (2009).
- [82] C. -h. Liu, S. R. Nagel, D. A. Schecter, S. N. Coppersmith, S. Majumdar, O. Narayan and T. A. Witten, ”Force Fluctuations in Bead Packs”, *Science* , **269**, 513 (1995).
- [83] T. S. Majmudar, and R. P. Behringer, ”Contact force measurements and stress-induced anisotropy in granular materials”, *Nature*, **435**, 1079 (2005).

- 
- [84] A. R. T. van Eerd, W. G. Ellenbroek, M. van Hecke, J. H. Snoeijer, and T. J. H. Vlugt, "Tail of the contact force distribution in static granular materials", *Phys. Rev. E*, **75**, 060302(R) (2007).
- [85] G. Parisi and F. Zamponi, "Mean-field theory of hard sphere glasses and jamming", *Rev. Mod. Phys.* **82**, 789 (2010).
- [86] C. S. O'Hern, S. A. Langer, A. J. Liu, and S. R. Nagel, "Force distributions near jamming and glass transitions", *Phys. Rev. Lett.* **86**, 111 (2001)
- [87] A. R. T. van Eerd, W. G. Ellenbroek, M. van Hecke, J. H. Snoeijer, and T. J. H. Vlugt, "Tail of the contact force distribution in static granular materials", *Phys. Rev. E* **75**, 060302(R) (2007).
- [88] J. Zhou and A. D. Dinsmore, "A statistical model of contacts and forces in random granular media", *J. Stat. Mech.* **5**, L05001 (2009).
- [89] P. Chaudhuri, L. Berthier, and S. Sastry, "Jamming transitions in amorphous packings of frictionless spheres occur over a continuous range of volume fractions", *Phys. Rev. Lett.* **104**, 165701 (2010).
- [90] M. P. Ciamarra, M. Nicodemi, and A. Coniglio, "Recent results on the jamming phase diagram", *Soft Matt.* **6**, 2871 (2010).
- [91] C. F. Schrek, C. S. O'Hern, and L. E. Silbert, "Tuning jammed frictionless disk packings from isostatic to hyperstatic", *Phys. Rev. E* **84**, 011305 (2011).
- [92] D. Vagberg, P. Olsson, and S. Teitel, "Glassiness, rigidity, and jamming of frictionless soft core disks", *Phys. Rev. E* **83**, 031307 (2011).
- [93] H. A. Makse, D. L. Johnson, and L. M. Schwartz, "Packing of compressible materials", *Phys. Rev. Lett.* **84**, 4160 (2000).



- 
- [94] S. Ostojic, E. Somfai, and B. Nienhuis, “Scale invariance and universality of force networks in static granular matter”, *Nature* **439**, 16 (2006).
- [95] S. Henkes, K. Shundyak, W. van Saarloos, and M. van Hecke, “Local contact numbers in two-dimensional packings of frictional disks”, *Soft. Matt.* **6**, 2935 (2010).
- [96] S. F. Edwards and P. W. Anderson, “Theory of spin glasses”, *J. Phys. F: Metal. Phys.* **5**, 965 (1975).
- [97] D. Sherrington and S. Kirkpatrick, “Solvable model of a spin-glass”, *Phys. Rev. Lett.* **35**, 26 (1975).
- [98] E. Marinari, G. Parisi, and F. Ritort, “Replica field theory for deterministic models: II. A non-random spin glass with glassy behaviour”, *J. Phys. A: Math. Gen.* **27**, 7647 (1994).
- [99] F. Barahona, “On the computational complexity of Ising spin glass models”, *J. Phys. A: Math. Gen.* **15**, 3241 (1982).
- [100] C. K. Thomas and A. A. Middleton, “Matching Kasteleyn cities for spin glass ground states”, *Phys. Rev. B* **76**, 220406(R) (2007).
- [101] G. Pardella and F. Liers, “Exact ground states of large two-dimensional planar Ising spin glasses”, *Phys. Rev. E* **78**, 056705 (2008).
- [102] A. J. Bray and M. A. Moore, “Chaotic nature of the spin-glass phase”, *Phys. Rev. Lett.* **58**, 57 (1987).
- [103] F. Ritort, “Static chaos and scaling behavior in the spin-glass phase”, *Phys. Rev. B* **50**, 6844 (1994).
- [104] C. De Dominicis and I. Kondor, “Eigenvalues of the stability matrix for Parisi solution of the long-range spin-glass”, *Phys. Rev. B* **27**, 606 (1983).

- 
- [105] M. Ney-Nifle and A. P. Young, “Chaos in a Two-Dimensional Ising Spin Glass”, *J. Phys. A: Math. Gen.* **30**, 5311 (1997).
- [106] S. Feng and P. N. Sen, “Percolation on elastic networks: New exponent and threshold”, *Phys. Rev. Lett.* **52**, 216 (1984).
- [107] D. J. Jacobs and M. F. Thorpe, “Generic rigidity percolation: The pebble game”, *Phys. Rev. Lett.* **75**, 22 (1995).
- [108] C. Moukarzel and P. M. Duxbury, “Stressed backbone and elasticity of random central-force systems”, *Phys. Rev. Lett.* **75**, 4055 (1995).
- [109] J. C. Maxwell, “On the calculation of the equilibrium and stiffness of frames”, *Philos. Mag.* **27**, 294 (1864).
- [110] D. J. Jacobs and B. Hendrickson, “An algorithm for two-dimensional rigidity percolation: The pebble game”, *J. Comp. Phys.* **137**, 346 (1997).
- [111] G. Laman, “On graphs and rigidity of plane skeletal structures”, *J. Engrg. Math.* **4**, 331 (1979).
- [112] W. G. Ellenbroek, Z. Zeravic, W. van Saarloos, and M. van Hecke, “Non-affine response: Jammed packings vs. spring networks”, *Eur. Phys. Lett.* **87**, 34004 (2009).
- [113] X. Mao, N. Xu, and T. C. Lubensky, “Soft modes and elasticity of nearly isostatic lattices: Randomness and dissipation”, *Phys. Rev. Lett.* **104**, 085504 (2010).
- [114] G. Parisi, “Toward a mean field theory for spin glasses”, *Phys. Lett.* **73A**, 203 (1979).
- [115] M. Mezard, G. Parisi, and M. A. Virasoro *Spin glass theory and beyond*, World Scientific, New Jersey (1987).

- 
- [116] D. S. Fisher and D. A. Huse, “Ordered phase of short-ranged Ising spin-glasses”, *Phys. Rev. Lett.* **56**, 1601 (1986).
- [117] D. S. Fisher and D. A. Huse, “Equilibrium behavior of the spin-glass ordered phase”, *Phys. Rev. B* **38**, 386 (1988).
- [118] D. W. Howell, R. P. Behringer, and C. T. Veje, “Fluctuations in granular media”, *Chaos* **9**, 559 (1999).
- [119] T. S. Majumdar and R. P. Behringer, “Contact force measurements and stress-induced anisotropy in granular materials”, *Nature* **435**, 1079 (2005).
- [120] A. J. Bray and M. A. Moore, “Evidence for massless modes in the ‘solvable model’ of a spin glass”, *J. Phys. C: Sol. St. Phys.* **12**, L441 (1979).
- [121] A. J. Bray and M. A. Moore, “Replica symmetry and massless modes in the Ising spin glass”, *J. Phys. C: Sol. St. Phys.* **12**, 79 (1979).
- [122] M. Mailman and B. Chakraborty, “Unjamming of Granular Packings as a Constraint Satisfaction Problem: Evidence for a Growing Static Length Scale in Frictionless Packings”, arXiv:1007.0266.
- [123] F. Krzakala and J. Kurchan, “Constraint optimization and landscapes”, *Eur. Phys. J. B* **64**, 563 (2008).
- [124] R. Mari, F. Krzakala, and J. Kurchan, “Jamming versus Glass Transitions”, *Phys. Rev. Lett.* **103**, 025701 (2009).
- [125] C. Toninelli, G. Biroli, and D. S. Fisher, “Spatial structures and dynamics of kinetically constrained models of glasses”, *Phys. Rev. Lett.* **92**, 185504 (2004).

- 
- [126] J. M. Schwarz, A. J. Liu, and L. Q. Chayes, “The onset of jamming as the sudden emergence of an infinite  $k$ -core cluster”, *Eur. Phys. Lett.* **73**, 560 (2006).
- [127] J. A. Adler, R. G. Palmer, and H. Meyer, “Transmission of order in some unusual dilute systems”, *Phys. Rev. Lett.* **58**, 882 (1987).
- [128] J. E. S. Socolar, D. G. Schaeffer, and P. Claudin, “Directed force chain networks and stress response in static granular materials”, *Eur. Phys. J. E* **7**, 353 (2002).
- [129] R. Blumenfeld, “Stresses in isostatic granular systems and emergence of force chains”, *Phys. Rev. Lett.* **93**, 108301 (2004).
- [130] S. Henkes and B. Chakraborty, “A statistical mechanics framework for static granular matter”, *Phys. Rev. E* **79**, 061301 (2009).
- [131] R. Metzler and J. Klafter, “The random walker’s guide to anomalous diffusion: A fractional dynamics approach,” *Phys. Rep.* **339**, 1 (2000).
- [132] J. Klafter, M. F. Shlesinger, and G. Zumofen, “Beyond Brownian motion,” *Phys. Today* **49**, 33 (1996).
- [133] R. Hilfer, ed., *Applications of Fractional Calculus in Physics* (World Scientific, New York, 2000).
- [134] B. J. West, M. Bologna and Paolo Grigolini, *Physics of Fractal Operators* (Springer, New York, 2003).
- [135] N. Laskin, “Fractals and quantum mechanics,” *Chaos* **10**, 780 (2000).
- [136] N. Laskin, “Fractional quantum mechanics,” *Phys. Rev. E* **62**, 3135 (2000).

- 
- [137] N. Laskin, “Fractional quantum mechanics and Lévy path integrals,” *Phys. Lett. A* **268**, 298 (2000).
- [138] X. Guo and M. Xu, “Some physical applications of fractional Schrödinger equation,” *J. Math. Phys.* **47**, 082104 (2006).
- [139] J. Dong and M. Xu, “Some solutions to the space fractional Schrödinger equation using momentum representation method,” *J. Math. Phys.* **48**, 072105 (2007).
- [140] N. Laskin, “Lévy flights over quantum paths,” *Comm. Nonlin. Sci. Num. Sim.* **12**, 2 (2007).
- [141] A. Zoia, A. Rosso, and M. Kardar, “Fractional Laplacian in Bounded Domains,” *Phys. Rev. E* **76**, 021116 (2007).
- [142] J. Dong and M. Xu, “Applications of continuity and discontinuity of a fractional derivative of the wave functions to fractional quantum mechanics,” *J. Math. Phys.* **49**, 052105 (2008).
- [143] N. Laskin, “Fractional Schrödinger equation,” *Phys. Rev. E* **66**, 056108 (2002).
- [144] R. Bañuelos, T. Kulczycki, and P. J. Méndez-Hernández, “On the Shape of the Ground State Eigenfunction for Stable Processes,” *Pot. Anal.* **24**, 205 (2006).
- [145] S. V. Buldyrev, M. Gitterman, S. Havlin, A. Y. Kazakov, M. G. E. de Luz, E. P. Raposo, H. E. Stanley and G. M. Viswanathan, “Properties of Lévy flights on an interval with absorbing boundaries,” *Physica A* **302**, 148 (2001).

- 
- [146] B. Dybiec, E. Gudowska-Nowak and P. Hanggi, “Lévy Brownian motion on finite intervals: Mean first passage time analysis,” *Phys. Rev. E* **73**, 046104 (2006).
- [147] M. E. Cates, J. P. Wittmer, J.-P. Bouchaud, and P. Claudin, “Jamming, force chains, and fragile matter”, *Phys. Rev. Lett.* **81**, 9 (1998).
- [148] B. H. Zimm, “Dynamics of polymer molecules in dilute solution: Viscoelasticity, flow birefringence, and dielectric loss”, *J. Chem. Phys.* **24**, 269 (1956).
- [149] R. K. P. Zia and D. J. Wallace, “Critical behaviour of the continuous  $n$ -component Potts model”, *J. Phys. A: Math. Gen.* **8**, 1495 (1975).
- [150] G. Cwlich and T. R. Kirkpatrick, “Mean-field theory and fluctuations in Potts spin glasses: I”, *J. Phys. A: Math. Gen.* **22**, 4971 (1989).
- [151] A. B. Harris, T. C. Lubensky, and J.-H. Chen, “Critical properties of spin-Glasses”, *Phys. Rev. Lett.* **36**, 8 (1976).
- [152] D. J. Gross, I. Kanter, and H. Sompolinsky, “Mean-field theory of the Potts glass”, *Phys. Rev. Lett.* **55**, 304 (1985).
- [153] G. Kotliar, P. W. Anderson, and D. L. Stein, “One-dimensional spin-glass model with long-range random interactions”, *Phys. Rev. B* **27**, 1 (1983).
- [154] M. A. Moore, “One-dimensional Ising spin-glass model with long-range interactions”, *J. Phys. A: Math. Gen.* **19**, L211 (1986).
- [155] M.-C. Chang, “Field-theoretical formulation of the spin-glass transition in the Potts model with short-ranged random-exchange interaction”, *Phys. Rev. B* **28**, 11 (1983).

- 
- [156] H. G. Katzgraber and A. K. Hartmann, “Ultrametricity and clustering of states in spin glasses: A one-dimensional view”, *Phys. Rev. Lett.* **102**, 037207 (2009).
- [157] D. Larson, H. G. Katzgraber, M. A. Moore, *et al.*, “Numerical studies of a one-dimensional three-spin spin-glass model with long-range interactions”, *Phys. Rev. B* **81**, 064415 (2010).

## VITA

NAME OF AUTHOR: Shiliyang Xu

PLACE OF BIRTH: Hefei, China

DATE OF BIRTH: April 9, 1987

DEGREES AWARDED:

B.Sc., Physics, University of Science and Technology of China (2006)

PROFESSIONAL EXPERIENCE:

Syracuse University, Department of Physics, Graduate Teaching/Research  
Assistant (2006-2011)